NITROGEN MUSTARD INDUCES EARLY CHANGES IN SKIN PROTEIN

EXPRESSION: POTENTIAL TARGETS FOR THERAPEUTIC INTERVENTION

by

GABRIELLA WAHLER

A dissertation submitted to the

School of Graduate Studies

Rutgers, The State University of New Jersey

In partial fulfillment of the requirements

For the degree of

Doctor of Philosophy

Graduate Program in Toxicology

Written under the direction of

Jeffrey D. Laskin and Laurie B. Joseph

And approved by

_____

_____

_____

_____

_____

New Brunswick, New Jersey

January, 2020

ABSTRACT OF THE DISSERTATION

Nitrogen Mustard Induces Early Changes in Skin Protein Expression:

Potential Targets for Therapeutic Intervention

By GABRIELLA WAHLER

Dissertation Directors:

Jeffrey D. Laskin, PhD; Laurie B. Joseph, PhD

Exposure to mustard gas is a current issue. Recently there has been resurgence in chemical warfare attacks, specifically in the Middle East. In August 2015, artillery shells were fired at Isnibil, a village east of Marea, Syria leaving 23 individuals hospitalized with signs of poisonous mustard gas exposure. Mustard gas attacks in Iraq and Syria resulted in victims presenting with respiratory problems, irritation to the eyes, vomiting, and damage to the skin which included blisters and burns. Skin barrier integrity is essential to human health and wellbeing. The stratum corneum, the outermost layer of the skin, is crucial for the body's defense against environmental toxins. Disruptions, which occur following chemical exposures, are associated with delayed wound healing and chronic wounds. Nitrogen mustard (NM, bis (2-chloroethyl) methylamine, mechlorethamine), an analog of the chemical warfare agent sulfur mustard (SM, bis (2-chloroethyl) sulfide), is a bifunctional alkylating agent that can induce oxidative stress, DNA damage and inflammation resulting in extensive skin damage. Since sulfur mustard is both lipophilic and volatile, dermal exposure can be localized using vapor cup models. In contrast, NM is hydrophilic; thus, direct application in solvents results in spreading over a relatively large area of skin. This makes quantification of tissue

damage difficult to assess. Key to elucidating the mechanism of action of mustards and testing potential countermeasures is the ability to generate reproducible injury in localized areas of the skin in experimental animal models. Despite extensive research, mechanisms underlying the chronological events of NM induced skin injury are not clearly understood, which makes it difficult to develop effective treatments for mitigating vesicant induced damage to the skin. Further understanding the effects of mustards on the skin will help determine potential therapies that can be used to mitigate toxicity. My proposed project focuses on chemical warfare agents and how alterations in oxidative stress and DNA damage proteins can alter skin re-generation following exposure. More specifically, it aims to examine the early chronology of NM damage on skin epithelium. The proposed studies will use a modified semi-occlusive patch test model developed in our laboratory to study skin injury following NM exposure to elucidate the underlying mechanism of action for the development of potential therapeutics.

aunt Lauretta Socci for her continued motivation. Finally, I would like to thank my god daughter Olivia June for bringing so much joy into my life.

DEDICATION

I dedicate this to my son Frank Edgar Wahler. Frank, I was pregnant with you during my

last year as a graduate student and you kept me strong during my defense. Mommy and

Daddy will love you always and forever. You have brought us a love we didn't know was

possible, and we can't wait to see you grow and achieve your dreams.

ACKNOWLEDGEMENT OF PREVIOUS PUBLICATIONS

CHAPTER 2

Gabriella M. Composto, Jeffrey D. Laskin, Debra L. Laskin, Donald R. Gerecke, Robert P. Casillas, Ned D. Heindel, Laurie B. Joseph, Diane E. Heck (2016). Mitigation of Nitrogen Mustard Mediated Skin Injury by a Novel Indomethacin Bifunctional Prodrug. *Experimental and Molecular Pathology*. 100(3); 522-31.

CHAPTER 3

Gabriella Wahler, Debra L. Laskin, Diane E. Heck, Jeffrey D. Laskin, Laurie B. Joseph (2019). Temporal Events in Mouse Epidermis Following Exposure to Nitrogen Mustard. *(In preparation for submission to Toxicology and Applied Pharmacology)*

CHAPTER 5

Gabriella Wahler, Laurie B. Joseph, Claire R. Croutch, Jieun Kang, Robert P. Casillas, Debra L. Laskin, Diane E. Heck, Jeffrey D. Laskin (2019). Wound Healing in Pig Skin Following Exposure to Sulfur Mustard Vapors. *(In preparation for submission to Experimental and Molecular Pathology)*

TABLE OF CONTENTS

LIST OF FIGURES

LIST OF TABLES

ABBREVIATIONS

AChE, acetylcholinesterase; AIDNX, prodrug NDH4338; B02, Rad51 inhibitor; BrdU, bromodeoxyuridine; CE, cornified envelope; CEES, 2-chloroethyl ethyl sulfide; COX-2, cyclooxygenase 2; DAB, diaminobenzidine ; D/E, dermal/epidermal; DSB, double strand breaks; H, humidity; HaCaT, human keratinocyte cell line; H&E, hematoxylin and eosin; H4, histone H4; 4-HNE, 4-hydroxynonenal; HO-1, hemeoxygenase 1; HRR, homologous recombination repair; ICLs, interstrand crosslinks; iNOS, inducible nitric oxide synthase; MC, mast cells; MEVM, mouse ear vesicant model; ML, moisture level; NHEJ, non-homologous end joining; NM, nitrogen mustard (bis (2-chloroethyl) methylamine); Nu7026, DNA-PK inhibitor; OBS, overall barrier score; 8-oxo-2'-dG, 8-oxo-2'-deoxyguanosine; pADPr, poly ADP ribose; PAM212, mouse keratinocyte cell line; PARP, poly ADP ribose polymerase; PCNA, proliferating cell nuclear antigen; PEG 400, poly ethylene glycol 400; PGD2, prostaglandin D2; PGE2, prostaglandin E2; phospho-H2A.X, phosphorylated histone H2A.X; PI, propidium iodide; pp53, phosphorylated p53; ROS, reactive oxygen species; SBS, skin barrier strength; SC, stratum corneum; SCH, stratum corneum hydration; SM, sulfur mustard (bis (2-chloroethyl) sulfide); SOD, superoxide dismutase; SSB, single strand breaks; T, temperature; TEWL, trans epidermal water loss; TPA, 12-O-tetradecanoylphorbol-13-acetate; TrxR, thioredoxin reductase

CHAPTER 1: INTRODUCTION

1.1 Vesicating Agents

Sulfur mustard (bis (2-chloroethyl) sulfide; SM) and its structural analog nitrogen mustard (bis (2-chloroethyl) methylamine; NM) are blistering agents which cause extensive damage to various tissues and organs including the skin, eyes and lungs following exposure (Graham *et al.*, 2013; Kehe *et al.*, 2005). Although NM has never been used in warfare it was developed as a chemical warfare agent in the 1940s by Germany and the United States and poses a similar threat as SM for use as a warfare agent (Inturi *et al.*, 2014). As a bifunctional alkylating agent, SM induces tissue injury by reacting with a variety of cellular macromolecules including nucleic acids, proteins and lipids (Joseph *et al.*, 2018; Papirmeister *et al.*, 1985). In aqueous solutions both SM and NM spontaneously lose a chloride ion and undergo nucleophilic substitution to form a cyclic aziridinium ring **(Fig. 1.1)** (Inturi*, et al.*, 2014; Mann, 2010). This intermediate is reactive, forming a second aziridinium ion which reacts with nearby nucleophilic sites resulting in adducts and crosslinks (Inturi*, et al.*, 2014). This results in alterations in tissue structure and function, erythema and pruritis which are among the first signs of vesicant-induced dermal injury (Joseph*, et al.*, 2018; Laskin *et al.*, 2010). Subsequently, degradation of the epidermis can result in the formation of fluid filled blisters and necrotic lesions (Graham*, et al.*, 2013; Joseph*, et al.*, 2018; Kehe *et al.*, 2008; Rice, 2003). Like SM, cutaneous exposure to NM causes toxicity to the dividing basal epidermal cells leading to cell death and delayed vesication, prolonged healing with chronic inflammation, tissue remodeling and scarring (Inturi*, et al.*, 2014; Joseph*, et al.*, 2018).

1.1.1 Skin Structure and Function

The skin is the largest organ of the body providing a physical barrier to foreign substances (Blattner *et al.*, 2014). The skin is composed of three primary layers, the epidermis, dermis and subcutaneous fat (Richardson, 2003) **(Fig. 1.2)**. The outermost layer of the epidermis, the stratum corneum (SC), contains corneocytes embedded in a lipid matrix held together by corneodesmosomes (Elias, 2014; Murphrey *et al.*, 2019). Ceramides, cholesterol, and free fatty acids in an equimolar ratio provide the permeability barrier which contributes to the hydrophobic nature of the skin (Blattner*, et al.*, 2014; Elias, 2014; Menon *et al.*, 2012). Lipolytic and proteolytic enzymes and anti-microbial peptides contribute to the ongoing biochemical activities in the SC (Barrett *et al.*, 1964; Dutagaci *et al.*, 2014; Menon*, et al.*, 2012; Raymond *et al.*, 2008). The epidermis is divided into several layers the SC, the uppermost layer, followed by the stratum lucidum, granulosum, spinosum and basale **(Fig. 1.2)**. Cells of the stratum basale, or basal layer of the skin, move upward through the spiny and granular layers to the top layer, the SC (Wickett *et al.*, 2006; Yousef *et al.*, 2019). The predominant cell type of the epidermis is the keratinocyte which transforms into corneocytes at the SC (Raymond*, et al.*, 2008; Wickett*, et al.*, 2006). Additional cell types in the epidermis include melanocytes, Langerhans, and Merkle cells. Melanocytes are the pigment-producing cells of the skin and hair and Langerhans cells are dendritic immune cells of the skin which play an important role in immune barrier of the epidermis and in contact allergy (Yousef*, et al.*, 2019). Merkel cells are important in sensory function for fine touch. The basement membrane is a thin layer of protein fibers and glycosaminoglycans which separates the epithelium from the underlying dermis. The dermis varies in thickness and is made up of two components, the thin papillary region (the upper most layer), composed of fine and loosely arranged collagen fibers. The thick reticular layer is

the lower layer of the dermis and is composed of dense irregular connective tissue and is the primary location of dermal elastic fibers (Rissmann *et al.*, 2009) **(Fig. 1.2)**. Embedded within the fibrous tissue of the dermis are the dermal vasculature, lymphatics, and nerve cells (Zhu *et al.*, 2015). These components of the dermis allow for waste removal aiding in the defense system of the skin (Stenn *et al.*, 2010). The hypodermis or subcutaneous tissue is the deepest layer of skin and contains adipose lobules along with some skin appendages (hair follicles), sensory neurons, and blood vessels providing anchorage (Yousef*, et al.*, 2019) **(Fig. 1.2)**. Together, these components of the skin help to maintain the SC barrier and integrity of the skin.

1.1.2 Skin Barrier Disruption

When functioning properly, the skin prevents water loss providing a barrier to epidermal invasion of allergens and bacteria. Interfering with or altering the functional properties of the skin can weaken the barrier, decreasing an individual's protection from environmental insult. Changes in skin barrier leads to imbalances in epidermal lipids and result in water loss from the SC (Elias, 2008; Hogan *et al.*, 2012; Rosso *et al.*, 2016). It is considered that the rate of trans epidermal water loss (TEWL) correlates with skin barrier function which can provide quantitative measurements of skin damage caused by exposure to chemical agents such as NM and SM (Blattner*, et al.*, 2014; Lee *et al.*, 2012). *In-vivo* measurements of TEWL were conducted in our laboratory to provide a quantitative assessment of gross skin damage as a direct result of NM exposure. The severity and progression of the resulting skin lesions were quantified daily for three days, beginning on day 0, 1 hour following exposure. These studies employed the use of the GPower Skin Barrier Light® by GPOWER Inc. (Seoul, South Korea) (Ye *et al.*, 2019).

In these studies, skin barrier strength (SBS), moisture level (ML), stratum corneum hydration (SCH), temperature (T) and humidity (H) in addition to TEWL were measured. Following damage, readings were taken to obtain an overall barrier score (OBS) to determine the strength of the skin barrier. Initially, 1 hour post-NM exposure (day 0) SBS decreased by 88% while TEWL rates increased by 90%, compared to control **(Fig. 1.3; A)**. Twenty-four hours after damage (day 1), ML and SCH were increased by 80% and 45%, respectively. Forty-eight hours (day 2) revealed a 20% decrease in OBS and a 2.5-fold increase in punch biopsy weight **(Fig. 1.3; A & B)**. Histological staining on day 2 revealed decreased SC integrity and a 42% decrease in epidermal thickness, compared to control **(Fig. 1.3; C)**. These data represent the damage that occurs to the skin barrier following vesicant exposure. Understanding skin sensitivity to various toxins is important in protecting human health and for evaluating dermal toxicants to determine their mechanism of action for the preclinical testing of drugs as treatments. For this reason, development of a suitable *in-vivo* model is essential in studying dermal toxicants.

1.1.3 Model Development

Multiple animal models have been developed in order to test the sensitivity of the skin to different toxicants that alter the defense system (El Maghraby *et al.*, 2015; Fischer *et al.*, 1989; Ogiso *et al.*, 2001). Dermal toxicants range from sensitizers and irritants to mutagens and carcinogens with the ability to cause adverse events in humans and animals via skin contact (Farage *et al.*, 2011). Due to its nature, the skin is permeable to lipid-soluble substances and gases, but impermeable to water making it difficult for dermal toxicants solubilized in hydrophilic formulations to penetrate the skin (Anishkin *et al.*, 2014; Notman *et al.*, 2008).

Toxic compounds with varying physical and chemical properties have different affinities to the SC affecting their absorption through the skin (Barrett*, et al.*, 1964). Absorption is dependent on the integrity of the skin, and the anatomical site exposed (Ibrahim *et al.*, 2010). SC thickness varies depending on location being about 0.5 mm on the eyelid and about 2 mm on the back (Sandby-Moller *et al.*, 2003). These changes in thickness predispose certain areas to increased penetration of topical products (Chantasart *et al.*, 2012; Vieille-Petit *et al.*, 2015).

Mice, rats, guinea pigs and swine have proven to be adequate animal models when determining skin toxicity (Surh *et al.*, 2012). These animal models have helped to develop direct and indirect methods that test and recapitulate the effects of dermal toxicants. Direct skin contact models rely on the solubility of toxicants for penetration through the skin, while indirect models rely on the use of physical supports for dermal application. Direct skin contact models include topical application, and vapor cups (Anderson *et al.*, 2002; Casillas *et al.*, 2000; Singer *et al.*, 2011). Indirect skin contact models employ the use of gauze pads and filter paper for toxicant application (Hojer *et al.*, 2002; Hulten *et al.*, 2004).

1.2. Direct Contact Models

1.2.1 Topical Application

The mouse ear vesicant model (MEVM) of induced dermal toxicity allows for analysis of chemical agents on the skin of animals. The MEVM has been used to study a range of toxicants such as 2-chloroethyl ethyl sulfide (CEES), a blistering agent, 12-O-tetradecanoylphorbol-13-acetate (TPA), a common topical irritant, SM and NM (Casillas*, et al.*, 2000; Chang *et al.*, 2009; Chang *et al.*, 2013; Ricketts *et al.*, 2000). The MEVM is

recognized for its effectiveness in studying skin responses and damage following exposure to chemical irritants (Casillas*, et al.*, 2000; Monteiro-Riviere *et al.*, 1999; Ricketts*, et al.*, 2000). Casillas et al., 2000 exposed rats to a single 5 µl dose of varying concentrations of SM in dichloromethane on the outer surface of the ear. This method of application allowed for evaluation of edema as an index of inflammation and histopathologic response to SM following exposure. A comparative evaluation of the results indicated which dose was optimal for future studies, and how the inflammatory response proved to be an early indicator of SM induced skin damage.   Studies investigating the mouse ear allow for further examination of dermal edema and the inflammatory response.   Rodent ear skin has comparable permeability with that of human skin demonstrating that the ear is a reasonable model for studying the transport of drugs (King *et al.*, 2015). A drawback in evaluation of toxicants on the ear is that mice can easily reach and groom this region, and the area (cm^2) is limiting (Jung *et al.*, 2015). Methods to reduce these limitations include use of the dorsal or ventral region of the mouse for dermal application (Chaquour *et al.*, 1995; Goswami *et al.*, 2015; Joseph *et al.*, 2011).

The dorsal and ventral regions of the mouse provide a larger area for application and the dorsum is in a location that is difficult for the mouse to reach (Jung*, et al.*, 2015; Singer *et al.*, 2015). The hairless mouse model is a method that exposes the dorsal region of mice to dermal toxicants (Goswami*, et al.*, 2015; Kligman, 1996; Zhaorigetu *et al.*, 2003). With this model dermal toxicants can be analyzed following exposure on SKH1-Hr hairless mice (Chaquour*, et al.*, 1995; Goswami*, et al.*, 2015; Joseph*, et al.*, 2011). Application of a toxicant on the dorsum allows for easy entry to internal organs and an examination of penetration range (Batal *et al.*, 2014; Pan *et al.*, 2015). This type of application is ideal for toxicants that are not hydrophilic, however for those that are

application can prove to be difficult. When applied directly to the skin these hydrophilic substances may spread laterally leading to unpredictable penetration dynamics and increased skin surface area exposure **(Fig. 1.4)** (Saunders *et al.*, 1999; Vieille-Petit*, et al.*, 2015). To avoid lateral spreading a barrier can be created around the application area (Wormser *et al.*, 2002). One such barrier can be the creation of a well.

Wells can be constructed out of open-ended plastic cylindrical tubes adhered onto the dorsal region through a silicone sealing ointment placed along the edge ensuring no leakage (Wormser*, et al.*, 2002). Such a study would be effective in containing the toxic solution in a defined area (Wormser*, et al.*, 2002). A limitation to such a design is the skin irritation that occurs with the addition of extra adhesive material leading to variability in results. Some studies mark the damage site with a tattoo adding increased variability and skin injury (Gopee *et al.*, 2005; Graham *et al.*, 2000; Graham *et al.*, 2002). One way to analyze skin damage following direct toxicant exposure while still controlling for area exposed and additional irritation is the use of a vapor cup (Anderson*, et al.*, 2002; Mershon *et al.*, 1990).

1.2.2 Vapor Cup Model

The vapor cup model was originally developed in order to create an experimental model that reflected real world SM exposure (Anderson*, et al.*, 2002; Joseph*, et al.*, 2011; Kehe *et al.*, 2009; Mershon*, et al.*, 1990). In this model SM is delivered via a closed cup vapor system to the skin surface of the animal (Ricketts*, et al.*, 2000). A vapor cup is prepared by fitting it with Whatman filter paper discs, fixed above the rim and saturated with SM. The volume of SM should be enough to thoroughly wet the filter paper without running down the inside of the (Anderson*, et al.*, 2002; Joseph*, et al.*, 2011; Ricketts*, et al.*, 2000). This model has been used to analyze SM-induced skin injury in several animal

species including guinea pigs, hairless guinea pigs, haired neonatal mice, hairless mice and pigs (Anderson, *et al.*, 2002; Joseph, *et al.*, 2011; Mershon, *et al.*, 1990; Wormser, *et al.*, 2002). Variations in this method occur between species but overall the vapor cup model is aimed at exposing the dorsal area of the skin to dermal toxicants for a controlled delivery comparable to human exposure (Graham, *et al.*, 2000; Graham, *et al.*, 2002).

The SM vapor cup model is one of the most successful and utilized forms of exposure for chemical vapors (Anderson, *et al.*, 2002; Mershon, *et al.*, 1990; Snider *et al.*, 2014). When the production of a vapor is not possible or recommended, other forms of skin exposures must be investigated.

1.3 Indirect Skin Contact Models

1.3.1 Patch Test Models

The patch test as we know it today was popularized by Ladassohn in 1895 (Fischer, *et al.*, 1989). This test has been refined from its simple origins, in which a substance was placed under an adhesive bandage and left on the skin for several days (Fischer, *et al.*, 1989; Rietschel, 1989). More recently test substances are suspended in a matrix and applied to the back or volar surface of the arm under occlusive or semi-occlusive tape (Fischer, *et al.*, 1989). This procedure has been modified for animal use by the Buehler Method (Buehler, 1994). The occlusive patch test to analyze hypersensitivity reactions in guinea pigs and more recent modifications employ gauze pads and filter paper as supports (Buehler, 1994; Hojer, *et al.*, 2002; Wu *et al.*, 2012).

In these models, which have been used in both humans and animals, test chemicals are suspended in a matrix which is adhered to a designated area of the skin with occlusive

or semi-occlusive tape (Buehler, 1994; Farage*, et al.*, 2011; Fischer*, et al.*, 1989; Nicholson *et al.*, 1999). Patch models have also been used to evaluate treatments for chemical burns, and as a method for delivering hydrophilic substances to the skin (Hojer*, et al.*, 2002; Hulten*, et al.*, 2004).

Although many patch models can be extrapolated to human skin, there are limitations in skin permeability of test agents between humans and animals, as well as their ability to induce irritation reactions (Chew *et al.*, 2003; Simon *et al.*, 1998).

1.4 Discussion

The SC functions in host protection from foreign chemicals and bacteria, water loss prevention, and body temperature regulation (Blattner*, et al.*, 2014; Richardson, 2003; Talreja *et al.*, 2001). Epidermal barrier perturbation is a consequence of various environmental factors (Hosnuter *et al.*, 2015; Pan*, et al.*, 2015). Correctly designed exposure models are needed to evaluate skin damage due to dermal toxicants (Joseph*, et al.*, 2011; Jung*, et al.*, 2015; Zhu*, et al.*, 2015). In order to develop a reliable model for skin barrier disruption we need to be familiar with each animal model's characteristics as well as experimental methods (Talreja*, et al.*, 2001). Absorption of chemicals through the skin varies depending upon the composition and solubility of the chemical (Barrett*, et al.*, 1964; Notman*, et al.*, 2008). Many dermal toxicants are soluble in water and prove difficult to study due to the hydrophobic nature of the skin (Anishkin*, et al.*, 2014; Dutagaci*, et al.*, 2014). Methods to drive toxicants through the skin barrier include direct and indirect contact models and are successful in causing skin irritation allowing for dermal toxicity testing. Among the animal models developed some prove better in their ability for controlled application and enhanced SC permeability (Casillas*, et al.*, 2000; Hojer*, et al.*, 2002). Modification of these animal models helps to better evaluate skin damage, chemical toxicity and subsequent skin resolution (Avci *et al.*, 2013; King*, et al.*,

2015). Vapor cup studies in general have demonstrated that hair follicles and sebaceous glands are targets for induced toxicity in the skin and that basal cell damage resembled lesions of vesicant injury in man (Mershon*, et al.*, 1990). The development and use of direct skin contact models such as the vapor cup model, and indirect skin contact models such as the patch test are invaluable in understanding the consequences of chemical exposures on the skin and for delivering hydrophilic substances through the hydrophobic SC (Buehler, 1994; Fischer*, et al.*, 1989; Hadebe *et al.*, 2014; Hulten*, et al.*, 2004).

The patch test model was modified in our laboratory to study the effects of NM on the skin. Preliminary studies with NM revealed the dorsal lumbar region of the mice as an ideal location for evaluating dermal injury and providing reproducibility in wound development **(Fig 1.5).**

1.5 Research Objective and Hypothesis

A central hypothesis was developed from the information presented in this introduction: Vesicant exposures lead to excessive skin damage through alterations in early markers of damage and repair. Three specific aims were developed to evaluate the hypothesis presented in this thesis:

Aim 1. Characterize tissue damage induced by NM with the use of a cutaneous mouse model.

Aim 2. Identify macromolecules that mediate DNA damage and oxidative stress in isolated mouse skin epithelium exposed to NM.

Aim 3. Analyze kinetics of DNA damage and oxidative stress in mouse and human keratinocytes exposed to NM in relation to the cell cycle.

The prevalence of chemical warfare and lack of effective countermeasures make the risk of exposure a significant concern. This work is aimed at identifying the mechanisms underlying the function of mustard agents, toxins used in chemical warfare, through the development of suitable *in-vivo* and *in-vitro* models to ameliorate skin injury following exposure for the development of countermeasures. This research fills knowledge gaps in the fields of skin biology, dermal toxicology, and environmental exposure science.

12

Sulfur Mustard (SM)   **Nitrogen Mustard (NM)**
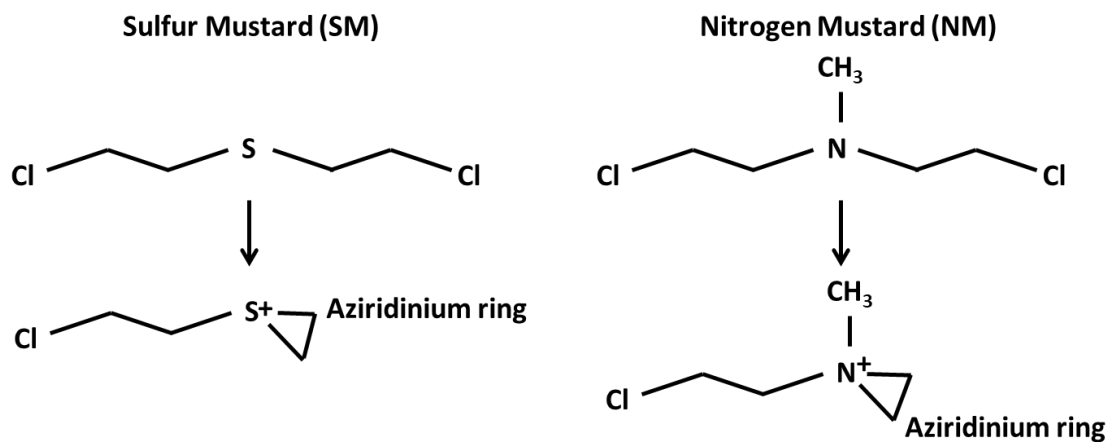
Figure 1.1 Aziridinium Ring Formation.

Both NM and SM form reactive aziridinium rings by intramolecular displacement of the chloride by the amine nitrogen. These aziridinium ions react with two bases on opposite strands of a DNA duplex to form a covalent linkage yielding adducts called DNA interstrand cross-links (ICLs). This prevents helix unwinding, blocking essential processes such as replication and transcription.

Stratum corneum

Stratum lucidum

Stratum granulosum

Epidermis

Stratum spinosum

Stratum basale

Basement membrane

Dermis

Adipose tissue
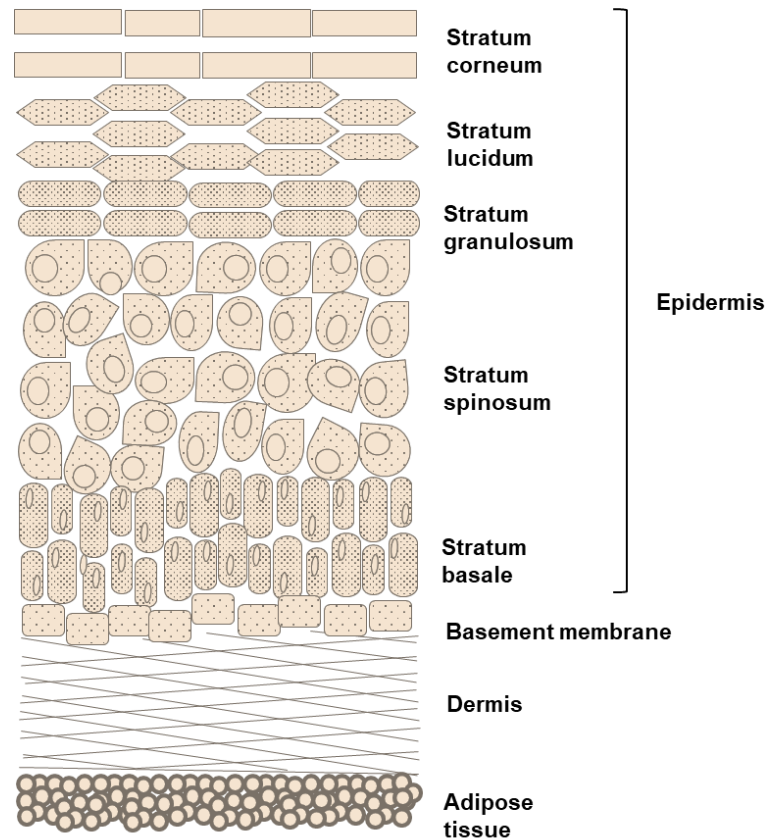
Figure 1.2 Figure Basic Skin Structure.

The image shows a simplified version of skin structure. The skin is divided into three main layers. The outermost layer, the epidermis, is composed of the stratum corneum, stratum lucidum, stratum granulosum, stratum spinosum and stratum basale. A basement membrane connects the epidermis and dermis. The dermis is composed of fine and loosely arranged collagen fibers which contain the dermal vasculature, lymphatics, and nerve cells (not depicted). Below the dermis is the hypodermis or adipose layer which contains adipose lobules (Wahler, 2019).

A.
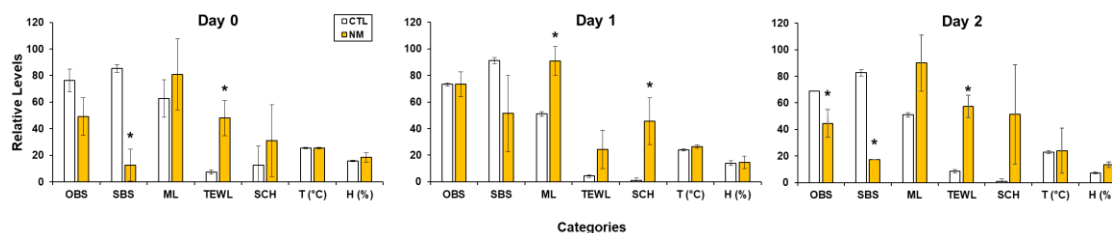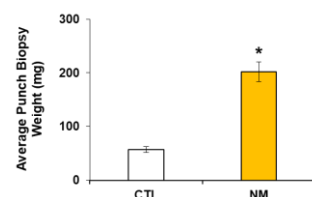
B. **C.**
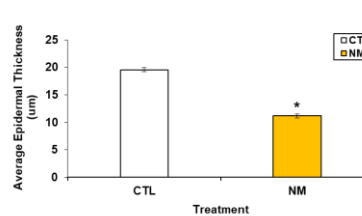
Figure 1.3 Changes in Skin Characteristics Following Treatment with Nitrogen Mustard.

The dorsal skin of female CD-1 mice was shaved and 20 μmol of NM in 20% deionized water/80% acetone (v/v) or vehicle control (CTL) was applied to the filters which were then covered with PARAFILM®. After 6 minutes, the filter discs were removed, and the skin analyzed for tissue damage 0-2 days following exposure using the GPower Skin Barrier Light® by GPOWER Inc. (Seoul, South Korea). **A.** The graphs show the relative levels of skin characteristics following exposure. **B.** The graph shows the average punch biopsy weight 2 days post-NM exposure. **C.** The graph shows the average epidermal thickness 2 days post-NM exposure. Comparison of the multiple groups was performed using one-way analysis of variance (ANOVA). The result is considered significant with p-value $\leq$ 0.05. *Significant from CTL (n = 3), the data are expressed as mean ± standard deviation (SD). **OBS**, overall barrier score; **SBS**, skin barrier strength; **ML**, moisture level; **TEWL**, trans epidermal water loss; **SCH**, stratum corneum hydration; **T**, temperature; **H**, humidity.

NM applied to the skin

Epidermis

Basement Membrane

Dermis

Hypodermis/Adipose tissue

Lateral Spreading

Limited Penetration
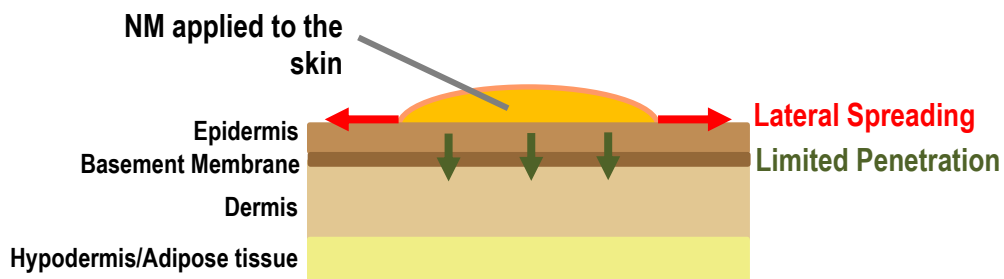
Figure 1.4 Limitations of the Hydrophobic Skin Barrier.

The diagram illustrates the difficulties of NM penetration through the hydrophobic skin barrier. The hydrophilic properties of NM results in diminished dermal penetration and lateral spreading resulting in excessive skin damage that is difficult to characterize.
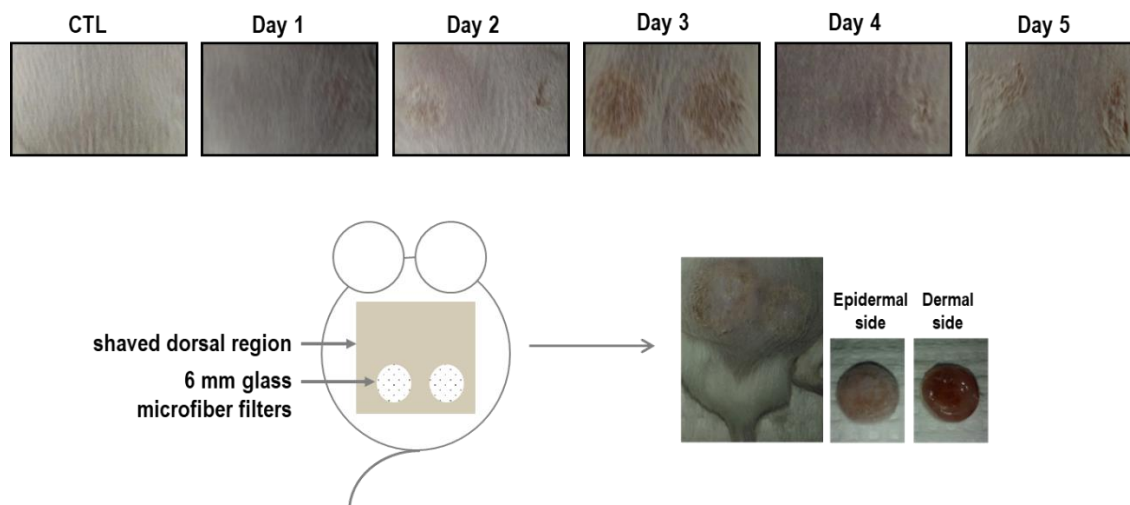
Figure 1.5 Mouse Model Results.

The dorsal skin of female CD-1 mice was shaved and exposed to 20 μmol of NM in 20% deionized water/80% acetone (v/v) or vehicle control (CTL). NM was applied to the filters which were then covered with PARAFILM®. After 6 minutes, the filter discs were removed, and the skin was analyzed for tissue damage 1-5 days following exposure. The patch test model was modified in our laboratory to study the effects of NM on the skin. The progression of wound development following NM exposure is depicted (*top panel*) along with filter placement and the punch biopsy obtained from the wound site (*lower right image*).

CHAPTER 2: DEVELOPING A NITROGEN MUSTARD MOUSE SKIN MODEL TO EVALUATE COUNTERMEASURES

Gabriella M. Composto[a], Jeffrey D. Laskin[a,b,c,d], Debra L. Laskin[a,b], Donald R. Gerecke[a,c], Robert P. Casillas[e], Ned D. Heindel[f], Laurie B. Joseph[a,b], Diane E. Heck[g]

[a] Joint Graduate Program in Toxicology, Rutgers University Graduate School of Biomedical Sciences, 170 Frelinghuysen Rd, Piscataway, NJ 08854, USA

[b] Department of Pharmacology and Toxicology, Rutgers University, 170 Frelinghuysen Rd, Piscataway, NJ 08854, USA

[c] Environmental and Occupational Health Sciences Institute, Rutgers University, 170 Frelinghuysen Rd, Piscataway, NJ 08854, USA

[d] School of Public Health, Rutgers University, 170 Frelinghuysen Rd, Piscataway, NJ 08854, USA

[e] Academy of Toxicological Sciences, Latham BioPharm Group, 101 Main Street, Cambridge, MA, 02142

[f] Department of Chemistry, Lehigh University, 27 Memorial Dr. W., Bethlehem, PA 18015, USA

[g] Department of Environmental Health Science, School of Health Sciences and Practice, New York Medical College, 40 Sunshine Cottage Rd., Valhalla, NY 10595, USA

2.1 Abstract

In the present studies, a modified cutaneous patch test model was developed in mice to characterize NM-induced injury and to evaluate the efficacy of an indomethacin pro-drug in mitigating toxicity. NM (20 µmol) or vehicle control was applied onto 6 mm glass microfiber filters affixed to the shaved dorsal skin of CD-1 mice for 6 minutes. This resulted in dermal absorption of approximately 4 µmol of NM. NM caused localized skin damage within 1 day, progressing to an eschar within 2-3 days, followed by wound healing after 4-5 days. NM-induced injury was associated with increases in skin thickness, inflammatory cell infiltration, reduced numbers of sebocytes, basal keratinocyte double strand DNA breaks, as measured by phosphorylated histone 2A.X (phospho-H2A.X) expression, mast cell degranulation and increases in inducible nitric oxide synthase (iNOS) and cyclooxygenase-2 (COX-2). Wound healing was characterized by epidermal hyperplasia and marked increases in basal cells expressing proliferating cell nuclear antigen (PCNA). A novel indomethacin-anticholinergic prodrug NDH4338 (AIDNX) designed to target cyclooxygenases and acetylcholinesterase (AChE), was found to markedly suppress NM toxicity, decreasing wound thickness and eschar formation. The prodrug also inhibited mast cell degranulation, suppressed keratinocyte expression of iNOS and COX-2, as well as markers of epidermal proliferation. These findings indicate that a novel bifunctional pro-drug is effective in limiting NM mediated dermal injury. Moreover, our newly developed cutaneous patch test model is a sensitive and reproducible method to assess the mechanism of action of countermeasures.

Abbreviations

AChE, acetylcholinesterase; CEES, 2-chloroethyl ethyl sulfide; COX, cyclooxygenases; D/E, dermal/epidermal; DSB, double strand breaks; H&E, hematoxylin & eosin; iNOS,

inducible nitric oxide synthase; MCs, mast cells; MEVM, mouse ear vesicant model; NM, nitrogen mustard (bis (2-chloroethyl) methylamine); PBS, phosphate buffered saline; PCNA, proliferating cell nuclear antigen; PGD2, prostaglandin D2; PGE2, prostaglandin E2; phospho-H2A.X, phosphorylated histone H2A.X; SC, stratum corneum; SM, sulfur mustard (bis (2-chloroethyl) sulfide); SSB, single strand breaks

2.2 Introduction

SM and NM are highly toxic bifunctional alkylating agents causing epidermal and dermal damage (Shakarjian *et al.*, 2010). In humans, depending on the dose and duration of exposure, mustards can cause acute injury, inflammation, the formation of ulcerative wounds, and blistering (Arck *et al.*, 2006; Ghabili *et al.*, 2010; Vogt *et al.*, 1984). Generally similar responses are observed in rodent models of cutaneous exposure to SM or NM (Tewari-Singh *et al.*, 2013).

Since SM is both lipophilic and volatile, dermal exposure can be localized using vapor cup models (Anderson*, et al.*, 2002; Mershon*, et al.*, 1990). In contrast, NM is hydrophilic; thus, direct application in solvents results in spreading over a relatively large area of skin. This makes quantification of tissue damage difficult to assess (Tewari-Singh*, et al.*, 2013; Tewari-Singh *et al.*, 2014; Vieille-Petit*, et al.*, 2015).

In the present studies, a modified semi-occlusive patch test model employing a glass microfiber filter delivery system was developed for cutaneous NM delivery in mice; our goal was to characterize skin injury and wound healing, and to assess the efficacy of a novel bifunctional anti-inflammatory prodrug, AIDNX, as a potential countermeasure. The advantage of microfiber dosing is that it provides an effective method of applying NM over defined areas of the skin, making it easier to quantify tissue damage. AIDNX was designed to target cyclooxygenases (COX), enzymes that generate proinflammatory

eicosanoids, and also to target acetylcholinesterase, an enzyme mediating hydrolysis of acetylcholine **(Fig. 2.1) (Kurzen *et al.*, 2007)**. The advantage of the prodrug is that it provides a simple dosage form for two drug targets in the skin and a facilitated mechanism for onsite controlled release of the individual therapeutic components. This provides an opportunity for therapeutic properties on the skin that exceed those of the component parts. In earlier studies we showed that AIDNX was effective in reducing sulfur mustard-induced edema, as well as degradation of the dermal-epidermal basement membrane; it also reduced expression of COX-2 and promoted wound re-epithelialization (Chang *et al.*, 2014). The present studies demonstrate that our modified cutaneous patch test model is highly reproducible and can be used to effectively evaluate candidate therapeutics with the potential to mitigate vesicant-induced skin injury.

2.2 Materials and Methods

Chemicals

Polyethylene glycol 400 and lanolin (C10-30 cholesterol/lanosterol esters) were from Croda Inc., Edison, NJ. Unless otherwise indicated NM (mechlorethamine HCl) and all other chemicals were purchased from Sigma-Aldrich (St. Louis, MO). AIDNX was synthesized as previously described (Young *et al.*, 2010).

Animals and Treatments

Female CD-1 mice (8 weeks; Charles River Laboratories, Wilmington, MA) were housed in filter-top micro isolation cages and maintained on food and water *ad libitum*. Mice received humane care in compliance with the Rutgers University guidelines, as outlined in the *Guide for the Care and Use of Laboratory Animals published by the National Institutes of Health*. Mice were anesthetized by intraperitoneal injection of ketamine (80 mg/kg) and xylazine (12 mg/kg), and randomly assigned to treatment groups. The

dorsal skin of the mice was shaved and then cleaned with deionized water. Six mm

glass microfiber filter discs (GE Healthcare, Buckinghampshire, UK) were placed on the

lumbar region of the shaved skin equidistant from the spine and adhered with 10 µl of

acetone **(Fig. 2.2; A)**. Twenty µl of freshly prepared 1 M NM (20 µmol) in 20% deionized

water/80% acetone, v/v, was then applied to the filters and immediately covered with

PARAFILM® (Pechiney, Menasha, WI). Control mice received the solvent without NM.

After 6 minutes, the filter discs were removed. In some experiments, mice were treated

topically with AIDNX four times per day beginning 1 hour after NM. For these

experiments, 20 µl of AIDNX (1% in a mixture of 49.5% lanolin and 49.5% polyethylene

glycol 400 (PEG400)) or vehicle control was applied directly to the skin and massaged in

using a finger cot (Thermo Fisher Scientific, Waltham, MA). Mice were euthanized 1-5

days post-NM and 12 mm full thickness biopsies of the exposure site and surrounding

tissue were immediately collected using a skin punch (Acuderm Inc., Ft. Lauderdale,

FL). Punch biopsies were trimmed and stored in ice cold phosphate buffered saline

(PBS) containing 3% paraformaldehyde/2% sucrose. The tissue was embedded in

paraffin and 6 µm sections prepared and stained with hematoxylin and eosin (H&E) or

Gomori's trichrome containing methyl (aniline) blue, for analysis of collagen I/III (Goode

Histolabs, New Brunswick, NJ). H&E stained tissue was scanned using a VS120-L100

Olympus virtual slide microscope (Waltham, MA). In some experiments, histological

sections were stained with toluidine blue O (Sigma Chemical, St. Louis MO) to visualize

metachromatic/basophilic granules in mast cells (MCs). Extrusion of basophilic toluidine

blue stained granules was evidence of MC degranulation (j). To quantify wound

thickness and nuclear size, measurements were performed on tissue sections using the

OlyVIA 2.7 viewer software (Olympus). Skin sections were divided into 4 equal parts

and measurements taken perpendicular from wound edge through the dermis, to the top

surface of the hypodermis. For nuclear size, wounds were divided in half, 10 random

nuclei from each half were measured by drawing a major axis (a) and minor axis (b) through each nuclei and calculating the area of an ellipse (area = π x ½ a x ½ b). To estimate absorption of NM from the filter discs, NM was applied to 6 weighed control discs and allowed to dry. The filters were then weighed again to determine filter bound NM. Twelve weighed discs treated with NM that had been applied to mice (treatment discs) were removed and dried. These filters were also weighed again to determine filter bound NM post-exposure. NM absorbed was based on the difference in the weight of NM on control discs and treatment discs. In these experiments, control discs were found to contain 3.93 ± 0.35 mg NM (mean ± SD, n = 6) while treatment discs contained 3.18 ± 0.37 mg NM (mean ± SD, n = 12). Differences in NM weight between control and treatment discs was 0.75 mg, thus approximately 20% of the NM applied to the skin was absorbed (~4 µmol or ~0.14 µmol NM/mm^2 of the filters discs).

Immunostaining

For immunohistochemistry, tissue sections (6 µm) were deparaffinized, and blocked with 25%-100% normal goat serum (Invitrogen, Grand Island, NY) at room temperature for 2 hours. Sections were then incubated overnight at 4°C with rabbit affinity purified polyclonal antibodies against phosphorylated histone 2A.X (phospho-H2A.X; Ser139, Cell Signaling, 1:50, Boston, MA), cyclooxygenase-2 (COX-2, Abcam, 1:200, Cambridge, MA), inducible nitric oxide synthase (iNOS, Abcam, 1:150), proliferating cell nuclear antigen (PCNA, Abcam, 1:500), or control rabbit IgG (Prosci, Atlanta, GA). After washing, the sections were incubated at room temperature for 30 minutes with biotinylated goat anti-rabbit secondary antibody (Vector Labs, Burlingame, CA). Antibody binding was visualized using a diaminobenzidine (DAB) Peroxidase Substrate Kit (Vector Labs).

Statistical analysis

Data are presented as mean ± SD (n = 6). A two-way analysis of variance was used to assess statistical significance (p ≤ 0.05).

2.3 Results

Effects of NM on mouse skin

Gross examination of the tissue revealed development of an indurated crusty wound 3 days post-NM exposure **(Fig. 2.2; B)**. Histologically, control skin consisted of a relatively thin epidermis 2-3 cell layers thick, with a contiguous stratum corneum (SC) **(Fig. 2.3; *left panels*)**. Loss of the SC was evident 1-2 days post-NM, along with an inflammatory cell infiltrate **(Fig. 2.3; *left panels*)**. Two-three days post-NM, an eschar developed over the wound site, accompanied by a general loss of dermal appendages including sebaceous glands and hair follicles. This was associated with an increase in wound and epidermal thickness **(Fig. 2.4),** as well as an increase in nuclear size within the thickened neo-epidermis **(Fig. 2.5)**. A thickened hyperplastic wound persisted in the skin 3-5 days post-NM. At this time, the eschar sloughed off leaving an acanthotic epidermis **(Fig. 2.3; *left panels*)**. Trichrome staining showed that NM exposure resulted in collagen deposition in the papillary dermis within 2 days **(Fig. 2.6; *left panels*)**. Three to four days post-NM, hemorrhage was evident within the thickened reticular dermis with hyperkeratosis superior to the hyperplastic epidermis. Three-five days post-NM, epidermal hyperplasia was also observed **(Fig. 2.6; *left panels*)**. After 5 days, hyperkeratosis was still evident, along with increased collagen deposition in both the reticular and papillary dermis **(Fig. 2.6; *left panels*)**.

As a bifunctional alkylating agent, NM is known to induce double strand DNA breaks (Clingen *et al.*, 2008). Phosphorylation of histone H2A.X, a variant of histone H2A, creates a recognition domain critical for DNA repair and is a marker of DNA damage

(Jowsey *et al.*, 2009; Mah *et al.*, 2010). Little or no phospho-H2A.X was evident in control skin **(Fig. 2.7;** *left panels***)**. NM caused a marked increase in phospho-H2A.X expression in the nuclei of basal and suprabasal cells of the interfollicular epidermis and the outer root sheath of hair follicles within 1-3 days **(Fig. 2.7;** *left panels***)**. Two-three days post-NM, phospho-H2A.X was also evident in infiltrating inflammatory cells beneath the eschar extending into the underlying dermis **(Fig. 2.7;** *left panels***)**. Interestingly, phospho-H2A.X persisted in the skin, primarily in the basal and suprabasal cells of the neo-epidermis, for at least 5 days post-NM **(Fig. 2.7;** *left panels***)**.

Nitric oxide is a reactive proinflammatory mediator generated in skin cells via an inducible isoform of nitric oxide synthase (iNOS) (Cals-Grierson *et al.*, 2004; Heck *et al.*, 1992). In control skin, iNOS expression was only noted in sebaceous glands **(Fig. 2.8)**; 1-2 days following NM, iNOS was evident in interfollicular epidermis and outer root sheath cells **(Fig. 2.8;** *left panels***)**. After 3-5 days, iNOS appeared in both the hyperplastic neo-epidermis and outer root sheath cells **(Fig. 2.8;** *left panels***)**. COX-2 is an enzyme that generates pro-inflammatory prostaglandins (Lee *et al.*, 2003). Low level COX-2 expression was detected in basal cells of the epidermis, outer root sheath cells and sebaceous glands in control tissue **(Fig. 2.9)**. COX-2 increased in basal cells and dermal inflammatory cells 1-2 days post-NM **(Fig. 2.9;** *left panels***)**. After 2 days, COX-2 expression was also increased in the epidermis and inflammatory cell infiltrate at the wound edge **(Fig. 2.9;** *left panels***)**. Three-five days post-NM, COX-2 was evident in the hyperplastic neo-epidermis **(Fig. 2.9;** *left panels***)**.

Evidence suggests that MCs in the skin play a role in the release of mediators important in inflammation and wound repair (Joseph*, et al.*, 2011; Tewari-Singh *et al.*, 2009). In control skin MCs were identified in the dermis, adjacent to dermal appendages and at the dermal/epidermal (D/E) junction **(Fig. 2.10;** *upper panels***)**. Approximately 23-36%

of the MCs were found to be degranulated. NM treatment had no effect on the number of MCs in the skin at the D/E junction **(Fig. 2.10;** *left graph***)**. However, a marked increase in degranulated MCs (50-75%) was noted after NM treatment **(Fig. 2.10;** *right graph***)**. PCNA, a marker of cellular proliferation and wound repair (Moldovan *et al.*, 2007; Park *et al.*, 2015) was expressed in basal cells in control mouse skin **(Fig. 2.11)**. NM treatment resulted in increased expression of PCNA in basal keratinocytes, as well as in inflammatory cells in the dermis within 1 day **(Fig. 2.11;** *left panels***)**. Two-three days post-NM, PCNA was detected in infiltrating inflammatory cells beneath the eschar at the D/E junction; after 4-5 days, PCNA expression was evident within basal keratinocyte nuclei of the neo-epidermis **(Fig. 2.11;** *left panels***)**.

Effects of AIDNX on NM-induced skin damage and inflammation

Treatment of mice with AIDNX beginning one hour after NM was found to mitigate tissue damage; thus, 1-3 days post-NM, the size and magnitude of the wound was reduced, along with inflammation **(Fig. 2.2; B & Fig. 2.3;** *right panels***)**. AIDNX also prevented the formation of an eschar and decreased overall wound thickness, epidermal hyperplasia and nuclear enlargement **(Fig. 2.3;** *right panels***, & Figs. 2.4-2.5)**. Additionally, AIDNX prevented the loss of sebaceous glands, as well as collagen deposition within both the reticular and papillary dermis, and hyperkeratosis and hemorrhage within the dermis **(Fig. 2.6;** *right panels***)**. This was associated with a marked reduction in iNOS and COX-2 expression as well as MC degranulation **(Figs. 2.8-2.9;** *right panels* **& Fig. 2.10)**. In contrast, AIDNX had no effect on PCNA expression in basal keratinocytes **(Fig. 2.11;** *right panels***)**, or on NM-induced expression of phospho-H2A.X **(Fig. 2.7;** *right panels***)**.

2.4 Discussion

Using a newly developed modified cutaneous patch test model, we characterized the progression of injury and wound healing on the dorsal skin of mice following NM exposure. Initially, an inflammatory response was evident which included edema and leukocyte infiltration. This was associated with alterations in skin structure including degradation of the SC, hyperkeratosis and acanthosis, along with increased collagen deposition and hemorrhage within the dermis followed by the formation of an eschar. Subsequently, increased proliferation of keratinocytes was observed at the wound margins, which extended under the eschar initiating the formation of a neo-epidermis. This generated a hyperplastic epidermis which replaced the eschar during the wound healing process. These data are consistent with earlier findings on the dermal responses of mice to SM, as well as NM (Au *et al.*, 2015; Casillas*, et al.*, 2000; Joseph*, et al.*, 2011; Smith *et al.*, 1997; Wormser*, et al.*, 2002). However, in earlier studies NM was applied to the dorsal skin in large volumes of either acetone or PBS over wide areas which limited the ability to evaluate candidate therapeutics. Our studies showing that NM-induced skin injury can be localized is important, not only for characterizing the wound response, but also for quantifying the efficacy of potential mustard countermeasures. NM is known to damage DNA causing both single (SSB) and double strand (DSB) breaks (Clingen*, et al.*, 2008). Excessive DNA damage can suppress keratinocyte proliferation resulting in persistent tissue injury (Barnes *et al.*, 2010; Inturi*, et al.*, 2014; Shahin *et al.*, 2001). Phosphorylation of the histone H2A variant, H2A.X, which recruits DNA damage response proteins, is critical for the repair of DNA DSBs (Mah*, et al.*, 2010; Scully *et al.*, 2013). Consistent with previous findings, we found that NM caused a rapid increase in phospho-H2A.X in the nuclei of basal and supra-basal cells of the interfollicular epidermis and the outer root sheath of hair follicles, presumably

a response to DNA damage. Two-three days post-NM, phospho-H2A.X was also evident in infiltrating neutrophils and macrophages, which are known to undergo apoptosis. High molecular weight DNA fragmentation occurs during apoptosis and this is associated with the phosphorylation of H2A.X (Rogakou *et al.*, 2000). Of interest were our findings that phospho-H2A.X persisted in basal cells of the neo-epidermis for at least 5 days post-NM. This suggests that despite extensive keratinocyte proliferation, DNA damage persists, which may contribute to aberrant or delayed wound repair. In this regard, SM has been shown to prolong wound healing in human skin (Ghabili*, et al.*, 2010; Rice, 2003). It is also possible that phospho-H2A.X is generated during DNA replication, and it may be that rapidly dividing/differentiating keratinocytes express this modified histone during the wound healing process (Mejia-Ramirez *et al.*, 2015; Sharma *et al.*, 2012; Williams *et al.*, 2010). iNOS and COX-2, are important in generating cytotoxic pro-inflammatory mediators in the skin (Lee*, et al.*, 2003; Moncada, 1999). Constitutive expression of both enzymes was noted in sebocytes of control skin, which is consistent with a role of reactive nitrogen species and eicosanoids generated from iNOS and COX-2, respectively, in regulating sebaceous gland function including lipid biosynthesis (Alestas *et al.*, 2006). Low constitutive levels of COX-2 were also noted in basal cells of the epidermis and outer root sheath cells in hair follicles in control skin where it also likely functions in epidermal homeostasis (Lee*, et al.*, 2003; Mitchell *et al.*, 1995; Williams *et al.*, 1999). NM exposure resulted in upregulation of iNOS and COX-2 in basal and suprabasal cells after 1-3 days. Increases in COX-2 expression are consistent with previous findings that SM, and the related half mustard, 2-chloroethyl ethyl sulfide (CEES), stimulate the release of prostaglandins from human and mouse keratinocytes, and that in mouse skin, SM-induced injury is associated with increased COX-2 (Black *et al.*, 2010; Joseph*, et al.*, 2011; Lefkowitz *et al.*, 2002). While sebocytes continued to express iNOS and COX-2 for 1 day post-NM, subsequently they

degenerated. The contribution of iNOS- and COX-2-derived mediators to sebaceous gland degeneration following mustard exposure remains to be determined. Four-five days post-NM, iNOS and COX-2 were localized throughout the hyperplastic neo-epidermis. These data are consistent with earlier findings that iNOS is upregulated in mouse skin after exposure to CEES (Jain *et al.*, 2014). Early increases in COX-2 and the generation of eicosanoids in the skin are thought to be important in initiating inflammation (Lefkowitz*, et al.*, 2002; Vane *et al.*, 1994). This is supported by findings that COX-2 inhibitors reduce SM induced inflammation in the mouse ear vesicant model (MEVM), and that SM-induced inflammation is reduced in COX-2 deficient mice (Casillas*, et al.*, 2000; Wormser *et al.*, 2004). Eicosanoids have been reported to stimulate keratinocyte growth, and it may be that elevated COX-2 in hyperplastic neo-epidermis is important in wound repair (Lee*, et al.*, 2003; Nyska *et al.*, 2001; Pentland *et al.*, 1986). This is supported by findings that the initial stages of acute inflammation in a full thickness incisional model of wound healing in mice are associated with the generation of proinflammatory prostaglandin PGE2, while wound repair is associated with production of anti-inflammatory prostaglandin PGD2 and its metabolites (Kapoor *et al.*, 2007). Our observation that iNOS is increased during wound healing are consistent with earlier studies showing that proliferating keratinocytes strongly express iNOS (Frank *et al.*, 2002; Jain*, et al.*, 2014). Findings that wound healing is also reduced in mice treated with iNOS inhibitors and in iNOS-deficient mice are in accord with the notion that nitric oxide contributes to the regulation of wound healing (Au*, et al.*, 2015; Frank*, et al.*, 2002; Heck*, et al.*, 1992). This may be due to nitric oxide-induced stimulation of growth factor and cytokine release by keratinocytes (Frank*, et al.*, 2002).

Degranulation of MCs is associated with the release of mediators important in inflammation and wound repair including histamine, cytokines, growth factors,

chemokines and bioactive lipids (Rao *et al.*, 2008; Shiota *et al.*, 2010; Weller *et al.*, 2006). MCs have been identified in the dermis, particularly in areas surrounding dermal appendages and at the basement membrane (Joseph*, et al.*, 2011; Weller*, et al.*, 2006). We found that NM induced injury in mouse skin is associated with significant and persistent MC degranulation without increases in the number of MCs in the tissue. Thus, whereas in control mouse skin only 23-36% of MCs were degranulated, 50-85% were degranulated after NM treatment for at least 5 days. This may contribute to propagating the inflammatory response to NM-induced injury. The fact that degranulated MCs persist at the wound site is consistent with the idea that they also contribute to the resolution of inflammation and the wound healing process (Ng, 2010; Noli *et al.*, 2001; Oehmichen *et al.*, 2009). Our data are in accord with earlier studies showing both increases in numbers of MCs and MC activation in mouse skin following SM and CEES induced skin injury in hairless mice (Joseph*, et al.*, 2011; Tewari-Singh*, et al.*, 2009).

PCNA is a nuclear protein and DNA polymerase cofactor important in controlling DNA replication and repair (Moldovan*, et al.*, 2007; Park*, et al.*, 2015). PCNA was constitutively expressed in basal cells in the interfollicular epidermis and in hair follicles, consistent with the fact that proliferation of these cells is required to replace cells lost during the epidermal differentiation process. Increases in the number of cells expressing PCNA in the epidermis was evident within 1-2 days after NM exposure, during the formation of an eschar, and in the neo-epidermis and hyperplastic epidermis during wound healing. These data are reflective of keratinocyte proliferation during wound repair (Laplante *et al.*, 2001; Patel *et al.*, 2006). Similar increases in PCNA expression during epidermal wound repair have been described in mouse skin following exposure to SM (Joseph*, et al.*, 2011; Joseph *et al.*, 2014).

Recent studies from our laboratory have demonstrated that a prodrug consisting of indomethacin, which targets cyclooxygenases, and an AChE inhibitor, which targets non-neuronal cholinergic anti-inflammatory signaling is effective in reducing SM-induced mouse skin inflammation and injury (Chang, *et al.*, 2014; Young, *et al.*, 2010; Young *et al.*, 2012). It is well known that the neurotransmitter, acetylcholine is produced by epithelial cells and immune cells. In the skin, acetylcholine participates in inflammation and the control of keratinocyte proliferation and differentiation (Grando *et al.*, 1993; Schlereth *et al.*, 2006; Wessler *et al.*, 2015). The present studies show that our bifunctional drug, AIDNX, is also effective in reducing NM-induced tissue injury. Thus, AIDNX reduced inflammation and wounding, as indicated by the lack of eschar formation in NM treated skin. This was associated with decreased epidermal hyperplasia and skin thickness, number of cells expressing PCNA, and reduced numbers of degranulated MCs and expression of iNOS and COX-2. Of interest was the fact that AIDNX did not alter NM-induced DNA damage, as reflected by expression of phospho-H2A.X. NM is known to directly damage DNA; these data indicate that DNA damage is not essential for inflammation and skin injury, and that strategies designed to interfere with inflammatory signaling pathways are sufficient to mitigate, at least in part, vesicant-induced skin injury. It should be noted that the precise role of indomethacin released from AIDNX in inhibiting cyclooxygenase activity in the skin is not known. Whereas COX-2 is important in regulating inflammation, COX-1 plays a role in skin homeostasis. The effects of COX-1 inhibition on wound healing in vesicant-treated skin remain to be determined.

2.5 Conclusion

In summary, the present studies characterize a semi-occlusive patch test model employing a glass microfiber filter delivery system to evaluate skin injury induced by vesicants. This highly reproducible model allowed us to evaluate the progression of NM-

induced inflammation, expression of inflammatory proteins, tissue damage, the formation of an eschar, and wound healing. Moreover, using this model, a novel bifunctional agent, AIDNX, was shown to be effective in reducing skin inflammation and injury. In subsequent experiments this model was useful in testing the efficacy of additional bifunctional agents that may be used as potential therapeutics **(Fig. 2.12)**. These data have potential clinical relevance as this prodrug may be further developed into an effective NM and SM countermeasure (Shakarjian*, et al.*, 2010).

The structural changes in the skin induced by NM in our patch model are consistent with the pathophysiology of SM-induced skin injury in humans. These data indicate that our patch model can be used to investigate mechanisms of action of vesicants, and to screen for potential candidate therapeutics that can be used to mitigate vesicant toxicity.

Although full thickness skin studies are important in understanding vesicant induced dermal damage, the addition of epidermal isolation studies can help to identify key factors that play a role in the early damage seen following vesicant exposures.
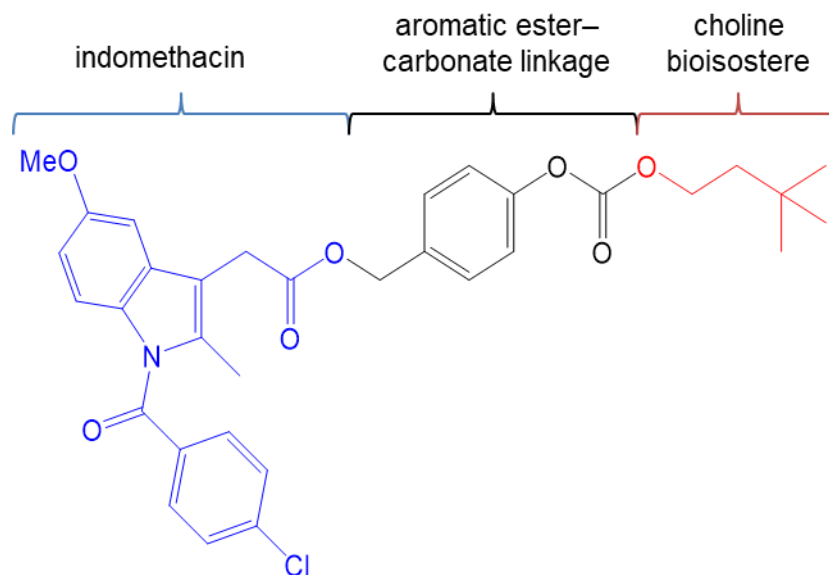
Figure 2.1 Chemical Structure of AIDNX.

AIDNX consists of an anti-inflammatory moiety, indomethacin (*blue*), and a choline bioisostere 3,3-dimethyl-1-butanol (*red*), linked via an aromatic ester-carbonate (*black*).

A.
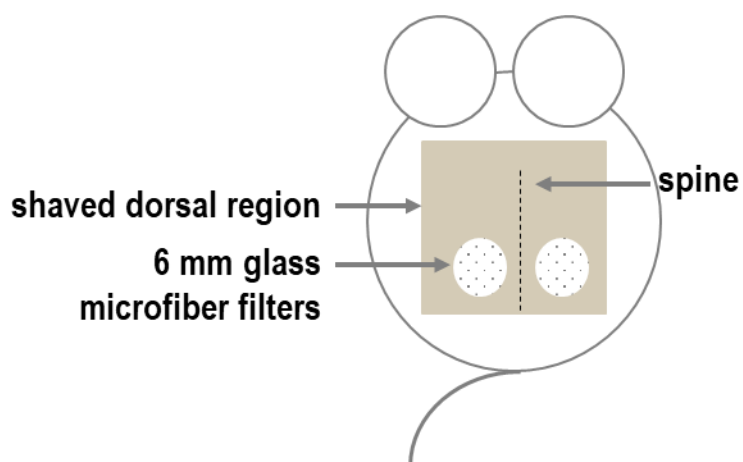
B.
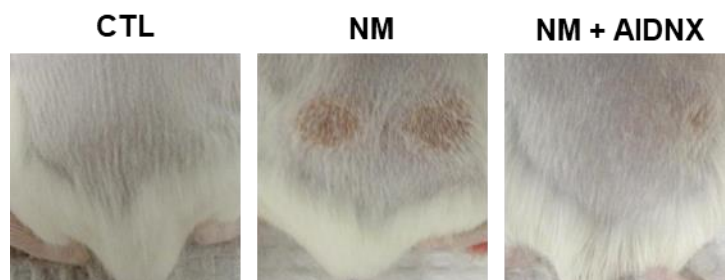
Figure 2.2 Modified Dorsal Skin Patch Model.

A. The dorsal skin of CD-1 mice was shaved and 6 mm glass microfiber filter discs were placed on the lumbar region of the skin equidistant from the spine (*upper panel*). Twenty microliters of a 1 M solution of NM in 20% deionized water/80% acetone (v/v) or vehicle control (CTL) was applied to the filters which were then covered with PARAFILM®. After 6 minutes, the filter discs were removed, and the skin analyzed for tissue damage 1-5 days post exposure. Mice were treated with AIDNX four times per day beginning 1 hour post-NM exposure. **B.** Panel shows the skin from CTL, NM and NM + AIDNX exposed skin 3 days post-NM.
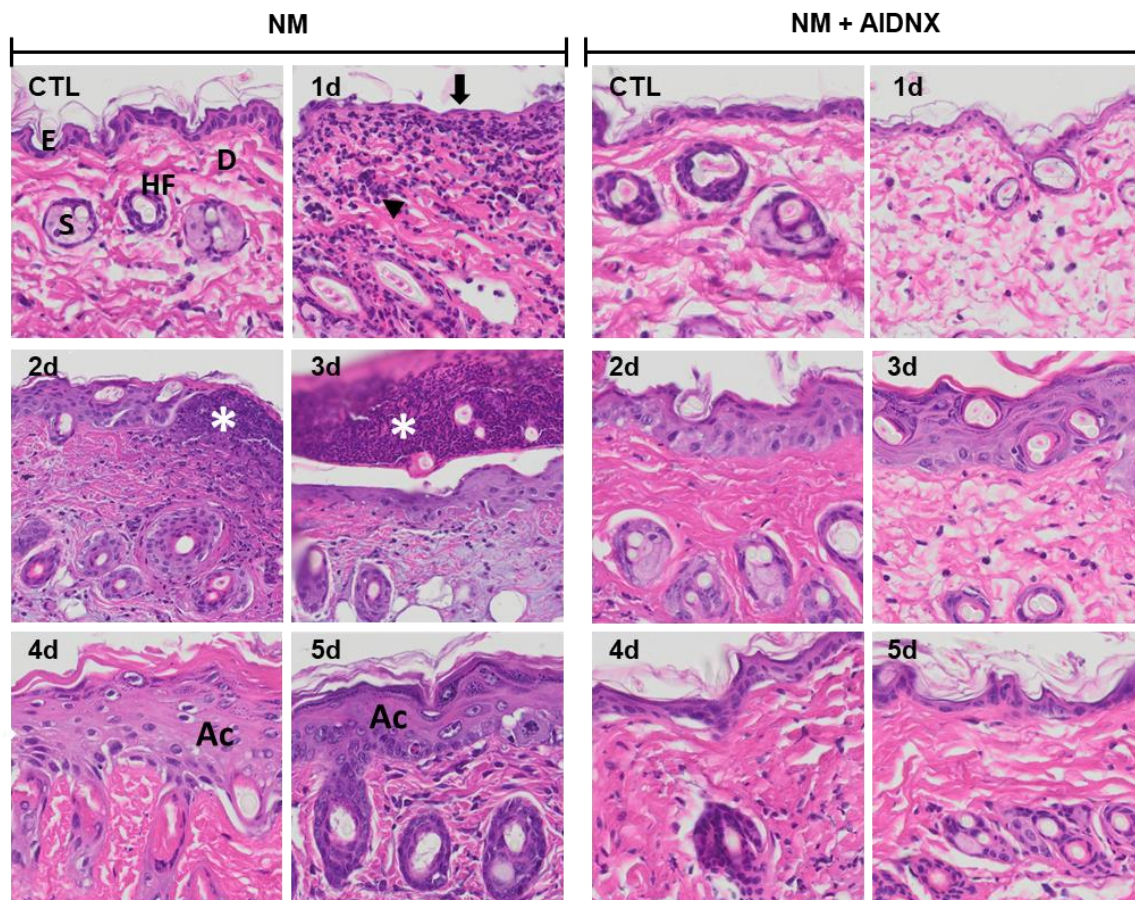
Figure 2.3 Hematoxylin and Eosin Staining of Mouse Skin Following NM Exposure.

Histological sections, prepared from control (CTL) mouse skin and mouse skin 1-5 days post-NM exposure, were stained with hematoxylin and eosin (H&E), which stains nuclei blue/black, and keratin and cytoplasm red. One representative section from 3 mice/treatment group is shown (original magnification, ×400). **E**, epidermis; **D**, dermis; **S**, sebaceous gland; **HF**, hair follicle; **asterisk**, eschar, **Ac**, acanthosis, **black arrow**, loss of SC; **black arrowhead**, inflammatory cell infiltrate. *Left panels*, mouse skin exposed to NM; *right panels*, mouse skin exposed to NM + AIDNX post-treatment.

Figure 2.4 Effects of NM on Mouse Skin Wound and Epidermal Thickness.

Histological sections, prepared from control (CTL) mouse skin and mouse skin collected 1-5 days post-NM, were stained with hematoxylin and eosin (H&E) and wound (*left graph*) and epidermal (*right graph*) thickness assessed as described in the Materials and Methods Section. Each point represents the mean ± SD (*n* = 6). *Significantly different from CTL mouse skin ($p \leq 0.05$); +significantly different from NM exposed mouse skin.
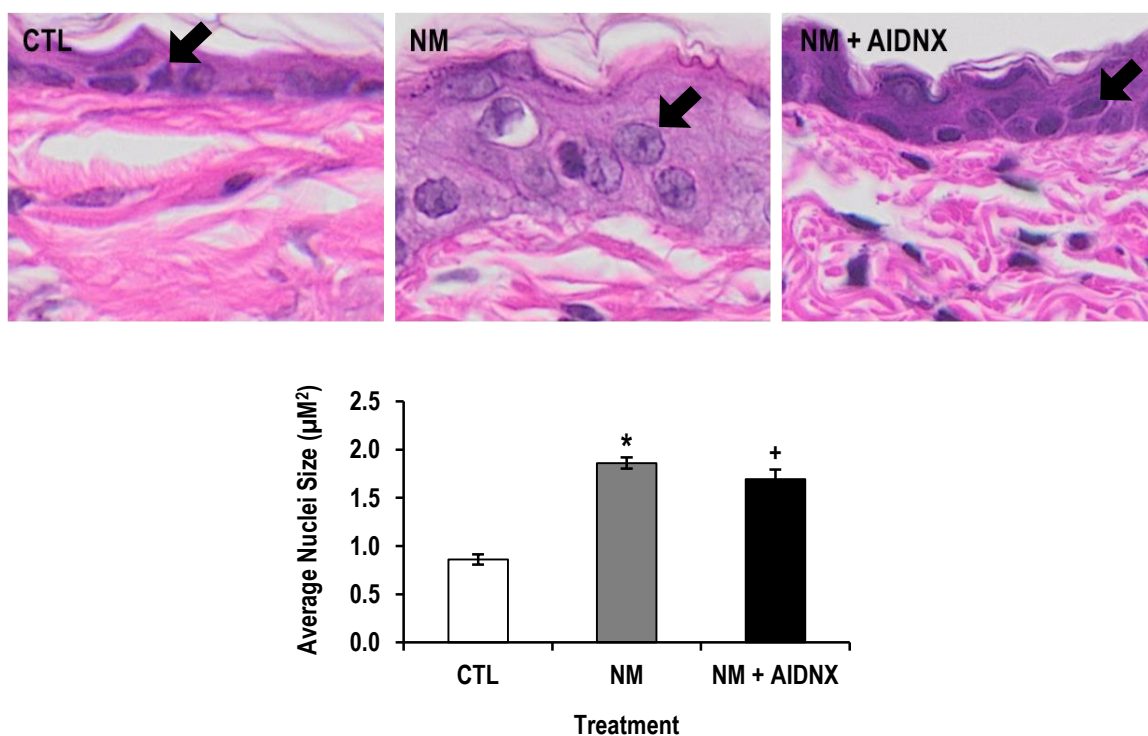
Figure 2.5 Effects of NM on Nuclear size.

A. Histological sections, prepared from control (CTL) mouse skin and mouse skin 3 days post-NM or NM + AIDNX, were stained with hematoxylin and eosin (H&E) and nuclear enlargement assessed as described in the Materials and Methods Section (original magnification, ×400). **B.** Graph represents the average nuclei size; each point represents the mean ± SD (n = 3). *Significantly different from CTL mouse skin; +significantly different from NM exposed mouse skin ($p \leq$ 0.05). **Black arrows**, nuclei.
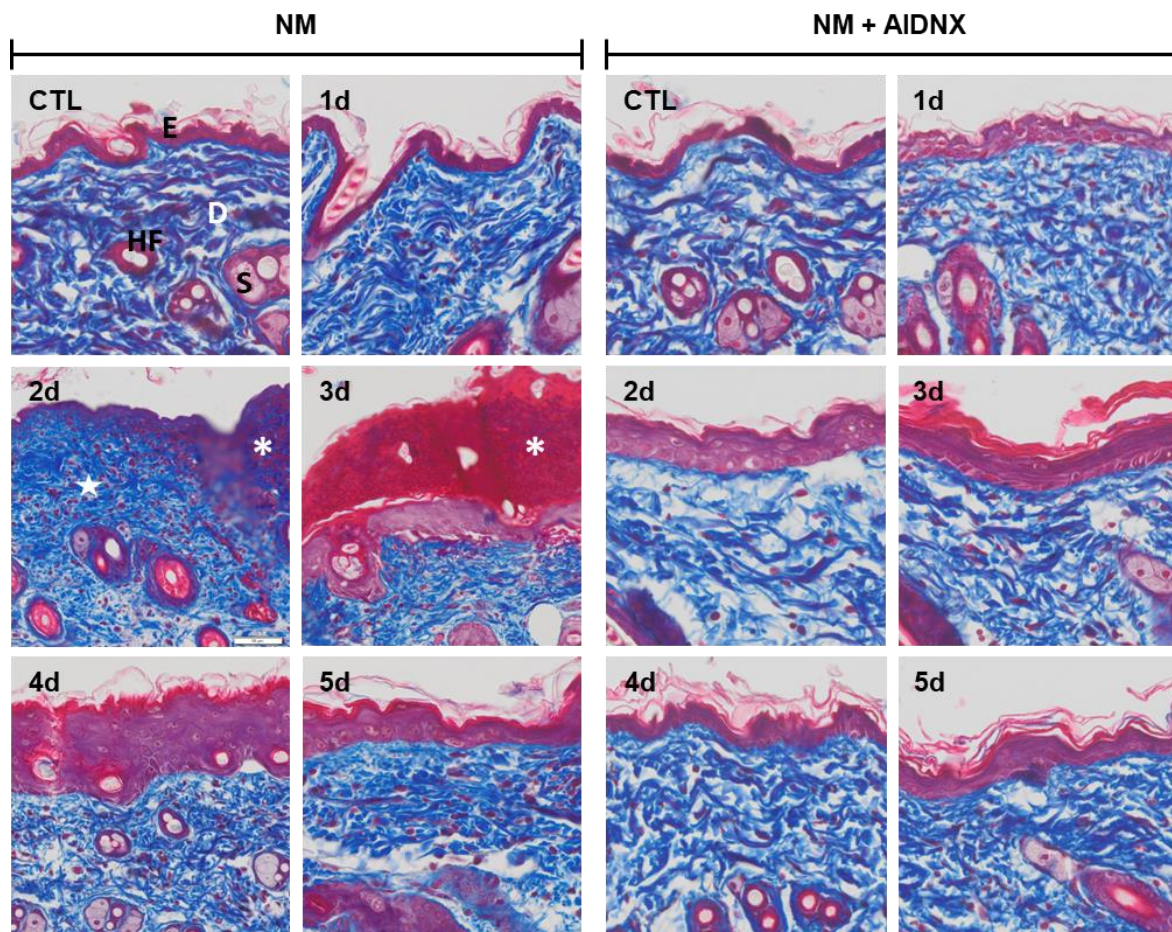
Figure 2.6 Trichrome Staining of Mouse Skin Following Exposure to NM.

Histological sections, prepared from control (CTL) mouse skin and mouse skin 1-5 days post-NM exposure, were stained with Gomori's trichrome containing hematoxylin, which stains nuclei blue/black, eosin which stains keratin and cytoplasm red, and aniline blue which stains collagen I/III royal blue. One representative section from 3 mice/treatment group is shown (original magnification, ×400). **E**, epidermis; **D**, dermis; **S**, sebaceous gland; **HF**, hair follicle; **asterisk**, eschar; **star**, collagen deposition. *Left panels*, mouse skin exposed to NM; *right panels*, mouse skin exposed to NM + AIDNX post-treatment.
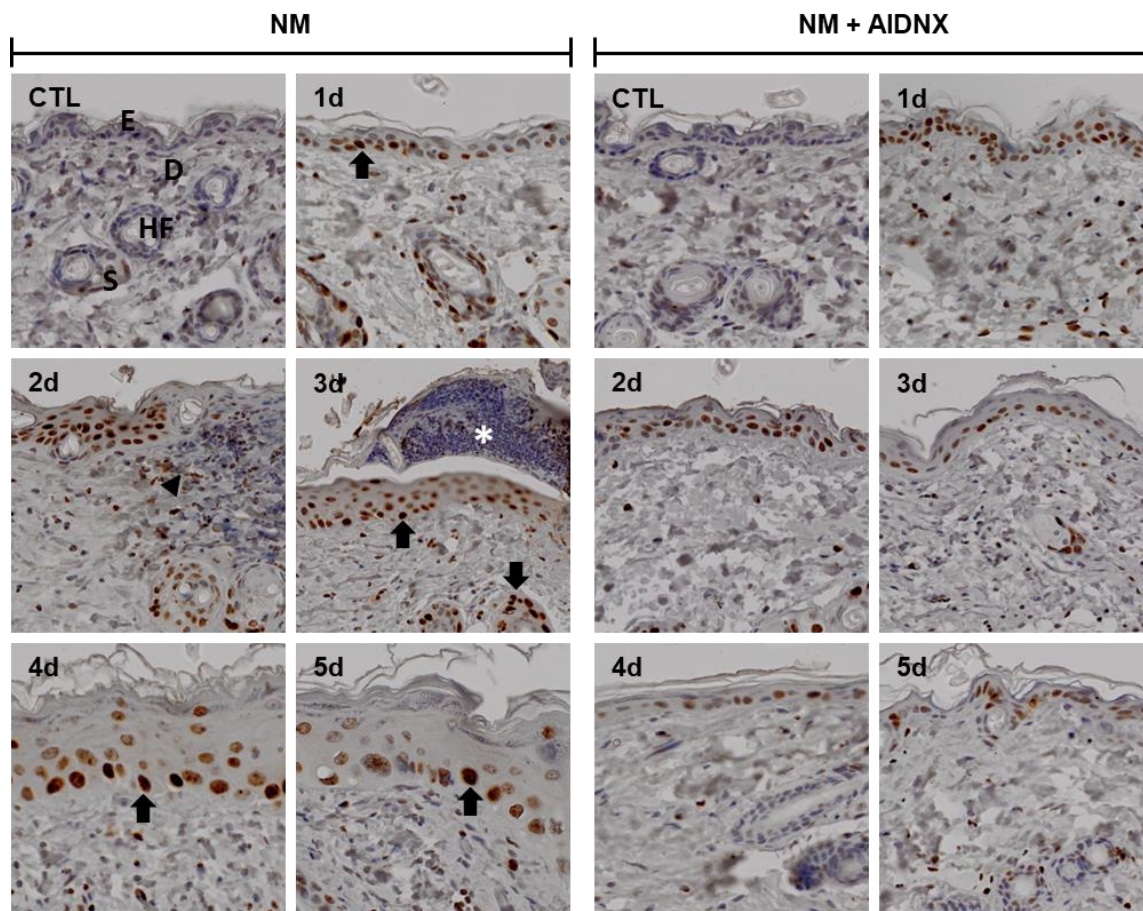
Figure 2.7 Effects of NM on Phospho-H2A.X Expression in Mouse Skin.

Histological sections, prepared from control (CTL) mouse skin and mouse skin 1-5 days post-NM exposure, were stained with an antibody to phospho-H2A.X. Antibody binding was visualized using a Vectastain Elite ABC kit. One representative section from 3 mice/treatment group is shown (original magnification, x400). **E**, epidermis; **D**, dermis; **S**, sebaceous gland; **HF**, hair follicle; **asterisk**, eschar; **black arrow**, keratinocytes expressing phospho-H2A.X; **black arrowhead**, inflammatory cell infiltrate. *Left panels*, mouse skin exposed to NM; *right panels*, mouse skin exposed to NM + AIDNX post-treatment.
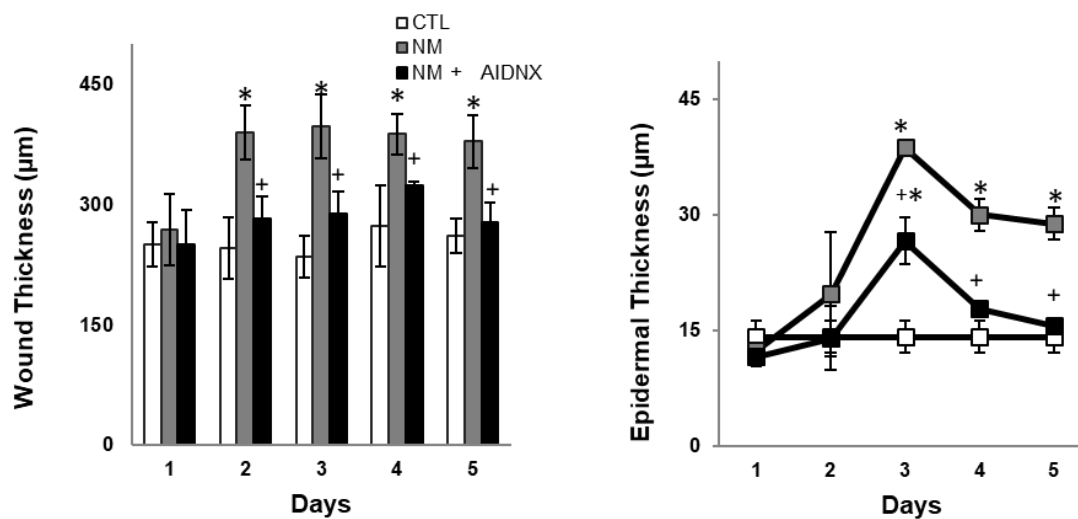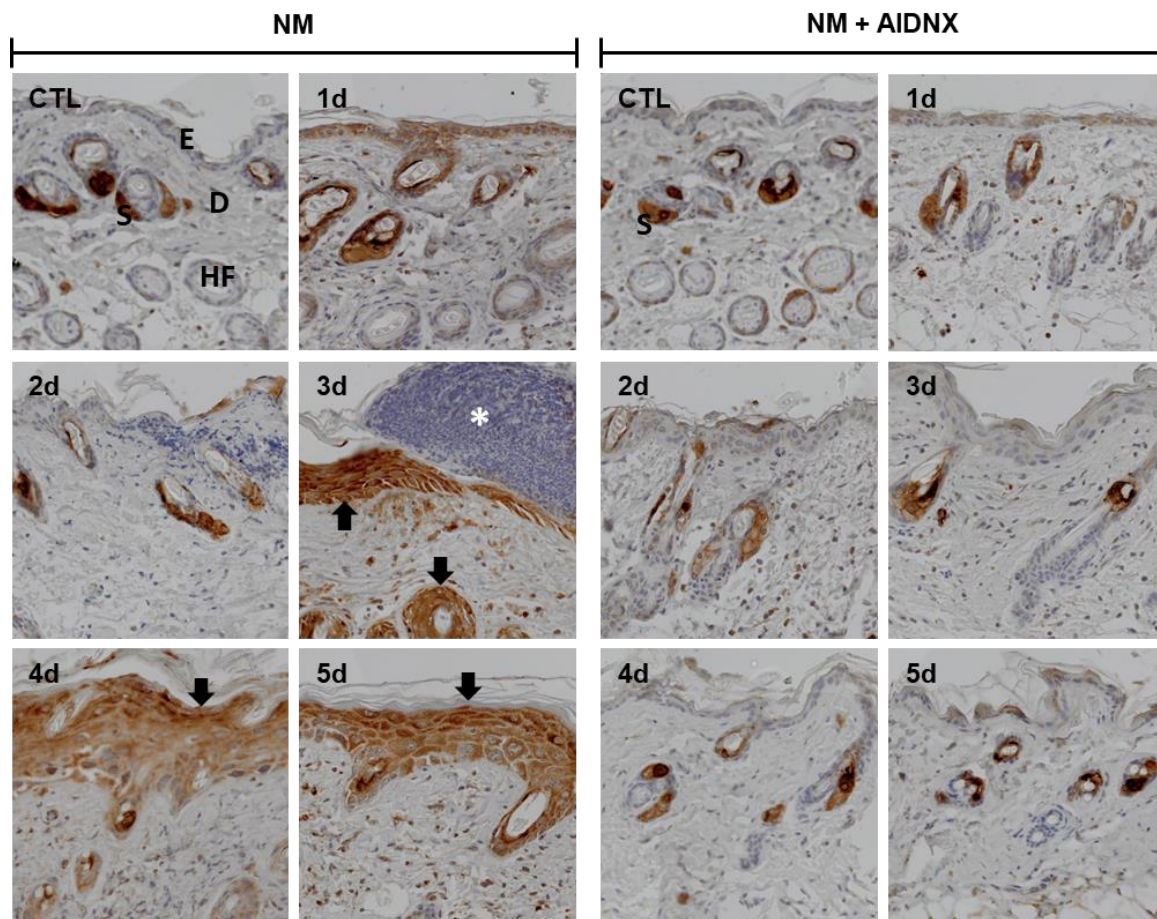
Figure 2.8 Effects of NM on iNOS Expression in Mouse Skin.

Histological sections, prepared from control (CTL) mouse skin and mouse skin 1-5 days post-NM exposure, were stained with an antibody to iNOS. Antibody binding was visualized using a Vectastain Elite ABC kit. One representative section from 3 mice/treatment group is shown (original magnification, x400). **E**, epidermis; **D**, dermis; **S**, sebaceous gland; **HF**, hair follicle; **asterisk**, eschar; **black arrows**, keratinocyte expression of iNOS. *Left panels*, mouse skin exposed to NM; *right panels*, mouse skin exposed to NM + AIDNX post-treatment.
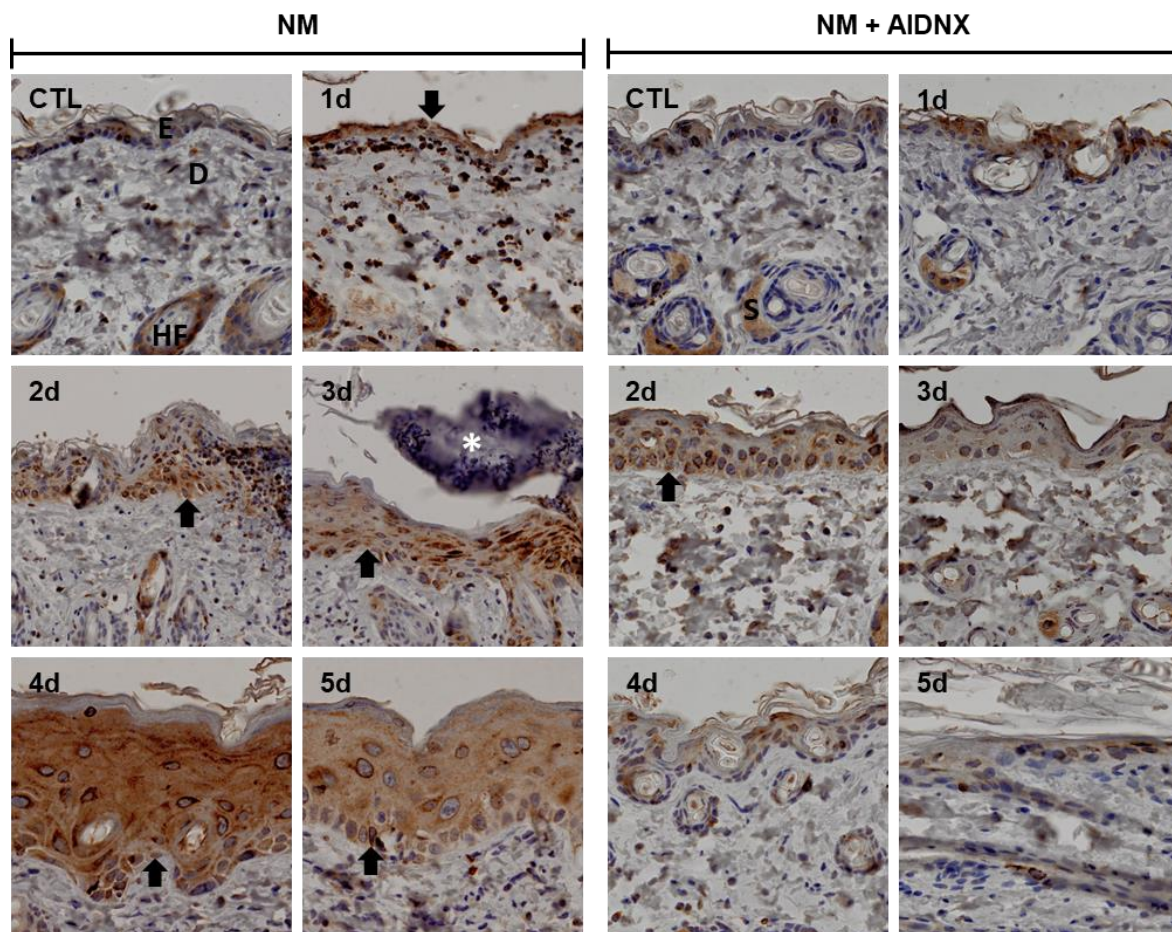
Figure 2.9 Effects of NM on COX-2 Expression in Mouse Skin.

Histological sections, prepared from control (CTL) mouse skin and mouse skin 1-5 days post-NM exposure, were stained with an antibody to COX-2. Antibody binding was visualized using a Vectastain Elite ABC kit. One representative section from 3 mice/treatment group is shown (original magnification, ×400). **E**, epidermis; **D**, dermis; **S**, sebaceous gland; **HF**, hair follicle; **asterisk**, eschar; **black arrows**, keratinocyte expression of COX-2. *Left panels*, mouse skin exposed to NM; *right panels*, mouse skin exposed to NM + AIDNX post-treatment.

A.
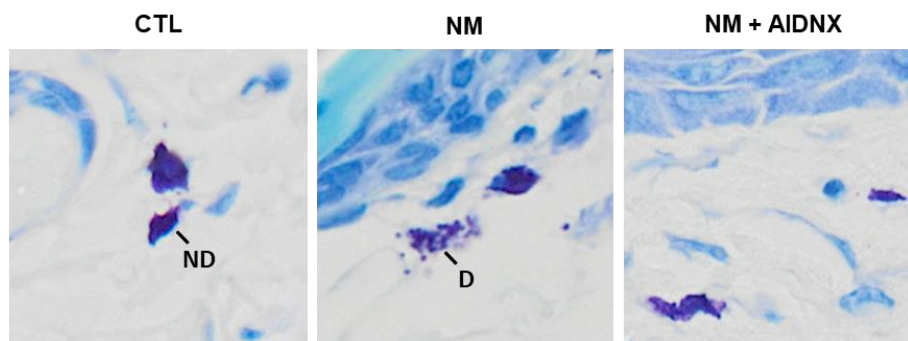
B.
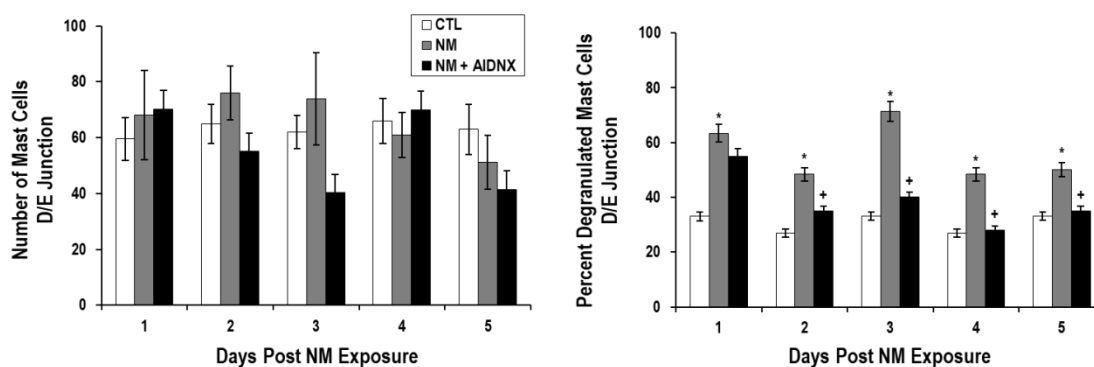
Figure 2.10 Effects of NM on Mast Cell Degranulation.

A. Histologic sections prepared from control (CTL) mouse skin and mouse skin 3 days post-NM or NM + AIDNX were stained for mast cells (MCs) using toluidine blue (original magnification, ×400). Insets show intact and degranulated MCs in CTL skin and NM treated skin; **ND**, no degranulation; **D**, degranulation. **B.** Shows the number of MCs at the D/E junction in CTL, NM and NM + AIDNX treated skin *(left graph)* and the percentage of MCs that were degranulated *(right graph)*. Each bar is the mean ± SD (*n* = 3) of 10 fields at 40x magnification. *Significantly different from CTL ($p \leq 0.05$); +significantly different from NM treatment.
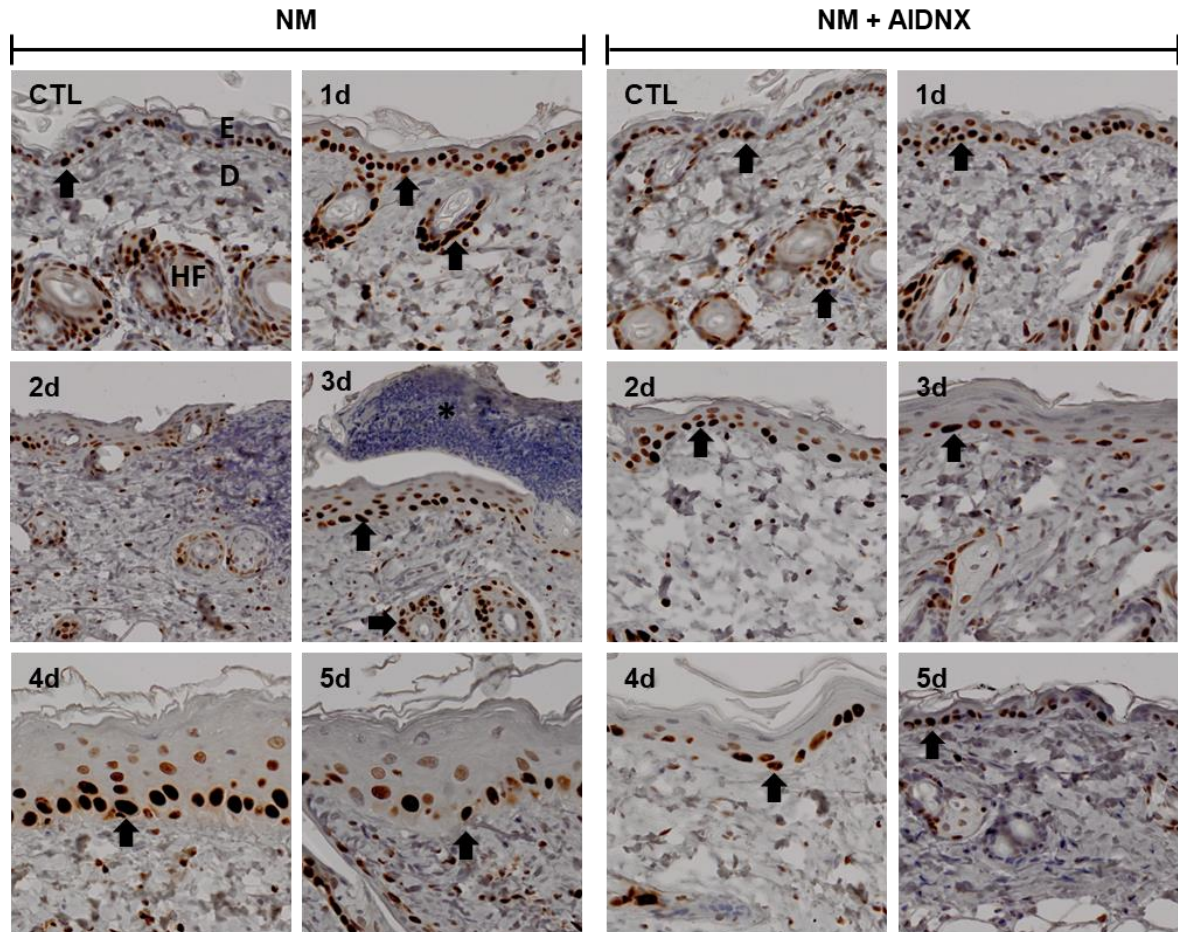
Figure 2.11 Effects of NM on PCNA Expression in Mouse Skin.

Histological sections, prepared from control (CTL) skin and skin 1-5 days post-NM, were stained with an antibody to PCNA. Antibody binding was visualized using a Vectastain Elite ABC kit (original magnification, x400). One representative section from 3 mice/treatment group is shown. **E**, epidermis; **D**, dermis; **HF**, hair follicle; **asterisk**, eschar; **black arrows**, keratinocyte expression of PCNA. *Left panels*, mouse skin treated with NM; *right panels*, mouse skin treated with NM + AIDNX post-treatment.
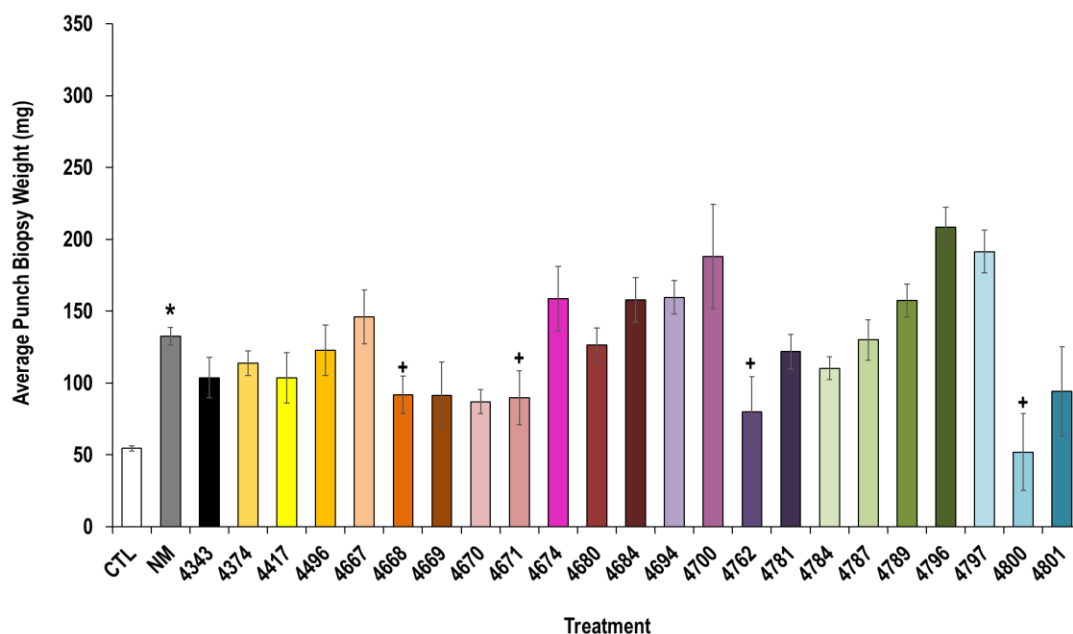
Figure 2.12 Effects of Various Multi-Functional Anti-Inflammatory Combination Drugs on NM Induced Skin Damage.

Punch biopsies from control (CTL) mouse skin and mouse skin 3 days post-NM exposure or NM + NDH compounds were weighed to assess edema. NDH compounds: Olvanils: 4343, 4417, 4496; NSAIDs: 4374, 4496; Caffeic acids: 4667, 4668, 4669, 4670, 4671, 4684; Flavanoids: 4674; Dodecyl Carbamates: 4680; Terpenes: 4694; Ferulic acids: 4700; N-As: 4762, 4781, 4784, 4787, 4789, 4796, 4797, 4800; Polyamines: 4801. All NDH compounds were received from Dr. Ned Heindel at Lehigh University. Each point represents the mean ± SD (n = 3-6). *Significantly different from CTL mouse skin; +significantly different from NM exposed mouse skin ($p \leq 0.05$).

CHAPTER 3: TEMPORAL EVENTS IN MOUSE EPIDERMIS FOLLOWING EXPOSURE TO NITROGEN MUSTARD

Gabriella Wahler[a], Debra L. Laskin[a,b], Diane E. Heck[c], Jeffrey D. Laskin[a,b,d,e], Laurie B. Joseph[a,b]

[a] Joint Graduate Program in Toxicology, Rutgers University Graduate School of Biomedical Sciences, 170 Frelinghuysen Rd, Piscataway, NJ 08854, USA

[b] Department of Pharmacology and Toxicology, Rutgers University, 170 Frelinghuysen Rd, Piscataway, NJ 08854, USA

[c] Department of Environmental Health Science, School of Health Sciences and Practice, New York Medical College, 40 Sunshine Cottage Rd., Valhalla, NY 10595, USA

[d] School of Public Health, Rutgers University, 170 Frelinghuysen Rd, Piscataway, NJ 08854, USA

[e] Environmental and Occupational Health Sciences Institute, Rutgers University, 170 Frelinghuysen Rd, Piscataway, NJ 08854, USA

3.1 Abstract

The ability of SM to induce inflammation, edema and blistering is cause for concern. Although many studies investigating the damaging effects of SM have been conducted, the precise mechanism of SM-induced skin damage is still largely unknown. The present studies use a patch-test model to analyze early alterations in oxidative stress and DNA damage markers in isolated mouse epidermis post-exposure to the SM surrogate NM. NM (20 µmol in 80% acetone/20% water) or vehicle control was applied onto 24 mm filters affixed to the shaved dorsal skin of CD-1 mice for 6 minutes. Mice were sacrificed and epidermis removed and analyzed 0-24 hours post-NM exposure by western blot analysis and immunohistochemistry. Post-exposure, phospho-H2A.X, a marker of double strand DNA breaks was up-regulated 4-fold by 0.25 h along with the DNA damage marker phospho-p53 (pp53; 3-fold by 0.25 h). This was associated with a 3-fold increase in poly (ADP) ribose (pADPr), a polymer synthesized by enzymes necessary for DNA repair, and a 3-8 fold increase in markers of oxidative stress including hemeoxygenase-1 (HO-1), thioredoxin reductase (TrxR), an antioxidant important in cell growth and survival, proteins modified by 4-hydroxynonenal (4-HNE), a lipid peroxidation end product, and expression of 8-oxo-2'-deoxyguanosine (8-oxo-2'-dG), a product of DNA oxidation. Alterations in DNA replication and subsequent cell cycle progression were investigated following NM exposure. An upregulation (10-fold) of the nucleoside bromodeoxyuridine (BrdU) 12 hours post-NM was evident along with a decrease in the cell cycle protein cyclin D2 by 0.5-fold at 1 hour. Infiltration of macrophages, neutrophils and mast cell (MC) degranulation suggested that cytokines, chemokines and lipid mediators released post-NM exposure contributed to oxidative stress. These data indicate that NM-induced epidermal injury is associated with

oxidative stress and DNA repair. Antioxidants as well as agents that enhance DNA repair may be important countermeasures to mitigate mustard-induced epidermal injury.

Abbreviations

BCA, bicinchoninic acid; BrdU, bromodeoxyuridine; DAB, diaminobenzidine; D/E, dermal/epidermal; HO-1, hemeoxygenase-1; 4-HNE, 4-hydroxynonenal; ICLs, interstrand crosslinks; MC, mast cell; NM, nitrogen mustard (bis (2-chloroethyl) methylamine); pADPr, poly ADP ribose; phospho-H2A.X, phosphorylated histone H2A.X; pp53, phosphorylated p53; ROS, reactive oxygen species; SC, stratum corneum; SM, sulfur mustard (bis (2-chloroethyl) sulfide); TrxR, thioredoxin reductase

3.2 Introduction

NM and SM are bifunctional alkylating agents that can induce oxidative stress, DNA damage and inflammation resulting in extensive skin damage (Arck*, et al.*, 2006; Composto *et al.*, 2016; Ghabili*, et al.*, 2010; Shakarjian*, et al.*, 2010; Vogt*, et al.*, 1984). The stratum corneum (SC), the outermost layer of the skin, is crucial for the body's defense against environmental toxins. Disruptions, which occur following chemical exposures, are associated with delayed wound healing and chronic wounds (Kondo *et al.*, 2010; Sandoval *et al.*, 2007; Shakarjian*, et al.*, 2010). Despite extensive research, mechanisms underlying the chronological events of mustard induced skin injury are not clearly understood, which makes it difficult to develop effective therapies for mitigating vesicant induced skin damage. The prevalence of mustard gas exposures in the Middle East are cause for concern due to the lack of effective countermeasures (Barnard *et al.*, 2017; Murdock, 2017; Shoumali *et al.*, 2015). Further understanding the effects of mustards on the skin will help develop candidate therapeutics that can be used to mitigate toxicity.

There is evidence that oxidative stress and DNA damage are key events in vesicant induced skin damage (Inturi*, et al.*, 2014; Jain *et al.*, 2011; Joseph*, et al.*, 2011; Jowsey*, et al.*, 2009). In particular, the formation of reactive oxygen species (ROS) in response to oxidative stress is a naturally occurring intracellular metabolic process which results when the production of ROS exceeds the capacity of antioxidant defense mechanisms (Paromov *et al.*, 2007). The production of ROS is altered following vesicant exposure resulting in damage to membrane lipids, proteins, and nucleic acids (Jafari, 2007; Kumar *et al.*, 2015; Zhang *et al.*, 2017). DNA damage occurs from alkylation by vesicants causing interstrand crosslinks (ICLs) which contributes to the epithelial toxicity of both SM and NM (Debiak *et al.*, 2016; Huang *et al.*, 2013; Kehe*, et al.*, 2008; Liu *et al.*, 2016). Vesicant induced DNA damage leads to the induction of cell cycle arrest, inhibition of DNA synthesis and cell replication in turn affecting the intracellular signaling pathway, PI3K/Akt, important in regulating the cell cycle (Inturi*, et al.*, 2014; Inturi *et al.*, 2013; Liu*, et al.*, 2016). The PI3K/Akt pathway is important in the regulation of transcription, proliferation, cell growth and apoptosis (Inturi*, et al.*, 2014). *In-vitro* studies demonstrating the role of mustard agents in alterations to the PI3K/Akt pathway have shown that the DNA chain break-activated nuclear protein, Poly (ADP) Ribose Polymerase (PARP), is activated in response to vesicant exposure in keratinocytes inducing apoptosis through PI3K/Akt pathway inhibition (Debiak*, et al.*, 2016; Kehe*, et al.*, 2008; Liu*, et al.*, 2016; Yamaguchi *et al.*, 2016). To develop mechanism-based therapies it is necessary to understand cellular injury and repair in detail, for this reason the use of *in-vivo* vesicant-exposed excised epidermis was studied to uncover potential mechanisms of vesicant induced skin injury.

The patch test model, as previously described, has shown to be a successful method for localized delivery of NM forming reproducible wounds on mouse skin (Composto*, et al.*,

2016). A modified version of this patch test model **(Fig. 3.1; A)** was used in these studies to examine the effects of *in-vivo* NM on skin epithelium isolated 0-24 hours post-exposure. Examining the early chronological events following topical NM exposure will elucidate the mechanisms of NM-induced skin damage that result in prolonged inflammation, delayed wound repair, cell cycle arrest and apoptosis.

3.3 Materials and Methods

Chemicals and Reagents

Unless otherwise indicated NM (mechlorethamine HCl) and all other chemicals were purchased from Sigma-Aldrich (St. Louis, MO).

Animals and Treatments

Treatment of mouse skin with NM was previously described with some modifications (Composto*, et al.*, 2016)*.* Female CD-1 mice 8 weeks of age (Charles River Laboratories, Wilmington, MA) were anesthetized by intraperitoneal injection of ketamine (80 mg/kg) and xylazine (12 mg/kg) randomly assigned to treatment groups and housed individually. The dorsal skin of the mice was shaved and washed with deionized water. One 24 mm glass microfiber filter disc (GE Healthcare, Buckinghampshire, UK) was placed on the lumbar region of the shaved skin and adhered with acetone **(Fig. 3.1 A)**. Freshly prepared NM solution (20 µmol) in 20% deionized water/80% acetone, v/v, was then applied to the filter and immediately covered with PARAFILM® (Pechiney, Menasha, WI). All control mice received the solvent without NM. After 6 minutes, the filter disc was removed. At appropriate times post-NM exposure, mice were euthanized, skin removed, and the epidermis isolated as previously described with modifications (Sternberg, 1999). Mouse skin is removed and placed on Parafilm® on dry ice and frozen for ~3 seconds and epithelium scraped off using a scalpel blade **(Fig. 3.2)**.

Isolated epithelium was lysed in cold RIPA buffer (50 mM Tris–HCl pH 7.4, 150 mM NaCl, 1% NP-40, 0.5% deoxycholic acid and 0.1% SDS) containing protease inhibitors and sonicated twice for 7 seconds on ice. Protein concentration was determined by bicinchoninic acid (BCA) assay (Pierce Biotechnology, Rockford, IL) using a bovine serum albumin standard. In some experiment's mice were treated topically with AIDNX once immediately following exposure to determine the benefits of the anti-inflammatory agent on the early damage induced by NM. For these experiments, 40 µl of AIDNX (1% in a mixture of 49.5% lanolin and 49.5% polyethylene glycol 400 (PEG400)) or vehicle control was applied directly to the skin.

In additional studies mice were euthanized 0-24 post-NM and 12 mm full thickness biopsies of the exposure site were immediately collected using a skin punch (Acuderm Inc., Ft. Lauderdale, FL). In some experiment's mice were injected *i.p.* with 200 µl of bromodeoxyuridine (BrdU; BD Biosceinces, San Jose, CA) 2 hours prior to NM exposure to determine the effects of NM on cellular division and cell cycle arrest.

Histology & Immunohistochemistry

Punch biopsies were trimmed and stored in ice cold phosphate buffered saline (PBS) containing 3% paraformaldehyde/2% sucrose. The tissue was embedded in paraffin and 6 µm sections prepared and stained with hematoxylin and eosin (H&E) (Histopathology Core Facility, Piscataway, NJ). H&E stained tissue was scanned using a VS120-L100 Olympus virtual slide microscope (Waltham, MA). In some experiments, histological sections were stained with toluidine blue O (Sigma Chemical, St. Louis MO) to visualize metachromatic/basophilic granules in mast cells (MCs). Extrusion of basophilic toluidine blue stained granules was evidence of MC degranulation (Joseph*, et al.*, 2011). To quantify wound thickness and nuclear size, measurements were performed on tissue

sections using the OlyVIA 2.7 viewer software (Olympus). Skin sections were divided into 4 equal parts and measurements taken perpendicular from wound edge through the dermis, to the top surface of the hypodermis. For nuclear size, wounds were divided in half, 10 random nuclei from each half were measured by drawing a major axis (a) and minor axis (b) through each nucleus and calculating the area of an ellipse (area = $\pi \times \frac{1}{2} a \times \frac{1}{2} b$). For immunohistochemistry, tissue sections (6 µm) were deparaffinized, and blocked with 100% normal horse serum (Invitrogen, Grand Island, NY) at room temperature for 2 hours. Sections were then incubated overnight at 4 °C with a mouse monoclonal antibody against 8-oxo-2'-deoxyguanosine (8-oxo-2'-dG, 1:200, Abcam), or control mouse IgG (Prosci, Atlanta, GA). After washing, the sections were incubated at room temperature for 30 minutes with biotinylated horse anti-mouse secondary antibody (Vector Labs, Burlingame, CA). Antibody binding was visualized using a diaminobenzidine (DAB) Peroxidase Substrate Kit (Vector Labs).

All animals received *humane care in compliance with the Rutgers University guidelines, as outlined in the Guide for the Care and Use of Laboratory Animals published by the National Institutes of Health*.

Western Blot Analysis

Proteins were reduced and separated on a 4-15% Tris-HCl gel (BioRad Laboratories, Hercules, CA). After transferring protein to nitrocellulose (Thermo Fisher Scientific, Waltham, MA), membranes were blocked with 5% nonfat dry milk in 0.1% TPBS for 30 minutes at 37 °C. Blots were incubated with primary antibodies against cyclooxygenase-2 (COX-2, 1:1,000, Abcam, Cambridge, MA), cyclin D2 (1:1,000, Cell Signaling Technologies, Danvers, MA), hemeoxygenase-1 (HO-1, 1:1000, Enzo Life Science Inc., Burlington, NC), 4-hydroxynonenal (4-HNE, 1:1,000, R&D systems, Minneapolis, MN),

phosphorylated histone H2A.X (phospho-H2A.X, 1:1000, Cell Signaling Technologies), phosphorylated p53 (pp53, 1:1,000, Cell Signaling Technologies), poly (ADP-ribose) (pADPr, 1:500, Abcam), and thioredoxin reductase (TrxR, 1:1,000, Santa Cruz Biotechnology, Dallas, TX). β-Actin (1:1,000, Cell Signaling Technologies), Histone H4 (H4, 1:1,000, Cell Signaling Technologies), and p53 (1:1,000, Cell Signaling Technologies) were used as loading controls. Proteins were visualized using HRP-linked secondary antibodies (anti-rabbit, or anti-mouse, 1:5,000, Cell Signaling Technologies) and Luminata Forte Western HRP substrate (Millipore, Billerica, MA) which forms chemiluminescent protein-antibody complexes visualized using a Fluorchem Imager (ProteinSimple, Santa Clara, CA). Semi-quantitative analysis of protein bands was performed using ImageJ Software version 1.5.

BrdU Assay

Histological sections were deparaffinized, and blocked with 100% normal goat serum (Invitrogen, Grand Island, NY) at room temperature for 2 hours. Sections were then incubated overnight at 4 °C with rabbit affinity purified polyclonal antibody against bromodeoxyuridine (BrdU, BD Biosciences, 1:50, San Jose, CA) or control rabbit or mouse IgG (Prosci, Atlanta, GA). After washing, the sections were incubated at room temperature for 30 minutes with biotinylated goat anti-rabbit secondary antibody (Vector Labs, Burlingame, CA). Antibody binding was visualized using a DAB Peroxidase Substrate Kit (Vector Labs). Photographs were taken at 400x magnification using a VS120 Olympus microscope (Waltham, MA). Calculation of percent positive BrdU nuclei were performed on tissue sections using the OlyVIA 2.7 viewer software (Olympus).

Statistical analysis

The data are expressed as mean $\pm$ SD ($n = 3$). Comparison of the multiple treatment groups was performed using one-way analysis of variance. The result is considered significant with p-value ≤ 0.05.

3.4 Results

Effects of NM on Full Thickness Mouse Skin

Histologic examination of full thickness skin biopsies from a time course of mice topically exposed to NM was analyzed. Control skin contained a 1-2 cell layer thick epidermis, with a contiguous SC **(Fig. 3.1; B)**. No changes were observed in NM exposed skin until 12 hours post-exposure where an inflammatory cell infiltrate was noted at the dermal/epidermal (D/E) junction **(Fig. 3.1; B)**. By 24 hours epidermal hyperplasia and dermal edema were evident **(Fig. 3.1; B)**. An 83% increase in biopsy weight (edema) was observed 12 hours post-NM exposure when compared to CTL, increasing to twice the CTL weight by 24 hours **(Fig. 3.3; *upper graph*)**. Epidermal thickness was doubled by 24 hours when compared to CTL **(Fig. 3.3; *lower graph*)**.

Mast Cell Degranulation in Mouse Skin Following Exposure to NM

MC degranulation is associated with the release of histamine, cytokines and growth factors, which induce inflammation and subsequent wound repair (Ng, 2010; Rao*, et al.*, 2008; Weller*, et al.*, 2006). Previous studies from our laboratory have shown an increase in MC degranulation following vesicant exposure by 24 hours (Composto*, et al.*, 2016; Joseph*, et al.*, 2018; Joseph*, et al.*, 2011). The present studies investigated MC degranulation 0-24 hours post-NM exposure. MCs were observed in the dermis, adjacent to the dermal appendages and at the D/E junction **(Fig. 3.4; A)**. In general, the number of MCs in the skin remained constant **(Fig. 3.4 B; *left graph*)**. Approximately

30-40% of MCs in control skin were degranulated; the percentage of degranulated MCs increased to 55-75%, 3-24 hours post-NM exposure **(Fig. 3.4 B; *right graph*)**. From our previous studies using SM it was determined that MC degranulation persists for at least 14 days (Joseph*, et al.*, 2018; Joseph*, et al.*, 2011), together these data indicate that NM readily increased MC degranulation, suggesting a role for MCs in both the early and late stages of vesicant induced skin injury and repair.

NM Associated DNA and Protein Damage in Mouse Epidermis is Time Dependent

DNA damage is a known consequence of exposure to vesicating agents such as NM and is associated with an increased production of inflammatory cytokines and mediators of oxidative stress (Graham *et al.*, 2005; Kehe*, et al.*, 2009; Paromov*, et al.*, 2007; Shakarjian*, et al.*, 2010; Tewari-Singh *et al.*, 2016). Because of its ability to induce DNA damage, NM is able to activate the DNA repair protein, PARP, which synthesizes the DNA-repair signal pADPr **(Liu*, et al.,* 2016)**. PARP activation and subsequent pADPr initiation can occur following activation of the PI3K-Akt pathway, an intracellular signaling element important in cell cycle regulation and apoptosis, a regulator of vesicant induced skin damage **(Aredia *et al.*, 2014; Liu*, et al.*, 2016)**.

In the current studies we analyzed downstream targets of the PI3K/Akt signaling pathway following NM exposure in isolated mouse skin epidermis over 24 hour time course. NM was found to increase the expression of pADPr by 8-fold 0.75 hours post-exposure **(Fig. 3.5)**. The pADPr response to NM was found to be biphasic, reaching a peak at 3 and 24 hours **(Fig. 3.5)**. NM was also found to induce biphasic response patterns in pp53 expression, a tumor suppressor and cell cycle regulator, along with the cell cycle protein cyclin D2 (Meyyappan *et al.*, 1998; Wang *et al.*, 2012). NM induced a 3-fold increase in pp53 at 0.25 hours and 1 hour increasing to 3.5-fold at 2 hours. Interestingly, cyclin D2 was down regulated 1 hour by 0.5-fold, increasing to control

levels by 2 hours **(Fig. 3.5)**. Additionally, the expression of pp53 decreased to control levels at 3 hours but was induced again by 2.5-fold at 6 hours when compared to control **(Fig. 3.5)**. Expression of the double strand DNA break marker phospho-H2A.X was upregulated 4-fold by 0.25 hours increasing 6-8-fold by 3-12 hours **(Fig. 3.5)**. In addition, nuclear expression of BrdU increased 12 hours post-NM exposure (a 10-fold increase in the percent of BrdU positive nuclei) indicating an increase in DNA replication. The percent of BrdU positive nuclei decreased by 24 hours to 5-fold indicating a decrease in DNA replication **(Fig. 3.6; B)**.

NM Induced 4-HNE Adduct Formation and Oxidative Stress in Mouse Epidermis

In the current studies oxidative stress in response to NM exposure in isolated epidermis was investigated. Due to increased stress events quantities of the lipid peroxidation end product, 4-HNE, are higher during oxidative stress. Western blot analysis of isolated epidermis revealed a 3-4 fold increase in 4-HNE protein adducts by 0.25 hours following exposure **(Fig. 3.7)**. In control epidermis, low levels of 4-HNE-protein adducts were detected **(Fig. 3.7)**. NM induced 4-HNE-protein adducts were associated with a marked increase in the expression of the antioxidant HO-1 (4.5 fold by 0.25 hours), a stress protein important in protecting the skin from oxidative stress induced injury (Gozzelino *et al.*, 2010; Park *et al.*, 2017). Like the DNA damage markers, 4-HNE elicited a biphasic response indicating a persistence of NM within the epidermis throughout the duration of the experiment **(Fig. 3.7)**. Concordant with 4-HNE and HO-1, TrxR, an antioxidant defense enzyme, was upregulated 8-fold within 0.25 hours following NM exposure **(Fig. 3.7)**. Basal cells of the epidermis expressing 8-oxo-2'-dG, an oxidized nucleoside of DNA and commonly studied DNA lesion following oxidative stress, was upregulated 0.25-24 hours post-exposure **(Fig. 3.8)** (Akasaka *et al.*, 2010; Emanuele *et al.*, 2014).

AIDNX Post NM Treatment Resulted in Reduced Epidermal Damage

To determine the role of AIDNX in resolving and reducing epidermal damage additional studies analyzed the effects of a single treatment of AIDNX applied to the dorsal region of the mouse immediately following exposure to NM. These studies observed the effects of the bifunctional NSAID on early NM damage. Interestingly, the addition of the one-time treatment with AIDNX resulted in a significant decrease in skin thickness, and MC degranulation (**Figs. 3.9 & 3.10)**. In addition, post-treatment with AIDNX resulted in a significant decrease in DNA damage, lipid peroxidation, and oxidative stress markers 0.25 hours post-NM **(Fig. 3.11)**. Although this decrease was significant, damage was still noted at later time points in the treatment group **(Fig. 3.11)**. This indicates the ability of AIDNX to diminish skin damage following NM exposure. This one-time treatment of AIDNX may not however, be enough to combat the damaging effects of the vesicating agent.

3.5 Discussion

Due to the latent nature of vesicant induced skin injury, studies investigating its effects have focused on lesions 24 hours following exposure. Previous i*n-vitro* studies and *in-vivo* skin models revealed inflammation, oxidative stress and DNA damage as the major contributors to vesicant induced skin injury while the cellular mechanisms affected are still poorly understood (Inturi*, et al.*, 2014; Kumar*, et al.*, 2015; Povirk *et al.*, 1994). Early events in NM induced skin injury need to be elucidated to uncover the mechanisms involved in skin damage following vesicant exposures for the study and development of therapeutics. Our laboratory has initiated characterization of the effects of *in-vivo* exposure of epidermis to NM followed by removal of the exposed epidermis isolated beginning 0.25 hours post-exposure. Using a version of our modified cutaneous patch test model Isolated full thickness skin revealed an inflammatory response 12 hours post-

exposure which included leukocyte infiltration and edema associated with alterations in skin structure (Composto et al., 2016). Previous studies from our laboratory have found increases in enzymes generating pro-inflammatory mediators including COX-2 and iNOS following vesicant exposures (Joseph, *et al.*, 2011). These findings correlated with extensive MC degranulation observed in the pathogenic response to vesicating agents (Joseph, *et al.*, 2011). MCs are known to release a variety of mediators that control hemostasis and inflammation during the early stages of tissue injury (Rao, *et al.*, 2008; Shiota, *et al.*, 2010; Weller, *et al.*, 2006). The observation that degranulated MCs were found as early as 3 hours following NM exposure in isolated mouse skin epidermis and persisted at the wound site throughout the time course demonstrate their importance in both the acute inflammatory phase as well as the wound healing process following exposure to vesicating agents.

Oxidative stress was observed as an initial event following exposure to NM. As a highly reactive aldehyde 4-HNE, in response to increased levels of ROS, induces cytotoxicity and modifies cellular components forming stable protein adducts with nucleophilic sites in both DNA and the side chains of histidine, lysine, and cysteine (Gutteridge, 1995; Zheng et al., 2013). The observed upregulation of 4-HNE at 0.25 hours followed by HO-1 at 12 hours post-exposure is consistent with earlier findings which showed that stress resulting from the reaction of lipid peroxidation products with cellular components upregulates HO-1 (Huang *et al.*, 2012; Zheng *et al.*, 2014; Zheng, *et al.*, 2013). Future studies will identify specific proteins modified by 4-HNE in the isolated epidermis and determine their role in mediating adaptive responses following exposure to mustard agents. Protection against oxidative stress can occur through the thioredoxin system which consists of TrxR, thioredoxin and NADPH. This system is a redox regulator and is targeted by vesicating agents resulting in an oxidative stress response 24 hours post-

exposure (Jan *et al.*, 2010; Jan *et al.*, 2014). In the present studies, the antioxidant enzyme TrxR was studied and was found to be upregulated by 0.25 hours, reaching its peak by 3-6 hours post-NM. The ability of NM to modulate epithelial cell expression of antioxidants such as HO-1 and TrxR suggests a possible role for antioxidants in protecting the skin from vesicant exposures.

DNA damage activates tyrosine kinases in cells and in turn activates signal transduction networks required to restore cellular homeostasis (Mahajan *et al.*, 2015; Valerie *et al.*, 2007). These signaling pathways are comprised of proteins critical for DNA repair and control of cell cycle checkpoints (Barnum *et al.*, 2014; Langerak *et al.*, 2011). The PI3K/Akt signaling pathway stimulates DNA double strand break repair through tyrosine kinase initiation and has been implicated in p53 phosphorylation in response to environmental stressors and DNA damage inducers through PARP activation (Elkholi *et al.*, 2014; Liu*, et al.*, 2016; Sandoval*, et al.*, 2007). Therefore, we investigated the effects of NM on the DNA repair protein pADPr, the cell cycle dependent proteins cyclin D2 and p53, and the marker of DNA double strand breaks phospho-H2A.X. Upregulation of pADPr was observed by 0.75 hours post-NM exposure, this was associated with a downregulation of phospho-H2A.X and pp53 in the isolated epithelium. Early increases in pp53 are likely important in DNA repair processes while later increases in pp53 are important in controlling cell cycle regulatory proteins (Jowsey *et al.*, 2015; Strozyk *et al.*, 2013)*.* These responses indicate a role for PARP activation in modulating DNA replication and repair. In addition, cyclin D2 was downregulated following NM-exposure. Cyclin D2, a subunit of cyclin dependent kinases, regulates the cell cycle through the phosphorylation of proteins critical for cell cycle progression (Meyyappan*, et al.*, 1998; Wang*, et al.*, 2012). The decrease in cyclin D2 observed

following NM exposure indicates a decrease in DNA replication and an increase in DNA damage and subsequent repair.

Of interest were our findings that oxidative stress and lipid peroxidation preceded NM-induced inflammation in the skin **(Table 3.1)**. Oxidative stress may stimulate initial NM injury accelerating the pro-inflammatory response through transcription factor activation. Understanding the complex system of signaling pathways involved in mustard-induced skin damage is critical. Use of our patch test model allows for clarification and insight into possible mechanisms of vesicants, such as a role of oxidative stress in these toxic consequences. In addition, a one-time AIDNX post-treatment aided in the reduction of initial NM induced skin injuries. Results suggest that repetitive treatment with AIDNX may be beneficial in combating the damaging effects of vesicating agents such as NM.

Taken together, these data suggest a role for oxidative stress in the early events following vesicant-induced skin injury. The mechanisms by which NM induces oxidative stress in isolated epithelium need to be further elucidated as does the role of antioxidants in protecting against tissue injury.

Currently, there are no effective therapies to mitigate the damage of vesicating agents. Studying the early chronological events following NM exposure will help to elucidate the mechanisms behind vesicant induced skin injury. These data contain new observations which are consistent with the effects of NM on the skin and demonstrate the utility of the patch test model for mechanistic studies on the action of vesicants (Composto*, et al.*, 2016; Goswami*, et al.*, 2015; Tewari-Singh*, et al.*, 2013; Tewari-Singh*, et al.*, 2014).
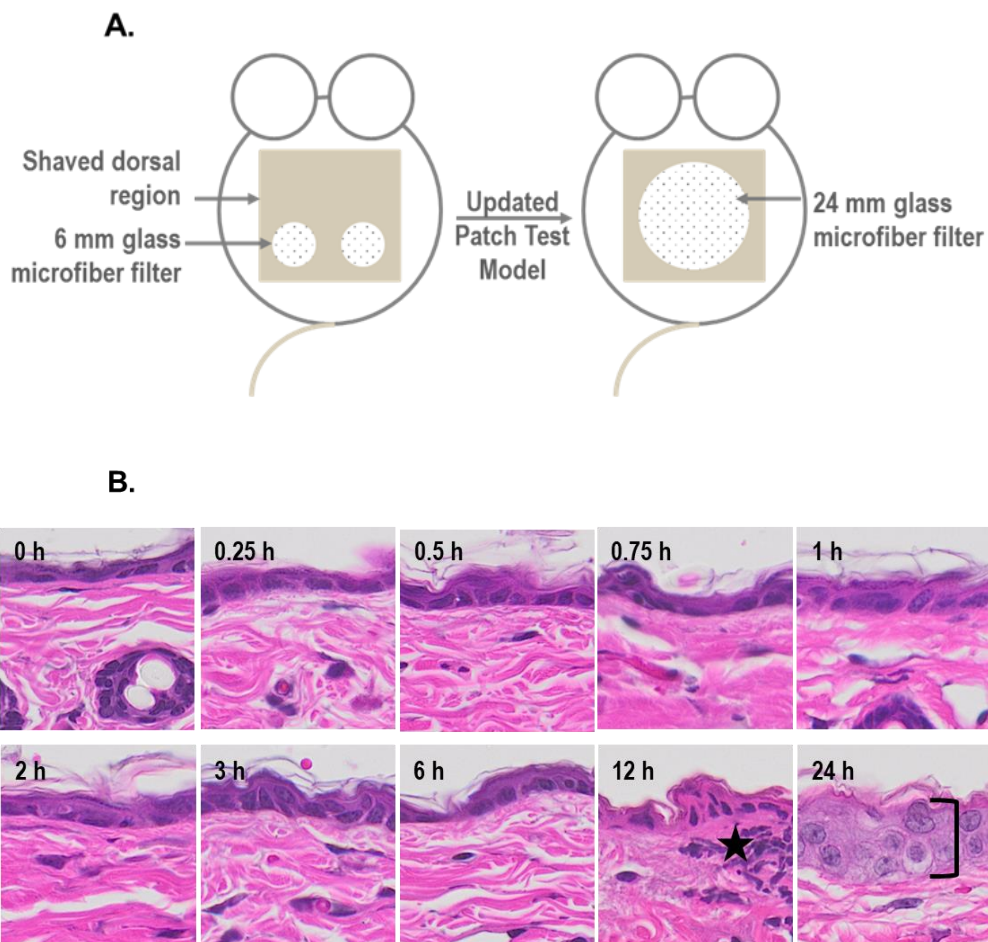
Figure 3.1 Modified Semi-occlusive Patch Test Model.

A. The dorsal skin of female CD-1 mice was shaved and one 24 mm glass microfiber filter disc was placed on the lumbar region of the skin, 120 μl of NM (20 μmol) in 20% deionized water/80% acetone (v/v) was applied to the filters which were then covered with PARAFILM® *(right figure)* - an updated version of our original patch test model (*left* figure). After 6 minutes, the filter discs were removed, and the excised epidermis analyzed for tissue damage 0-24 hours post exposure. **B.** Hematoxylin and eosin (H&E) staining of NM exposed tissue or matched control. One representative section from 4 mice/treatment group is shown (original magnification, x 400) **black star**, inflammation; **bracket**, epidermal thickening.
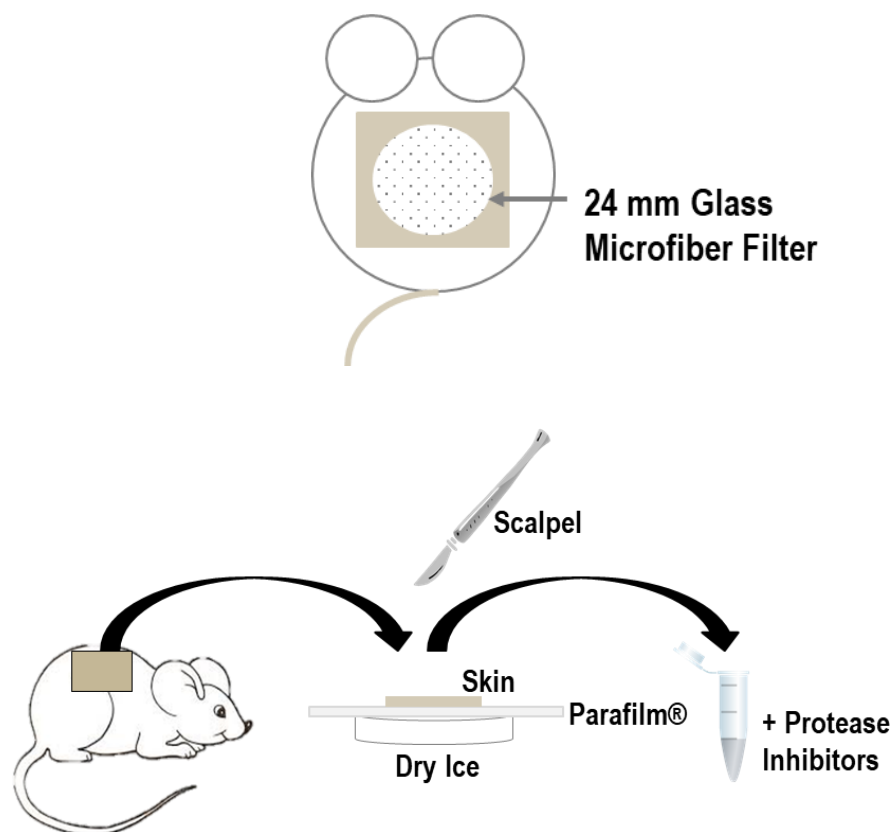
Figure 3.2 Epidermal Isolation Model.

The dorsal skin of female CD-1 mice was shaved and one 24 mm glass microfiber filter disc was placed on the lumbar region of the skin, 120 μl of NM (20 μmol) in 20% deionized water/80% acetone (v/v) was applied to the filters which were then covered with PARAFILM®. After 6 minutes, the filter disc and back skin was removed. The back skin was quickly laid out onto a piece of PARAFILM® and placed on a block of dry ice and allowed to freeze for ~3 seconds. The frozen skin had the epidermis gently scraped off using a scalpel blade. The excised epidermis was placed into a 1.5 ml Eppendorf tube containing protease inhibitors and stored at -80 °C until further processing.

A
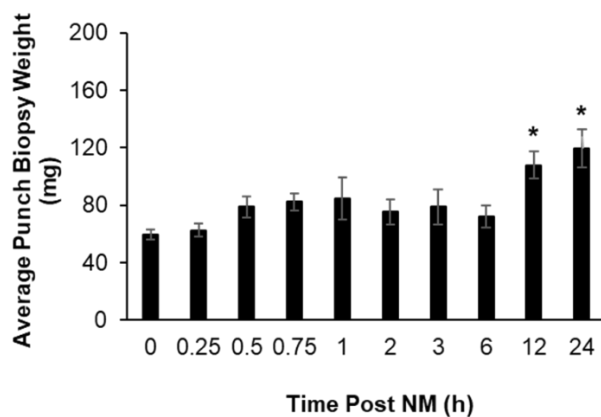
B
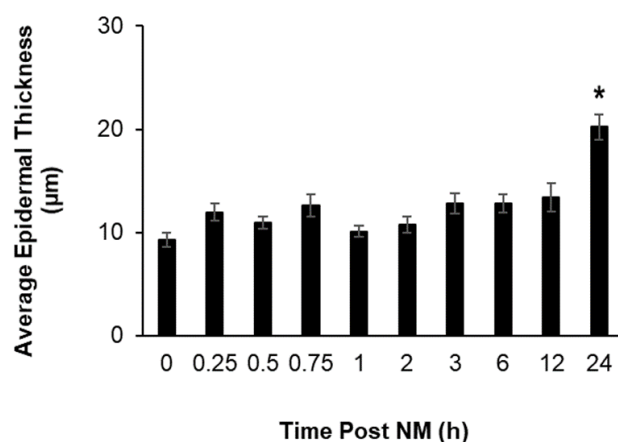
Figure 3.3 Effects of NM on Edema and Epidermal Thickness.

Punch biopsies from control (CTL) mouse skin and mouse skin collected 0-24 hours post-NM exposure, were weighed prior to embedding/sectioning and staining with hematoxylin and eosin (H&E). The epidermal thickness was measured from the H&E stained tissue sections. Wound weights (*upper panel*) and epidermal thickness (*lower panel*) were assessed as described in the Materials and Methods section. Data are presented as mean ± SD ($n = 4$). *Significantly different from CTL mouse skin ($p \leq 0.05$).

A.
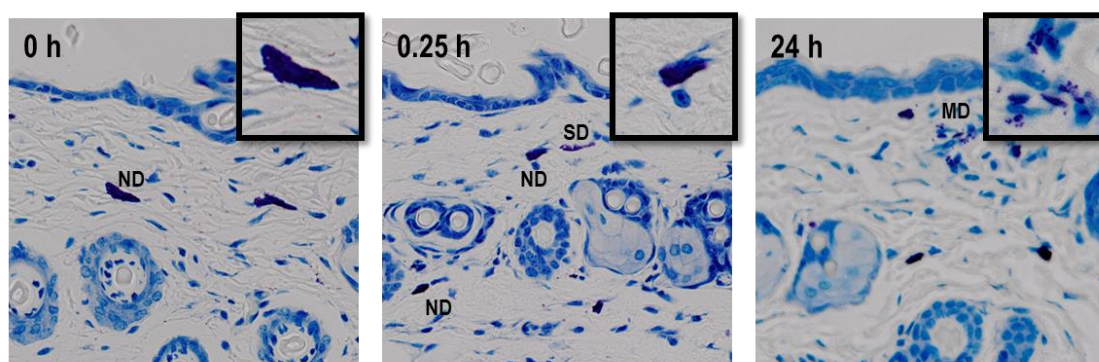
B.
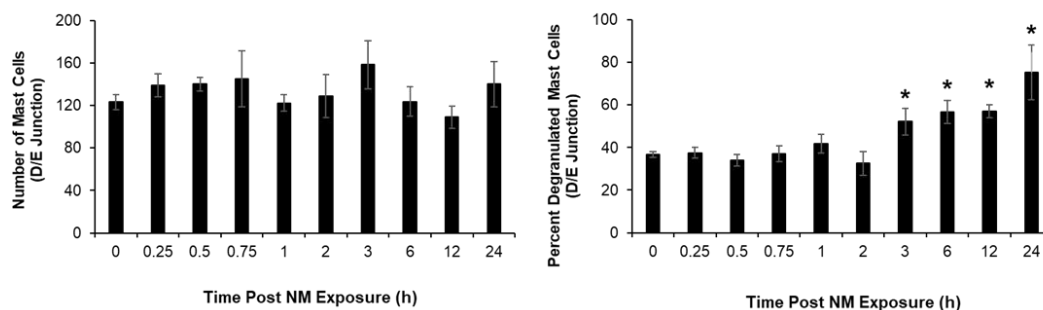
Figure 3.4 Effects of NM on Mast Cell Degranulation.

Histological sections, prepared from control (CTL) mouse skin and mouse skin collected 0-24 hours post-NM exposure, were stained for MCs using toluidine blue (*upper panels*, original magnification, x400). Insets show intact and degranulated MCs in CTL skin and NM treated skin, **ND**, no degranulation; **SD**, slight degranulation; **MD**, major degranulation. Lower panels show the number of MCs at the D/E junction in CTL and NM treated skin (*lower left graph*) and the percentage of MCs that were degranulated (*lower right graph*). Data are presented as mean ± SD ($n = 4$) of 10 fields at 40x mag. *Significantly different from CTL ($p \leq 0.05$).
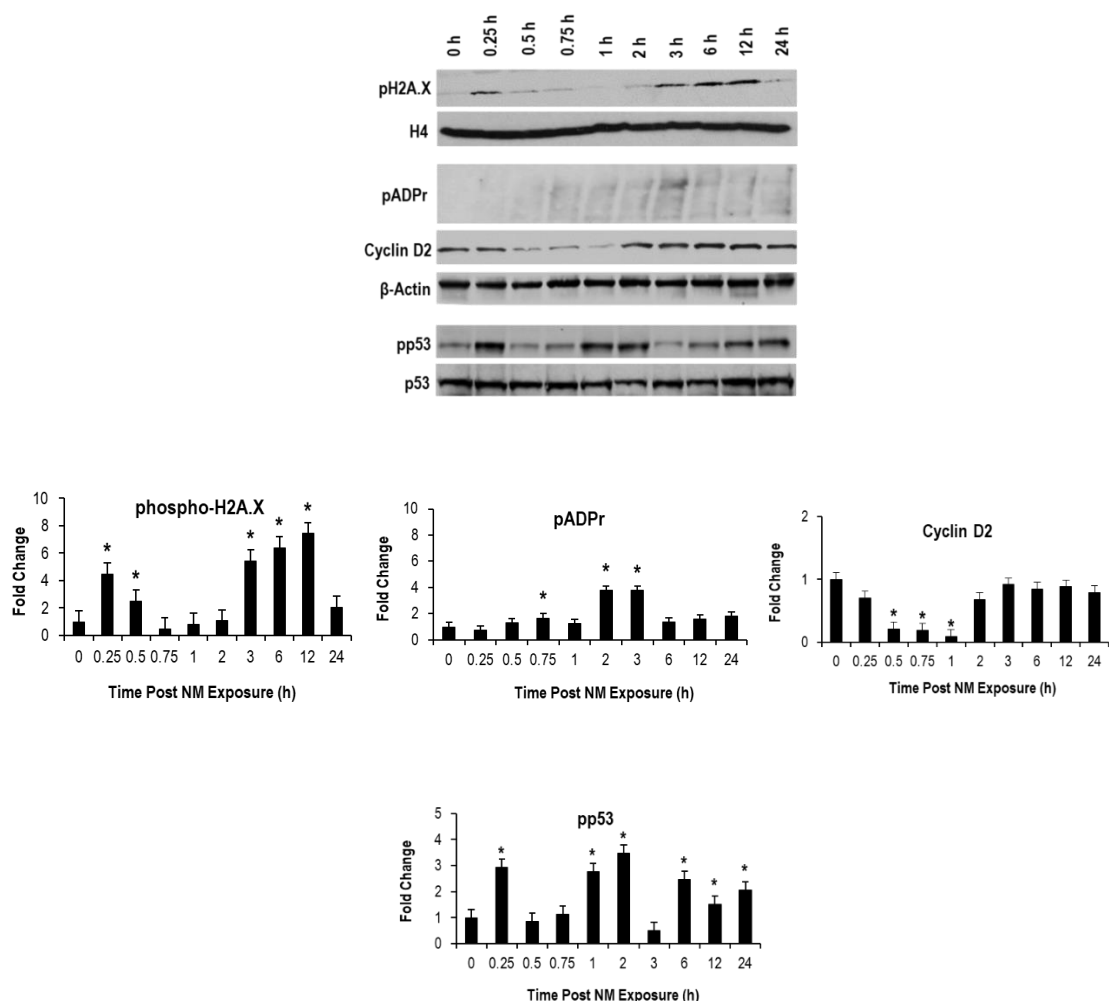
Figure 3.5 Effects of NM on Proteins Involved in DNA Damage Pathways.

Western blot analysis was performed on epidermis isolated from control (CTL) mice and mice exposed to 20 µmol NM 0-24 hours post exposure. Western blots show phospho-H2A.X, pADPr, cyclin D2 and pp53 expression from 1 representative experiment. H4 served as a loading control for phospho-H2A.X, β-Actin served as a loading control for pADPr and cyclin D2, and p53 served as a loading control for pp53. Protein expression was semi-quantified using densitometry of western blots from 3 independent experiments. Data are presented as mean ± SD ($n = 3$). *Significant from CTL; $p \leq 0.05$.
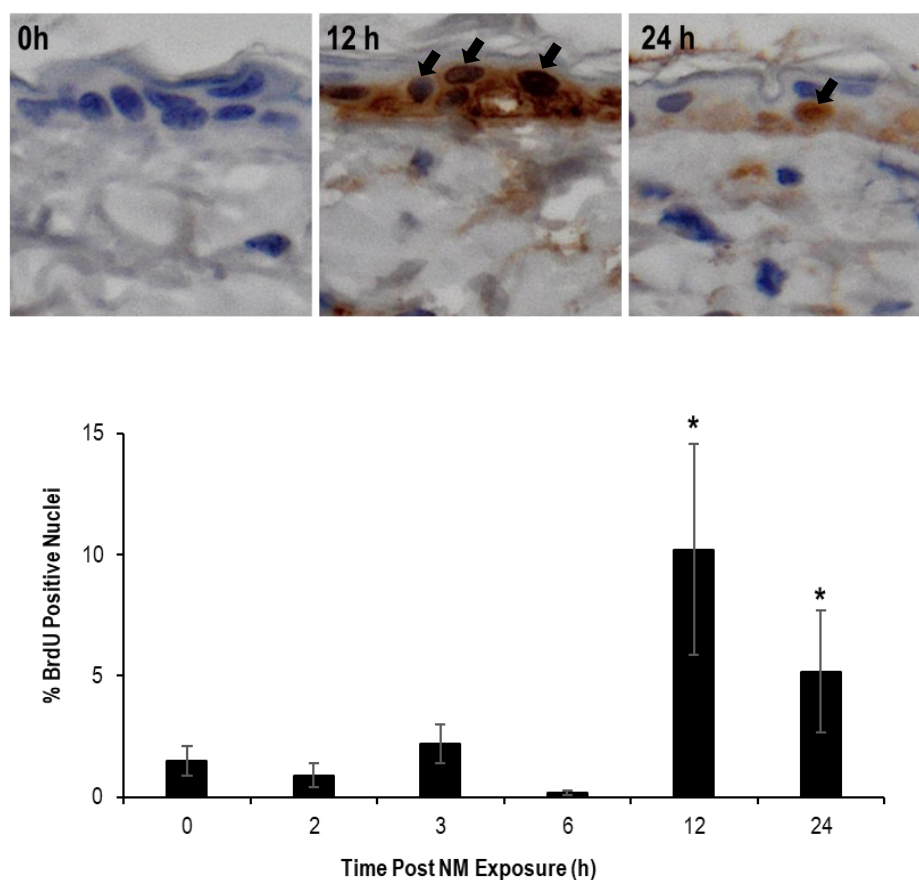
Figure 3.6 BrdU Incorporation Assay.

CD-1 mice were injected with 200 µl of BrdU. 2 hours after injection mice were exposed to 20 µmol NM in 20% deionized water/80% acetone (v/v) via the patch model. Histological sections prepared from mouse skin collected 0-24 hours post-NM exposure, were stained with an antibody to BrdU.   Antibody binding was visualized using a Vectastain Elite ABC kit.   One representative section from 3 mice/treatment group is shown for 12- and 24-hours post-NM exposure (u*pper panels*; original magnification, x400).   The brown colored diaminobenzidine (DAB) positive nuclei were BrdU positive and were counted in 10 randomly selected fields at 40x magnification (*Graph*). Data are presented as mean ± SD (*n* = 3). *Significantly different from CTL (*p* $\leq$ 0.05). **Black arrows**, BrdU positive cells.
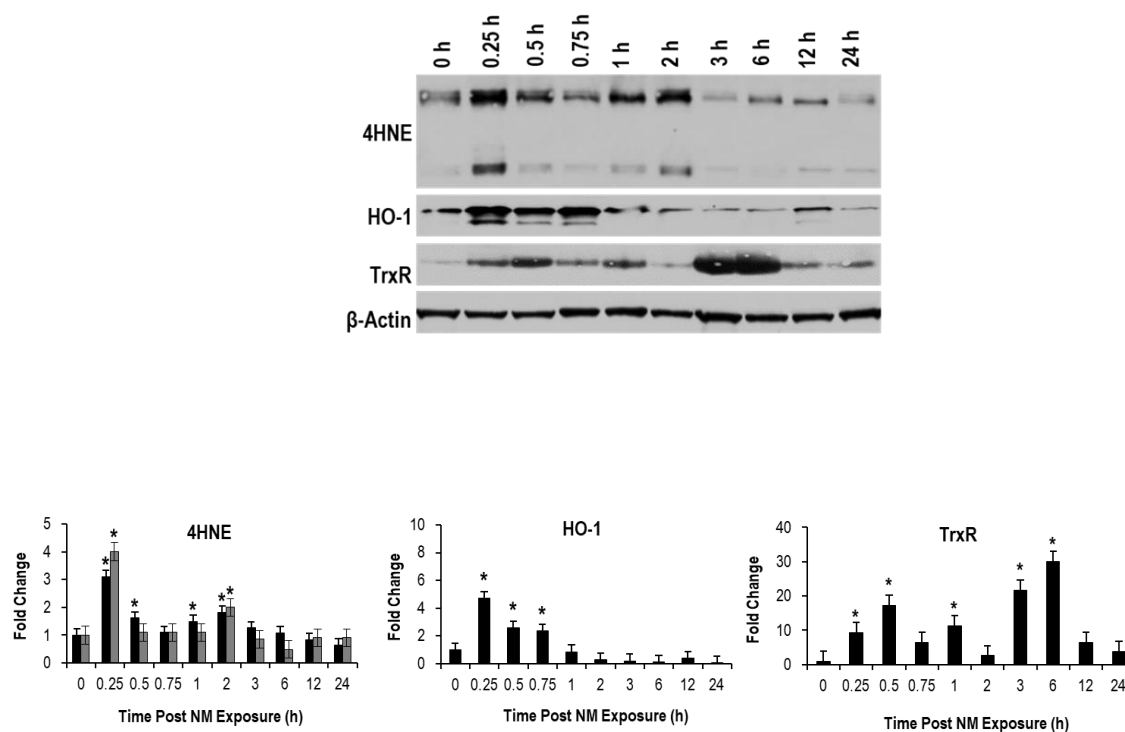
Figure 3.7 Effects of NM on Oxidative Stress Proteins.

Western blot analysis was performed on epidermis isolated from control (CTL) mice and mice exposed to 20 µmol NM 0-24 hours post exposure. Western blots show 4-HNE adducts of histidine residues (black bars represent higher molecular weight adducts, gray bars represent lower molecular weight adducts), HO-1, and TrxR expression from 1 representative experiment. β-Actin was used as a loading control. Protein expression was semi-quantified using densitometry of western blots from 3 independent experiments. Data are presented as mean ± SD (n = 3-4). *Significant; $p \leq 0.05$ compared to CTL.
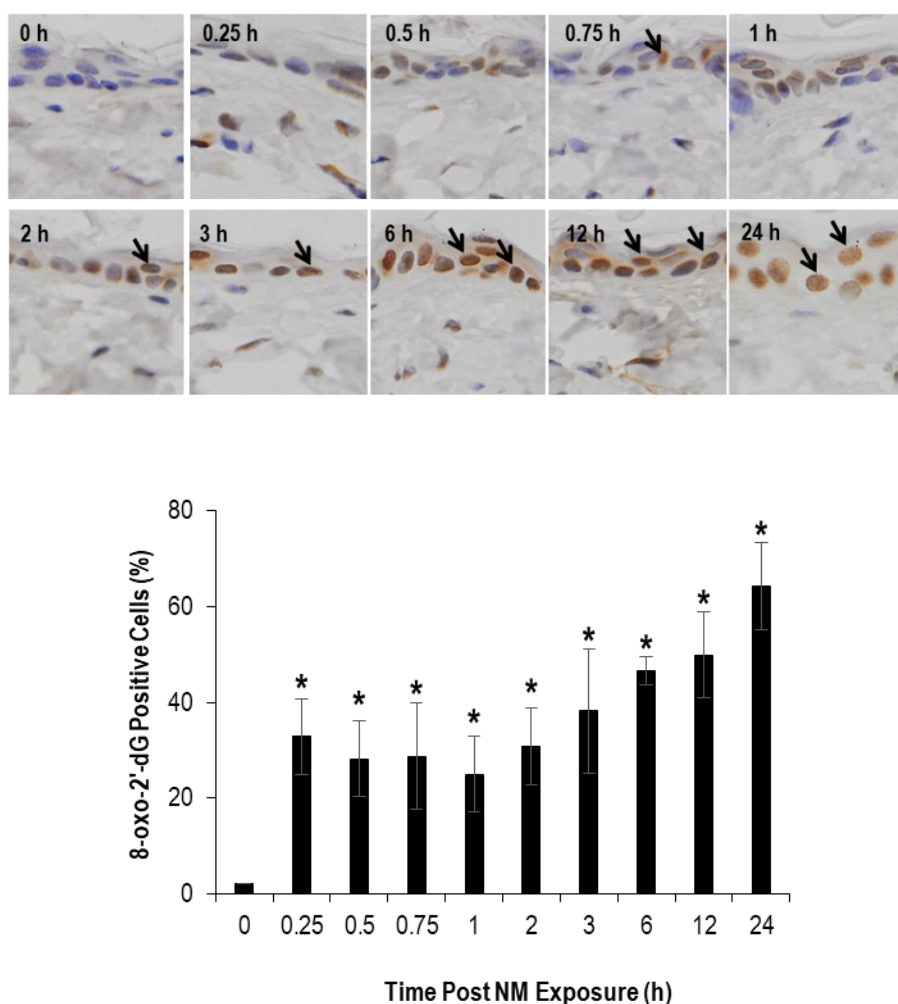
Figure 3.8 Effects of NM on 8-oxo-2'-deoxyguanosine in Mouse Skin.

Histological sections, prepared from control (CTL) mouse skin and mouse skin collected 0-24 hours post-NM exposure, were stained with an antibody to 8-oxo-2'-deoxyguanosine. Antibody binding was visualized using a Vectastain Elite ABC kit. One representative section from 4 mice/treatment group is shown (*Upper panels*; original magnification, x400). The brown colored diaminobenzidine (DAB) positive nuclei were 8-oxo-2'-dG positive and were counted in 10 randomly selected fields at 40x magnification (*Graph*). Data are presented as mean ± SD (*n* = 4). *Significantly different from CTL ($p \leq 0.05$); **black arrows**, 8-oxo-2'-dG positive cells.

Table 3.1 Events Following NM-Induced Skin Injury

Time Post-NM	Events
0.25 h	DNA Damage/Repair; Lipid Peroxidation; Oxidative Stress
0.5 h	DNA Damage/Repair; Oxidative Stress
1 h	Lipid Peroxidation; Cell Cycle Modifications
2 h	DNA Damage/Repair; Lipid Peroxidation; Cell Cycle Modifications
3 h	DNA Damage/Repair; Lipid Peroxidation; Oxidative Stress; Cell Cycle Modifications; Mast Cell Degranulation
6 h	DNA Damage/Repair; Oxidative Stress; Cell Cycle Modifications; Mast Cell Degranulation
12 h	DNA Damage/Repair; Oxidative Stress; Mast Cell Degranulation; Inflammation; Edema; Apoptosis
24 h	DNA Damage/Repair; Oxidative Stress; Cell Cycle Modifications; Mast Cell Degranulation; Inflammation; Edema
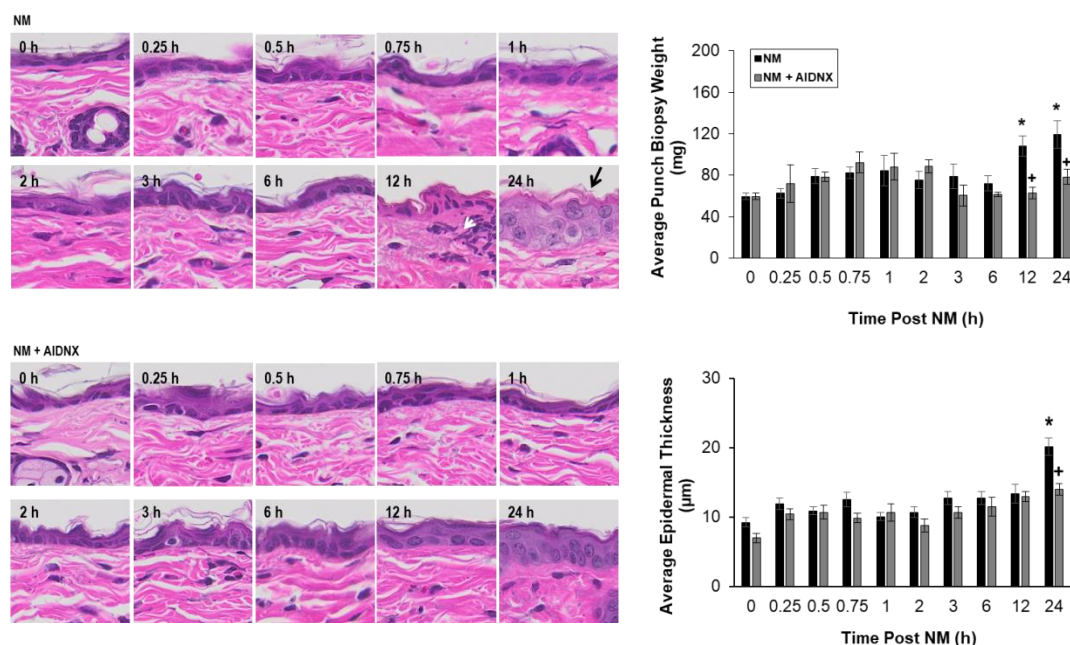
Figure 3.9 Effects of AIDNX on Mouse Skin Post-NM Exposure.

Histological sections prepared from control (CTL) mouse skin and mouse skin exposed to NM and NM + AIDNX were stained with hematoxylin & eosin (H&E) and punch biopsy weight and epidermal thickness measured 0-24 hours post exposure. **White arrowhead**, inflammatory cell infiltrate; **black arrow**, thickened neo-epidermis. One representative section from 3 mice/treatment group is shown (original magnification, ×400). Data are presented as mean ± SD (n = 3-5) *Significantly different from CTL; [+]significantly different from NM ($p \leq 0.05$).
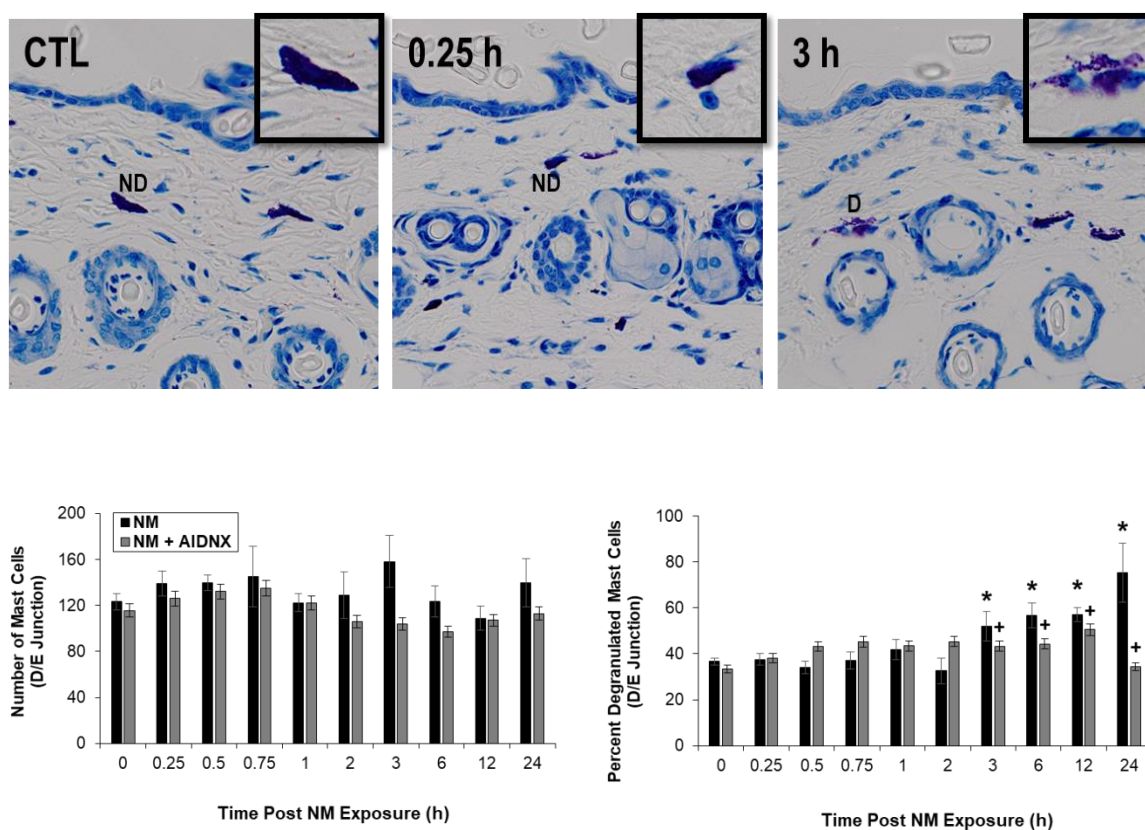
Figure 3.10 Effects of AIDNX on Mast Cell Degranulation Post-NM Exposure.

Histologic sections prepared from control (CTL) mouse skin and mouse skin 0-24 hours

post-NM or NM + AIDNX were stained for MCs using toluidine blue. The graphs show

the number of MCs at the D/E junction in CTL, NM and NM + AIDNX exposed skin (*left*

graph) and the percentage of MCs that were degranulated (*right graph*). Data are

presented as mean ± SD ($n = 3$) of 10 fields at 40× magnification. *Significantly different

from CTL; +significantly different from NM ($p \leq 0.05$). **ND**, no degranulation; **D**,

degranulation.
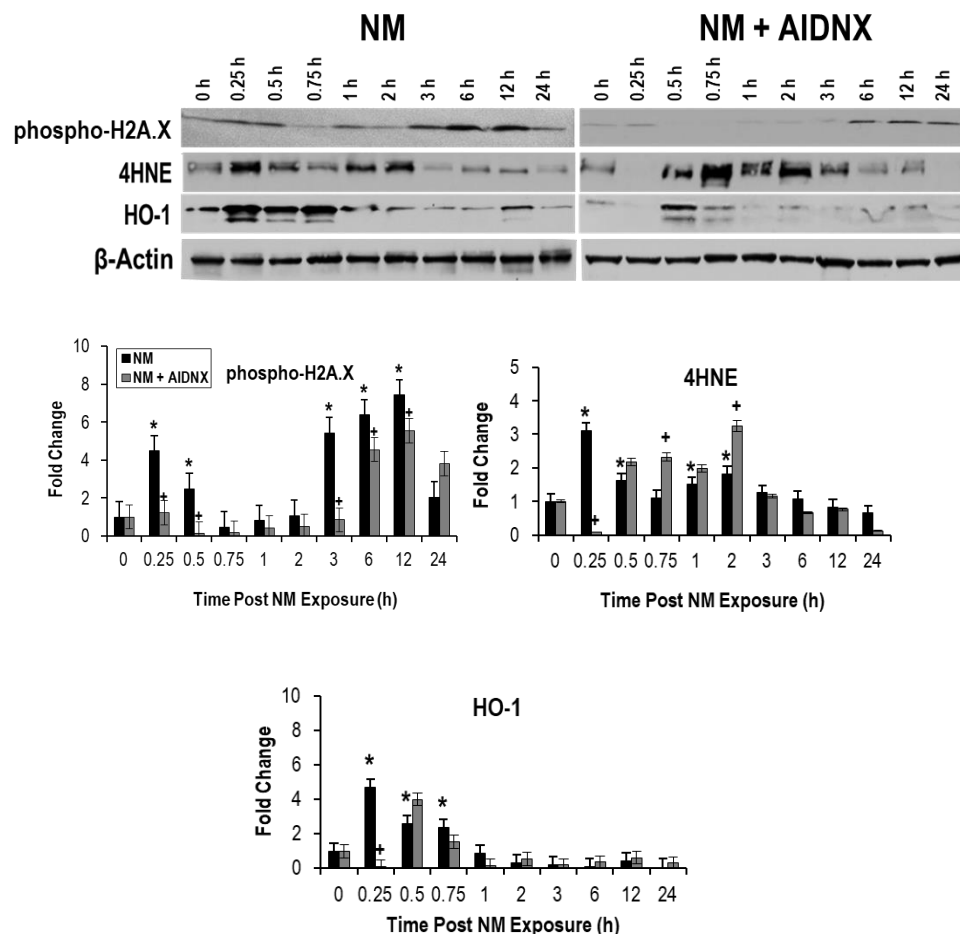
Figure 3.11 Effects of AIDNX on DNA Damage and Oxidative Stress Proteins in Isolated Mouse Skin Epithelium.

Western blot analysis was performed on epidermis isolated from CTL mice and mice exposed to 20 µmol NM and NM + AIDNX 0-24 hours post exposure. Western blots show phospho-H2A.X, 4-HNE, and HO-1 expression from 1 representative experiment. Protein expression was semi-quantified using densitometry of western blots from 3 independent experiments. Data are presented as mean ± SD (n = 3). *Significantly different from CTL; +significantly different from NM ($p \leq 0.05$).

CHAPTER 4: NITROGEN MUSTARD EXPOSURE ALTERS DNA DAMAGE REPAIR PATHWAYS IN MOUSE AND HUMAN KERATINOCYTES

Gabriella Wahler[a], Debra L. Laskin[a,b], Diane E. Heck[c], Jeffrey D. Laskin[a,b,d,e], Laurie B. Joseph[a,b]

[a] Joint Graduate Program in Toxicology, Rutgers University Graduate School of Biomedical Sciences, 170 Frelinghuysen Rd, Piscataway, NJ 08854, USA

[b] Department of Pharmacology and Toxicology, Rutgers University, 170 Frelinghuysen Rd, Piscataway, NJ 08854, USA

[c] Department of Environmental Health Science, School of Health Sciences and Practice, New York Medical College, 40 Sunshine Cottage Rd., Valhalla, NY 10595, USA

[d] School of Public Health, Rutgers University, 170 Frelinghuysen Rd, Piscataway, NJ 08854, USA

[e] Environmental and Occupational Health Sciences Institute, Rutgers University, 170 Frelinghuysen Rd, Piscataway, NJ 08854, USA

4.1 Abstract

Both SM and NM are bifunctional alkylating agents that target DNA, RNA, proteins and lipids forming adducts and crosslinks. In the present studies DNA damage and repair pathways following NM exposure were investigated to determine the rate of DNA damage and the major pathway involved in repair. *In-vitro* studies analyzing the effects of NM exposure on both mouse (PAM212) and human (HaCaT) keratinocytes were performed. NM was found to cause S phase arrest 16-24 hours post exposure which were associated with DNA double strand breaks (DSB). Increased comet tail extent was observed 24 hours post-NM exposure which was associated with increased levels of DNA DSB repair molecules phospho-H2A.X and pp53. Exposure to NM resulted in a 3-fold increase in pp53 by 1 hour increasing to 6-fold by 6 hours. Phospho-H2A.X expression increased 2-fold by 2 hours reaching its peak at 6 hours (3-fold). To further analyze DNA damage and repair following exposure to NM two pathways involved in DNA DSB repair, nonhomologous end joining (NHEJ) and homologous recombination (HRR) were studied. The DNA-PK inhibitor Nu7026 and the Rad51 inhibitor B02 were used to determine the role of NHEJ and HRR in DNA repair following NM exposure, respectively. Inhibition of NHEJ did not affect the amount of DNA damage occurring following exposure to NM. However, inhibition of the HRR pathway caused a significant increase in DNA damage indicating HRR as the key pathway involved in the repair of NM-induced DNA DSBs. Understanding the pathways involved in DNA repair could aid in the development of therapeutic strategies for the mitigation of vesicant-induced skin damage.

Abbreviations

B02, Rad51 inhibitor; DSB, double strand breaks; HaCaT, human keratinocyte cell line; HO-1, hemeoxygenase-1; HRR, homologous recombination repair; ICL, interstrand crosslinks; NHEJ, non-homologous end joining; Nu7026, DNA-PK inhibitor; PAM212, mouse keratinocyte cell line; phospho-H2A.X, phosphorylated histone H2A.X; PI, propidium iodide; pp53, phosphorylated p53; SSB, single strand breaks

4.2 Introduction

The genotoxic effects of chemical agents makes understanding the pathways involved in vesicant-induced DNA damage a major study of interest. As discussed in previous chapters, interstrand crosslinks (ICL) contribute to cytotoxicity and the induction of cell cycle arrest inhibiting DNA synthesis and cell replication. Following vesicant induced injury, DNA damage activates cell signaling pathways which promotes DNA repair and apoptosis by activating cell cycle checkpoints and inhibiting cell cycle progression. Molecules important in cell cycle regulation include the tumor suppressor protein, p53 and cyclin dependent kinases (CDKs). Both proteins are activated following DNA damage and play roles in ensuring DNA replication is halted so repair can take place (Senturk *et al.*, 2013). Repair involves DNA incision resulting in the formation of DNA DSBs. DNA DSBs can be repaired by the NHEJ or HRR pathway, among others (Inturi*, et al.*, 2014; Jasin *et al.*, 2013; Lieber, 2010; Mao *et al.*, 2008). The NHEJ pathway recruits the DNA-dependent protein kinase (DNA-PK) catalytic subunit forming DNA-PK holoenzyme. DNA-PK, when bound to the broken ends, becomes activated and undergoes auto-phosphorylation to repair the DNA (Lieber, 2010; Mao*, et al.*, 2008). Nu7026, a competitive inhibitor of DNA-PK, prevents Ku70 binding to strand breaks and recruiting DNA-PK catalytic subunit to facilitate rejoining of the DNA strands (Alagpulinsa *et al.*, 2014; Veuger *et al.,* 2003). In the HRR pathway, the tumor suppressor gene

BRCA2 interacts with the DNA repair protein, Rad51, and coordinates the binding of the Rad51 filament to the 3'ss DNA tails leading to DNA strand separation (Jasin*, et al.*, 2013; Mao*, et al.*, 2008). Annealing is catalyzed by BRCA2 and Rad51, completing the DNA DSB repair process (Jasin*, et al.*, 2013; Mao*, et al.*, 2008). The inhibitor used to block the HRR pathway is the specific Rad51 inhibitor known as B02. B02 prevents Rad51 from polymerizing onto single-stranded overhangs of DSBs, preventing reciprocal and nonreciprocal DNA strand exchange by homologous duplexes (Alagpulinsa*, et al.*, 2014; Veuger*, et al.*, 2003).

The use of specific DSB repair pathways inhibitors helped to uncover the major repair pathway involved in NM induced DNA damage in mouse and human keratinocytes.

4.3 Materials and Methods

Cell Culture and Treatments

PAM212 and HaCaT cells were obtained from the American Type Culture Collection (Manassas, VA) and cultured in Dulbecco's Modified Eagle's Medium, with 4.5 g/L Glucose, without L-Glutamine (DMEM, Lonza, Walkersville, MD) containing 10% fetal bovine serum (FBS) and 1% penicillin/streptomycin. Cells were grown under standard culture conditions at 37 °C in a humidified 5% CO_2 incubator. NM (mechlorethamine hydrochloride; 98%) was obtained from Sigma-Aldrich Chemical Co. (St. Louis, MO) and the stock solution of NM was prepared fresh in DMEM for the exposures. For inhibitor studies, Nu7026 and B02 were obtained from Sigma, and the stocks were prepared in dimethyl sulfoxide (DMSO). Cells were treated with either 10 μmol Nu7026 or B02 1 hour before NM exposure. Desired assays were carried out 24 hours following these treatments. Unless stated otherwise, the final concentration of DMSO in the culture medium during treatments did not exceed 0.1% (v/v). All NM preparations were carried

out in a continuously operated chemical and biological safety hood, and exposures were initiated under a safety laminar hood using all required and approved personal protective equipment.

Flow Cytometry

For cell cycle distribution studies cells were exposed to 1 μmol NM and harvested 8, 16, and 24 hours post exposure after trypsinization, washed with PBS and fixed in 3 ml ice-cold 70% ethanol drop-wise while vortexing. Cells were incubated in ethanol for 1 hour on ice then resuspended in PBS containing propidium iodide (PI, 1:100) and RNAse A (1:30) and incubated at 37 °C in a water bath with shaking for 1 hour prior to analysis. For inhibitor studies cells were harvested 24 hours post-treatments after trypsinization, washed twice with PBS and fixed in 1 ml ice-cold 70% methanol drop-wise while vortexing. Cells were incubated in methanol for 20 minutes at -20 °C. Cells were then washed twice with PBS and incubated in 100 μl of 0.5% IGEPAL in PBS. Cells were blocked in normal horse serum for 15 minutes at room temperature, washed twice with PBS and incubated with phospho-H2A.X antibody (1:300) for 1 hour at room temperature. Cells were washed twice with PBS and incubated in Alexa fluor-488 conjugated antibody (1:400) for 1 hour at room temperature in the dark. After incubation cells from all experiments were analyzed at the Rutgers University FACS core laboratory to determine cell cycle progression and intercellular phospho-H2A.X accumulation.

Western Blot Analysis

Following exposures, cell lysates were prepared, and protein concentration was determined by bicinchoninic acid (BCA) assay (Pierce Biotechnology, Rockford, IL) using a bovine serum albumin standard. Proteins were separated on a 4-15% Tris-HCl gel (BioRad). After transferring protein to nitrocellulose (Thermo Fisher Scientific, Waltham, MA), membranes were blocked with 5% nonfat dry milk in 0.1% TPBS for 30

minutes at 37 °C. Membranes were then incubated with primary antibodies against p53 (1:1,000, Cell Signaling Technologies, Danvers, MA), pp53 (1:1,000, Cell Signaling Technologies), HO-1 (1:1,000, Cell Signaling Technologies), phospho-H2A.X (1:1,000, Cell Signaling Technologies), and β-Actin (1:1,000, Cell Signaling Technologies) at 4 °C overnight. Membranes were then incubated in appropriate secondary antibody either rabbit or mouse (1:2,500; Cell Signaling Technologies). Luminata Forte Western HRP substrate (Millipore, Billerica, MA) which forms chemiluminescent protein-antibody complexes was used to visualize protein bands using a Fluorchem Imager (ProteinSimple, Santa Clara, CA). Semi-quantitative analysis of protein bands was performed using ImageJ Software version 1.5.

Comet Assay

About 3×10^5 HaCaT cells were plated onto 60 mm tissue culture plates. The cells were serum starved for 48 hours for synchronization. Cells were treated with 1 µmol NM or CTL (serum free media) for 24 hours. After treatment the cells were trypsinized and resuspended in PBS at a concentration of 1×10^6 cells/ml. Cells were pipetted into 1% low melting agarose on a comet assay slide containing a thin layer of agarose (Trevigen, Gaithersburg, MD) and incubated at 4 °C for 30 minutes. After incubation cells were lysed in lysis buffer (Trevigen, Gaithersburg, MD) overnight at 4 °C. The COMET assay slides were removed from the lysis buffer and immersed in 50 ml of 1x neural electrophoresis buffer for 30 minutes at 4 °C or in 50 ml of alkaline unwinding solution for 1 hour at 4 °C in the dark to unwind the DNA. The slides were immersed in 1x neutral or alkaline buffer in the slide tray of the Comet Assay ES unit (Trevigen, Gaithersburg, MD). The slides were covered with a slide tray overlay and electrophoresed at 21 volts for 45 minutes at 4 °C for the neutral assay (determination of SSBs and DSBs), or at 21

volts for 30 minutes at 4 °C for the alkaline assay (determination of SSBs). After electrophoresis, slides were immersed in DNA precipitation solution for 30 minutes at room temperature for the neutral assay. The slides were then fixed in 70% ethanol for 30 minutes at room temperature for the neutral assay or immersed twice in deionized water for 5 minutes to remove residual buffer then fixed in 70% ethanol for 5 minutes at room temperature for the alkaline assay. The samples were dried on a heat block at 37 °C for 15 minutes in order to bring all the cells to a single plane for observation. Slides were stained with 100 µl of 1 µg/ml PI diluted 1:100. The samples were incubated at room temperature for 30 minutes protected from light. After incubation the slides were washed in water for 5 minutes to remove any background PI. The slides were then dried on a heat block set to 37 °C and examined under a confocal fluorescent microscope at 10x magnification. The tail moment is the sum of half the radius of the comet head and half the length of the comet tail (Singh, 2016).

Statistical analysis

Data are presented as mean ± SD. A one-way analysis of variance was used to assess statistical significance ($p \leq 0.05$).

4.4 Results

Cell Cycle Progression Following NM Exposure

Cytograms of both HaCaT and PAM212 cells show a shift of cells into S phase at 16 hours and 24 hours, respectively following 1 µmol of NM treatment **(Fig 4.1)**. Analysis of the cytograms revealed that approximately 40% of HaCaT cells were arrested in S-phase by 16 hours, increasing to 50% by 24 hours **(Fig 4.2; *left graph*)**. Interestingly, NM didn't arrest PAM212 cells in S phase until 24 hours post exposure when 40% of the cells were arrested **(Fig 4.2; *right graph*)**.

NM Exposure Induces DNA DSBs in HaCaT Cells

Exposure of HaCaT cells to NM for 24 hours resulted in an increase in DNA DSBs. DNA breaks were visualized through increased tail moments and levels of the DNA damage markers phospho-H2A.X and pp53. Tail moments were only found to be significantly increased in the neutral assay following exposure to NM when compared to control **(Fig. 4.3)**. The neutral COMET assay detects DSBs in DNA while the alkaline COMET assay detects SSBs, indicating that NM is only causing DNA DSBs and not SSBs **(Fig. 4.3)**. These results were associated with increases in the levels of DNA DSB markers phospho-H2A.X and pp53 **(Fig. 4.4)**. NM caused a 3-fold increase in pp53 by 1 hour post exposure increasing to 6-fold by 6 hours **(Fig. 4.4)**. Phospho-H2A.X expression increased 2-fold by 2 hours reaching its peak at 6 hours (3-fold) **(Fig. 4.4)**. Taken together, these results indicate that exposure of HaCaT cells to NM induced DNA double-strand breaks rather than single-strand breaks.

NM Induced DNA Damage is Increased when Homologous Recombination Repair is Inhibited

Flow cytometric analysis of phospho-H2A.X was performed to determine the effect of DNA DSB repair pathways on NM induced DNA damage. Studies analyzed the percentage of phospho-H2A.X in control and NM exposed cells with or without DNA repair pathway inhibitors, NHEJ and HRR. NM treatment alone resulted in elevated phospho-H2A.X levels when compared to control **(Fig 4.5)**, indicating DNA damage following exposure to NM. Cells pretreated with the specific Rad51 inhibitor, B02, resulted in a 4-fold increase in phospho-H2A.X levels when compared to control **(Fig. 4.5)**. Cells pretreated with the competitive DNA-PK inhibitor, Nu7026, resulted in levels of phospho-H2A.X similar to those seen in the control **(Fig. 4.5)**. The intracellular levels of phospho-H2A.X correlated with protein levels observed following exposure to NM

(Fig. 4.6). NM exposure alone caused a 2.5-fold increase in the protein levels of

phospho-H2A.X when compared to control **(Fig. 4.6)**. The addition of Nu7026 resulted in

levels similar to control **(Fig. 4.6)**. Interestingly, the addition of B02 resulted in a 1.5-fold

increase in phospho-H2A.X levels when compared to control **(Fig. 4.6)**. Taken together,

these findings suggest HRR as the main pathway involved in the repair of NM induced

DNA DSBs in HaCaT cells.

4.5 Discussion

The use of mustard agents in warfare has been a cause for concern since the 1800s

(Jiang *et al.*, 2018). The toxic effects of mustard agents such as SM are well

documented, however treatment for such exposures is lacking. Similar to SM, NM

induces toxicity through adduct formation and crosslinking with DNA, RNA, and proteins.

The major target of NM in the skin are dividing epidermal keratinocytes. Due to their

relevance in NM induced skin damage both mouse and human keratinocytes were used

in our studies to analyze the kinetics of NM-induced cytotoxicity, DNA damage and

repair.

Studies analyzed the effect of NM on cell cycle progression and DNA damage. Specific

inhibitors, Nu7026 and B02, to repair pathways, NHEJ and HRR, necessary for the

repair of DNA damage, respectively, were used to determine the main pathway involved

following NM exposure. Cell cycle analysis demonstrated that HaCaT cells are more

sensitive to NM induced DNA damage indicated by S phase arrest 16 hours following

exposure as compared to PAM212 cells **(Fig. 4.2;** *left graph***)**. The sensitivity of HaCaT

cells to NM made them an ideal model to use for the inhibitor studies. Although both SM

and NM are known to cause DNA SSBs and DSBs, our studies demonstrate that

exposure of HaCaT cells to 1 μmol of NM for 24 hours causes only DSBs. Additional

studies will need to be performed to determine if SSBs occur at higher concentrations

and longer time points following exposure to NM. The increases in the DNA damage markers phospho-H2A.X and pp53 observed following NM exposure coincide with the increases in tail moment measured using the COMET assay.

DNA damage is a major event following exposure to mustard agents. Determining the repair mechanism involved can help for the development of effective therapeutics for NM, and possibly SM-induced skin injuries. These results revealed that the HRR pathway was the major pathway responsible for DNA repair following NM exposure. This pathway may be a beneficial target for the study of potential therapeutics as countermeasures.
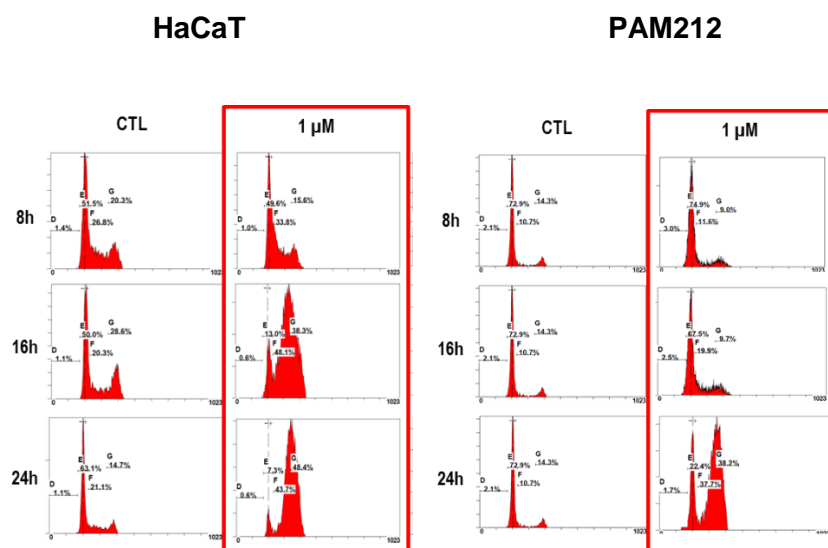
HaCaT　　　　　　　　　　　　**PAM212**

Figure 4.1 Effects of NM on Cell Cycle Distribution in HaCaT and PAM212 cells.

Cells were treated with 1 µmol NM or control (CTL) in serum-free medium. After 8, 16 or

24 hours, cell cycle distribution was analyzed by flow cytometry using propidium iodide

(PI) DNA staining. The representative cytograms show the cell cycle distribution of CTL

and NM-treated HaCaT (*left panels*) and PAM212 (*right panels*) cells.
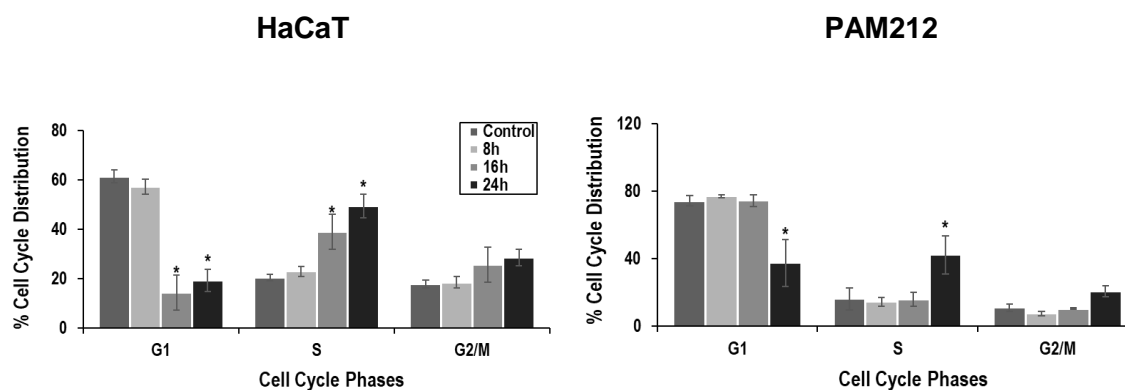
HaCaT **PAM212**

Figure 4.2 Effects of NM on Phases of the Cell Cycle in HaCaT and PAM212 cells.

Cells were treated with 1 µmol NM or control (CTL) in serum-free medium. After 8, 16 or 24 hours, cell cycle distribution was analyzed by flow cytometry using propidium iodide (PI) DNA staining. Data are presented as mean ± SD, $n = 3$. The graphs represent the percentage of HaCaT (*left graph*) and PAM212 (*right graph*) cells in each phase of the cell cycle following exposure to NM. *Significantly different from CTL; $p \leq 0.05$.

A.
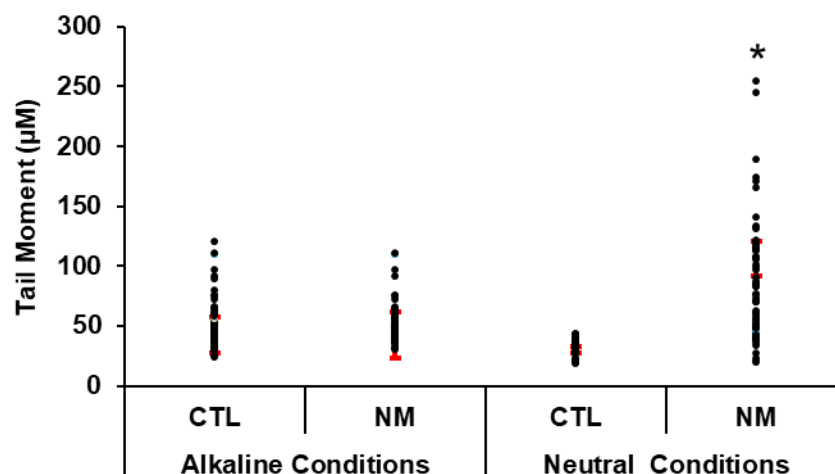
B.
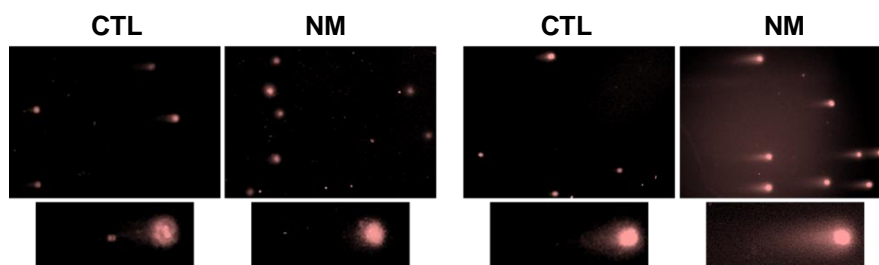
Figure 4.3 Effect of NM Exposure on the Formation of DNA Strand Breaks in HaCaT cells.

Cells were treated with 1 μmol NM or control (CTL) in serum-free medium. After 24 hours COMET assay was performed. **A.** Average tail moments of CTL and NM exposed cells under alkaline and neutral COMET assay conditions. **B.** Representative images of COMET assay tails from CTL and NM exposed cells under alkaline (*left panels*) and neutral (*right panels*) COMET assay conditions. The enlarged images show the COMET tail length in CTL and NM exposed cells under both assay conditions. Data are presented as mean ± SD, $n = 4$, *Significantly different from CTL, $p \leq 0.05$ (Singh, 2016).
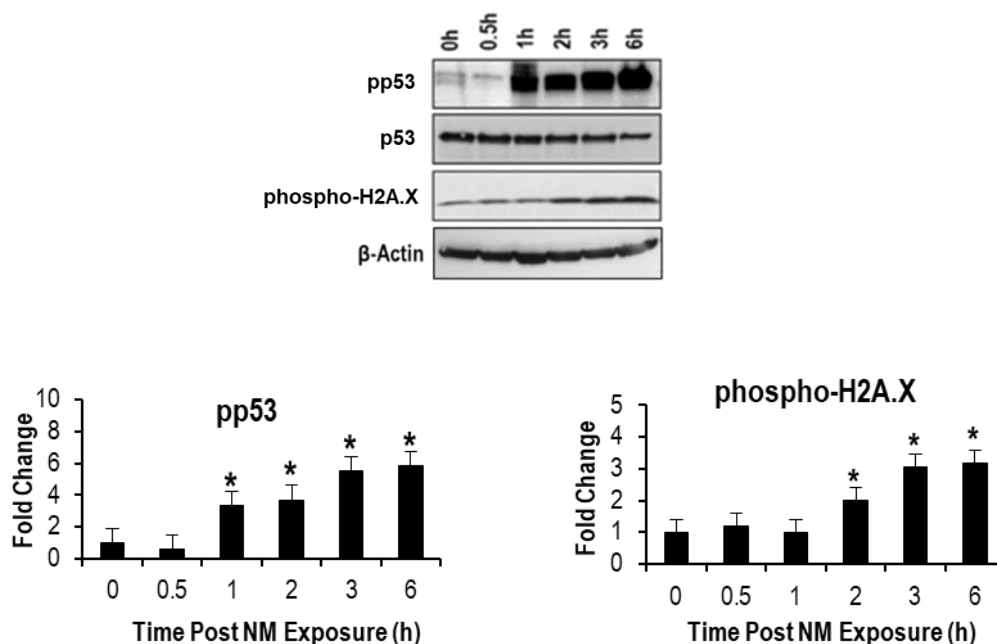
Figure 4.4 Effect of NM Exposure on the Activation of DNA Damage Response Molecules

Western blot analysis was performed on HaCaT cells exposed to 1 µmol NM examined 0-6 hours post exposure. Western blots show pp53, and phospho-H2A.X expression from 1 representative experiment. Total p53 and β-Actin were used as loading controls. Protein expression was semi-quantified using densitometry of western blots from 3 independent experiments. Data are presented as mean ± SD (n = 3). *Significant; $p \leq$ 0.05.
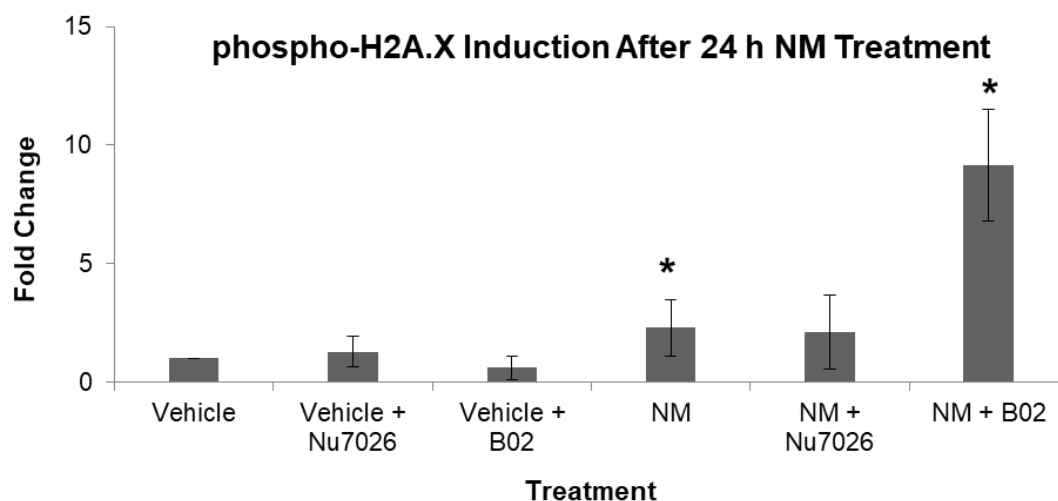
Figure 4.5 Flow Cytometric Analysis of DNA DSB Repair Pathways NHEJ and HRR Post-NM Exposure.

To determine the activation of the NHEJ and HRR pathways, whole cell lysates prepared from HaCaT cells exposed to 1 μmol NM with or without inhibitors to NHEJ (Nu7026) or HRR (B02) for 24 hours, were analyzed by flow cytometry for phospho-H2A.X expression. Data are presented as mean ± SD ($n = 3$); *Significant $p \leq 0.05$.
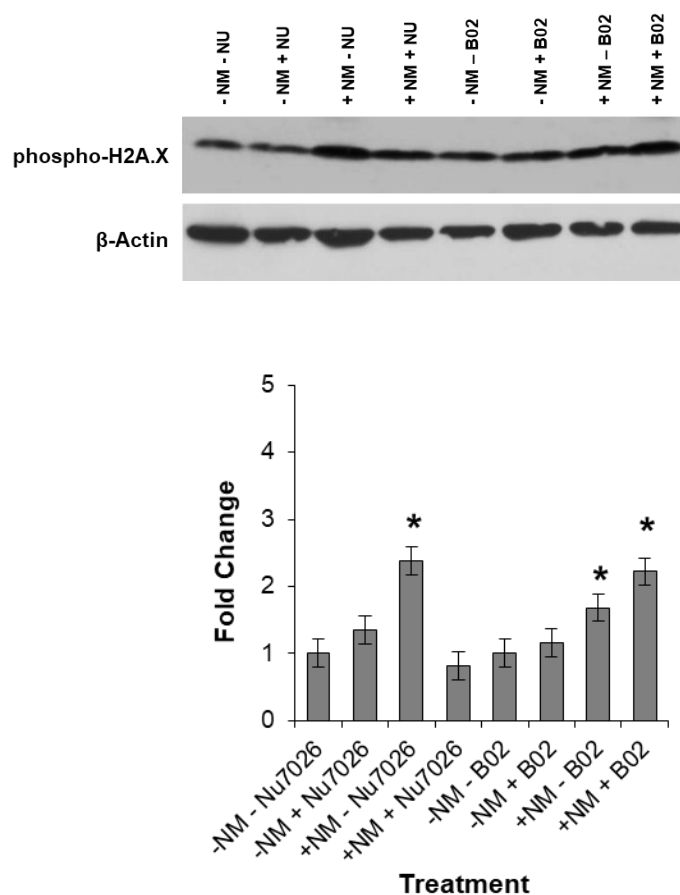
Figure 4.6 Effects of NM Exposure on the Activation of DNA DSB Repair Pathways NHEJ and HRR.

To determine the activation of the NHEJ and HRR pathways, whole cell lysates prepared from HaCaT cells exposed to 1 µmol NM with or without inhibitors to NHEJ (Nu7026) and HRR (B02) for 24 hours, were analyzed by western blot analysis using an antibody to phospho-H2A.X. Data are presented as mean ± SD ($n = 3$); *Significant $p \leq 0.05$.

CHAPTER 5: DEVELOPING A PIG SKIN MODEL FOR SULFUR MUSTARD INJURY

Gabriella Wahler[a], Laurie B. Joseph [a,b], Claire R. Croutch[c], Jieun Kang[d], Robert P. Casillas[e], Debra L. Laskin[a,b], Diane E. Heck[f], Jeffrey D. Laskin [a,b,g,h]

[a] Joint Graduate Program in Toxicology, Rutgers University Graduate School of Biomedical Sciences, 170 Frelinghuysen Rd, Piscataway, NJ 08854, USA

[b] Department of Pharmacology and Toxicology, Rutgers University, 170 Frelinghuysen Rd, Piscataway, NJ 08854, USA

[c] MRIGlobal, 425 Volker Blvd., Kansas City, MO 64110, USA

[d] Ernest Mario School of Pharmacy, Rutgers the State University of New Jersey, 160 Frelinghuysen Rd, Piscataway, NJ 08854, USA

[e] Academy of Toxicological Sciences, Latham BioPharm Group, 101 Main Street, Cambridge, MA, 02142

[f] Department of Environmental Health Sciences, School of Health Sciences and Practice, New York Medical College, 40 Sunshine Cottage Rd., Valhalla, NY 10595, USA

[g] School of Public Health, Rutgers University, 170 Frelinghuysen Rd, Piscataway, NJ 08854, USA

[h] Environmental and Occupational Health Sciences Institute, Rutgers University, 170 Frelinghuysen Rd, Piscataway, NJ 08854, USA

5.1 Abstract

Sulfur mustard (SM, bis (2-chloroethyl) sulfide) is a potent skin vesicant which is recognized as a chemical threat agent. Depending on the dose and time following exposure, SM causes epidermal erosions, dermal inflammation, edema and blistering. In the present studies we used a dermal minipig model to characterize the skin wound healing process following exposure to neat SM vapor. Saturated SM vapor caps were placed on the dorsal flanks of 3-month-old male Gottingen minipigs and 48 hours post SM exposure, control and wounded sites were debrided daily for 7 days with wet to wet saline gauze soaks. After debridement, animals were sacrificed, and full thickness skin biopsies prepared for histology and immunohistochemistry. Following H&E staining, control skin contained a 3-4 cell layer thick epidermis with a prominent stratum corneum. Nine days post-SM, a well-developed eschar covered the skin, however, the epidermis beneath the eschar displayed significant wound healing with a well differentiated epidermis. Epidermis from SM-treated skin was hyperplastic (8-12 cell layers thick), a thick granular layer was evident. Control epidermis ranged from 65 to 75 microns while the SM treated epidermis ranged from 600 to 980 microns. Stratum corneum shedding, basal cell karyolysis and elongated rete ridges composed of multilayered columnar cells were also evident in the neo-epidermis. Expression of proliferating cell nuclear antigen (PCNA) was contiguous along the basal epidermal layer of both control- and SM-treated skin. PCNA was also evident in the hyperplastic rete ridges, in dermal fibroblasts, and in inflammatory cells in SM-treated skin. Trichrome staining of control skin revealed a well-developed collagen network with no delineation between the papillary and reticular dermis. A major delineation was observed in the SM-exposed dermis which contained a web-like papillary dermis composed of filamentous extracellular matrix, while the lower reticular dermis contained compacted collagen fibrils. These data demonstrate significant epidermal regeneration following SM exposure in the minipig skin model.

Further studies analyzing the wound healing process will be important to understand SM-induced skin damage and to provide a model to evaluate potential vesicant countermeasures.

Abbreviations

D/E, dermal/epidermal; H&E, hematoxylin & eosin; NM, nitrogen mustard; PCNA, proliferating cell nuclear antigen; SM, sulfur mustard

5.2 Introduction

Sulfur mustard (SM, bis (2-chloroethyl sulfide) is a potent skin vesicant that has been used in chemical warfare (Inturi*, et al.*, 2014; Jiang*, et al.*, 2018). Toxicity induced by SM is both dose- and time-dependent and is noted for its ability to cause epidermal erosions, dermal inflammation and edema, necrosis and blistering (Arck*, et al.*, 2006; Ghabili*, et al.*, 2010; Shakarjian*, et al.*, 2010; Vogt*, et al.*, 1984). These skin lesions can be slow to heal and may require months of intensive care (Alrobaiea *et al.*, 2016; Chilcott *et al.*, 2007).

Several *in-vivo* models have been established to characterize SM-induced cutaneous injury to understand the mechanism of action of SM for the development of therapeutics. This includes mouse, rat, guinea pig, rabbits and pig skin (Brown *et al.*, 1997; Chilcott*, et al.*, 2007; Joseph*, et al.*, 2011; Margulis *et al.*, 2007). Responses of human skin to SM have also been studied using mice grafted with human skin (Greenberg et al., 2006). Previous variations of this model used biopsied partial thickness human skin as graft tissue (Alrobaiea*, et al.*, 2016; Chilcott *et al.*, 2002).

The porcine model is widely accepted for chemical injury research because of its close resemblance both structurally and physiologically to the human skin (Chilcott*, et al.*, 2007; Margulis*, et al.*, 2007). The pig exhibits vesicles in the skin similar to those

observed after burns in humans (Chilcott, *et al.*, 2007; Margulis, *et al.*, 2007). The wound healing processes in the pig and human are also very similar. Most rodents heal wounds through contraction reducing wound surface size, humans and pigs heal wounds by an outgrowth from the edges of the wounds (Chilcott, *et al.*, 2007; Margulis, *et al.*, 2007).

Previous studies from our laboratory have shown that SM exposure in SKH-1 hairless mice induces histopathological changes, inflammation and DNA damage 24 hours post-exposure which persists for at least 7 days. By 14 days, there was epidermal regeneration with extensive hyperplasia (Joseph, *et al.*, 2011). The current studies use a dermal minipig model to characterize the skin wound healing process following exposure to neat SM vapor 9 days post exposure. We are looking at the formation of a neo-epidermis following exposure to determine the rate of wound healing. These studies will help examine the effects of SM exposure in pig skin and determine the extent of SM induced skin injury and repair.

5.3 Materials and Methods

Animals and Treatments

All animal experiments and SM treatments were performed at MRIGlobal Kansas City, MO. Animals received humane care in compliance with the institution's guidelines, as outlined in the *Guide for the Care and Use of Laboratory Animals published by the National Institutes of Health*. The SM vapor cap method was used to induce dermal injuries using three-month-old male Gottingen minipigs. Minipigs were anesthetized for induction of SM injuries, saline debridement, and subsequent wound care. Briefly, to generate dermal injuries, neat liquid SM (10 µl) was applied to the filter paper in the vapor caps which were then placed onto a glass surface for at least 5 minutes to allow for the formation of a vapor. Vapor caps were then placed on the dorsal skin of the animals and removed after 30 minutes. Control caps did not contain SM. After 48 hours,

SM- and control-treated skin was debrided using wet-to-wet gauze soaks, debridement continued daily for 7 days. After each debridement, exposed sites were covered with a saline gauze dressing (0.9% NaCl, sterile; Hospira, Inc., Lake Forest, IL) which was changed daily. At the end of the debridement period animals were sacrificed, and 10 mm punch biopsies of control skin and skin at wound sites were taken and immediately fixed in 10% formalin and embedded in paraffin.

Histology and Immunostaining

Tissue sections (6 µm) were prepared from paraffin embedded tissues and stained with hematoxylin and eosin (H&E) or Gomori's trichrome containing methyl (aniline) blue for analysis of collagen I/III (Histopathology Core Facility, Rutgers University, Piscataway, NJ). For immunohistochemistry, tissue sections were deparaffinized, and blocked at room temperature with either goat serum or 1% horse serum for 2 hours, and then incubated at room temperature for 30 minutes or overnight at 4 °C with primary rabbit affinity purified polyclonal antibodies to loricrin (1:400, Abcam, Cambridge, MA), vimentin (1:1200, LSBio, Seattle, WA) cytokeratin 10 (1:200, Covance, Princeton, NJ) or monoclonal antibodies against E-cadherin (1:300, Cell Signaling, Danvers, MA) and PCNA (1:300, Millipore, Burlington, MA). Mouse IgG (ProSci Inc., Poway, CA) or rabbit IgG (ProSci Inc.) was used as a control. After washing, tissue sections were incubated for 30 minutes with biotinylated goat anti-rabbit- or goat anti-mouse-secondary antibodies (Vector Labs, Burlingame, CA). Antibody binding was visualized using a DAB Peroxidase Substrate Kit (Vector Labs). Images from tissue sections were acquired at high resolution using an Olympus VS120 Virtual Microscopy System and viewed using OlyVIA software version 2.9 (Center Valley, PA).

5.4 Results

SM-induced structural changes in pig skin

In initial studies we analyzed morphological changes in pig skin during wound healing after SM treatment. H&E and Gomori's trichrome staining of control dorsal skin sections showed a well-developed laminated stratum corneum overlying a differentiated epidermis **(Figs. 5.1 & 5.3)**. The differentiated epidermis was composed of a well-defined basal layer with keratinocytes displaying prominent nuclei. Overlying the basal layer was a 4-6-cell layer thick stratum spinosum and a distinct 3-4 cell layer thick granular layer (stratum granulosum) and stratum lucidum. Hair follicles, sebaceous glands and sweat glands as well as capillaries were scattered throughout the dermis. In SM treated skin, there was extensive wound healing as evidenced by the presence of a thickened hyperplastic neo-epidermis **(Figs. 5.1 & 5.3)**. A 2-3 cell layer thick basal layer was evident which was comprised of disorganized cuboidal and columnar cells. The epidermis also contained a hyperplastic stratum spinosum with flattened keratinocytes. A thickened stratum lucidum, and a stratum granulosum containing 4-5 cell layers was also evident. Numerous birds-eye nuclei were noted in basal and suprabasal keratinocytes. The epidermis of SM treated skin was also covered by an eschar directly above the stratum lucidum; despite extensive wound healing, no contiguous stratum corneum was evident.

In control skin, a homogenous dermis was also evident with a filamentous matrix connecting reticular collagen fibrils to the basement membrane. Following SM exposure, the reticular dermis appeared to be disorganized and edematous near the basement membrane; also noted was an influx of inflammatory cells including macrophages and neutrophils at the dermal/epidermal (D/E) junction. Whereas control skin revealed a well-developed collagen network with no delineation between the papillary and reticular

dermis, following SM treatment, there was a marked delineation in the SM treated dermis **(Fig. 5.3)**. Stratum corneum shedding, basal cell karyolysis and elongated rete ridges composed of multilayered columnar epithelial cells were also evident in the neo-epidermis during wound healing following SM treatment **(Figs. 5.1 & 5.3)**.

SM exposure resulted in a significant increase in both epidermal and full thickness skin **(Fig. 5.2)**. Epidermal thickness increased 25% in skin exposed to SM when compared to control **(Fig. 5.2;** *left graph***)**. Full skin thickness increased 60% in skin exposed to SM when compared to control **(Fig. 5.2;** *right graph***)**.

Markers of proliferation, differentiation and wound healing

PCNA, a marker of cellular proliferation, was expressed within the nuclei of basal cells of the epidermis and hair follicles in control skin (Moldovan, 2007). An increase in the number of PCNA expressing cells was evident in the basal cell layer following SM treatment; these cells expressed greater levels of PCNA when compared to control cells **(Fig. 5.4)**. In both control and SM-treated skin, scattered PCNA expressing cells were evident in the flattened suprabasal cells.

Cytokeratins are intermediate filaments expressed in keratinocytes and are known to be important in regulating proliferation, differentiation and wound healing in the skin (Bragulla *et al.*, 2009; Moll *et al.*, 2008). We found that in both control and SM-treated pig skin, keratin 10, which is normally expressed in post-mitotic, differentiating keratinocytes, was selectively expressed in suprabasal epidermal keratinocytes **(Fig. 5.5)** (Santos et al., 2002). Basal cells expressed no or low levels of keratin 10. Increased levels of keratin 10 were expressed in keratinocytes in hair follicles following SM treatment **(Fig. 5.5)**.

Only low levels of keratin 17, a keratin known to be expressed largely in epidermal appendages but not interfollicular keratinocytes, were found in the epidermis of control pig skin **(Fig. 5.6)** (Mazzalupo *et al.*, 2003; Yang *et al.*, 2019). A marked increase in keratin 17 was noted in both basal and suprabasal keratinocytes following treatment with SM. Increased expression of keratin 17 was evident within the cytoplasm of the basal keratinocytes. Hair follicles from both control and SM treated skin expressed a high level of keratin 17 in the cytoplasm of outer root sheath cells **(Fig. 5.6)**.

Loricrin, a glycine-serine-cysteine-rich insoluble envelope protein, is known to be highly enriched in cornified envelopes of keratinocytes (Kim *et al.*, 2008; Nithya *et al.*, 2015)}. In control and SM-treated pig skin, loricrin was expressed in the granular layer of the epdiermis **(Fig. 5.7)**. In control skin, loricrin was expressed in a tight band of cells just below the stratum corneum while in SM-treated skin expression was spread over several layers just below the eschar. Loricrin was also expressed at the surface of hair follicles in SM-treated skin **(Fig. 5.7)**.

E-cadherin is an intracellular adhesion protein essential for the formation and maintenance of epithelial adherens junctions (Bruser *et al.*, 2017; Mendonsa *et al.*, 2018). In control skin, E-cadherin was primarily expressed in cell-cell junctions of differentiating suprabasal cells within the epidermis **(Fig. 5.8)**. The protein was also expressed within the cytoplasm of basal and suprabasal cells, but not in the stratum corneum. Less E-cadherin was expressed in the epidermis of SM-treated skin. The protein was largely confined to epithelial adherens junctions of suprabasal cells below the granular layers **(Fig. 5.8)**. Hair follicles also expressed E-cadherin in epithelial adherens junctions in the outer root sheath; the protein was expressed in hair follicles from both control and SM-treated skin **(Fig. 5.8)**.

5.5 Discussion

Sulfur mustard is a potent vesicant causing severe skin damage (Requena et al. 1988).
The formation of large, fluid-filled blisters and delay in wound healing can result in
increased infection and decreased quality of life. The biochemical basis of the
pathogenesis of SM induced skin injuries is still largely unknown. Observations of
Gottentin minipigs 9 days following challenge with SM vapor revealed ultrastructural
changes in the both the papillary and reticular dermis, as well as basal and suprabasal
keratinocytes of the epidermis. These changes included increased stratification,
parakeratosis, epidermal edema, a disorganized basal layer and dermal vacuolization.

Markers of barrier integrity were studied to determine the degree of wounding and repair
occurring 9 days post-SM exposure. The epidermal cornified cell envelope (CE) is a
complex protein-lipid composite that replaces the plasma membrane of terminally
differentiated keratinocytes (Candi *et al.*, 2005). This lamellar structure is essential for
the barrier function of the skin preventing the loss of water and ions and to protect from
environmental hazards. The major protein of the epidermal CE is loricrin. Loricrin is
expressed in the granular layer of all keratinized epithelial cells of mammals. Disruption
of the loricrin gene can lead to inherited skin diseases. Our studies observed expression
of loricrin in the stratified layer of control skin, which drastically decreased in SM
exposed skin. Similar to loricrin expression, the expression of Keratin 10, a structural
protein found in the suprabasal layers of the epidermis, was decreased in skin exposed
to SM when compared to control. This decrease may be because cells are rapidly
proliferating to cover the wound site, indicated by increased expression of PCNA in the
basal of layer of SM exposed skin.

The decrease observed in loricrin and keratin 10 expression was associated with decreases in the tight junction protein E-cadherin following SM exposure. Tight junctions are important for cell adhesion and integrity of the skin barrier. A decrease in E-cadherin, along with the other structural proteins found in the epidermis is an indication of epidermal barrier disruption.

Taken together, these data suggest that exposure of pig skin to SM leads to epidermal barrier disruption and delayed wound healing associated with increased epidermal thickness, eschar formation and. The decreased expression of epidermal structural proteins 9 days post-SM indicates the prevalence of SM in the skin and persistent epidermal damage. Understanding the mechanisms of SM induced skin injury in not only mouse models but in the minipig model as well will fill gaps in vesicant induced skin injury. This will aid in the development of potential therapeutics as treatments.

Figure 5.1 Structural Changes in Pig Skin Following Exposure to SM.

Histological sections, prepared from control (CTL) pig skin and pig skin 9 days post SM, were stained with H&E (original magnification, ×400). **A.** Panels show H&E staining in the epidermal layers of CTL (*upper panels*) and SM (*lower panels*) exposed skin at low (*left panels*) and high (*right panels*) magnification. **B.** Panels show H&E staining in the hair follicles of CTL (*upper panels*) and SM (*lower panels*) exposed skin at low (*left panels*) and high (*right panels*) magnification. Left scale bars = 100 µm; right scale bars = 20 µm. **E**, epidermis; **D**, dermis; **SC**, stratum corneum; **SL**, stratum lucidum; **SG**, stratum granulosum; **SS**, stratum spinosum; **SB**, stratum basale; **HF**, hair follicles.
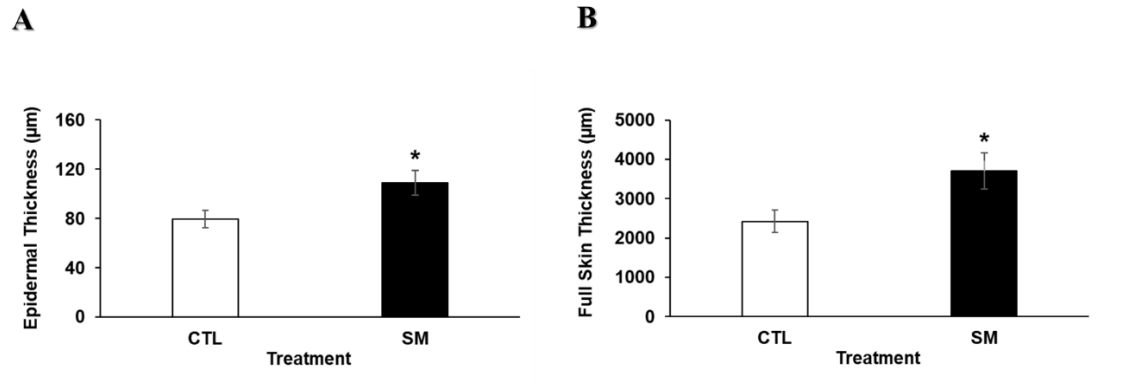
Figure 5.2 Effect of SM on Skin Thickness in Pig

Hematoxylin & Eosin (H&E) stained sections of control (CTL) pig skin and pig skin 9 days post SM exposure were analyzed and measured for epidermal and full skin thickness (μm). **A**. Epidermal thickness increased 25% in skin exposed to SM when compared to CTL. **B.** Full skin thickness increased 60% in skin exposed to SM when compared to CTL. Data are presented as mean ± SD (n = 3) *Significant from control $p \leq$ 0.05.
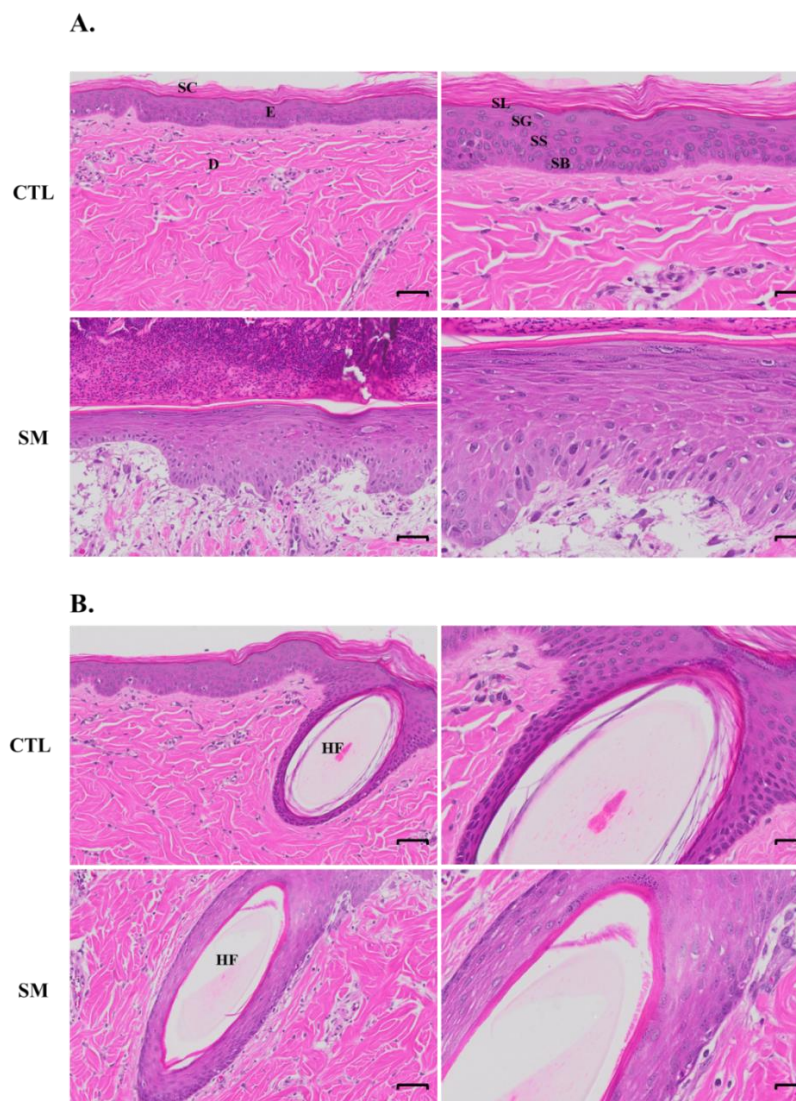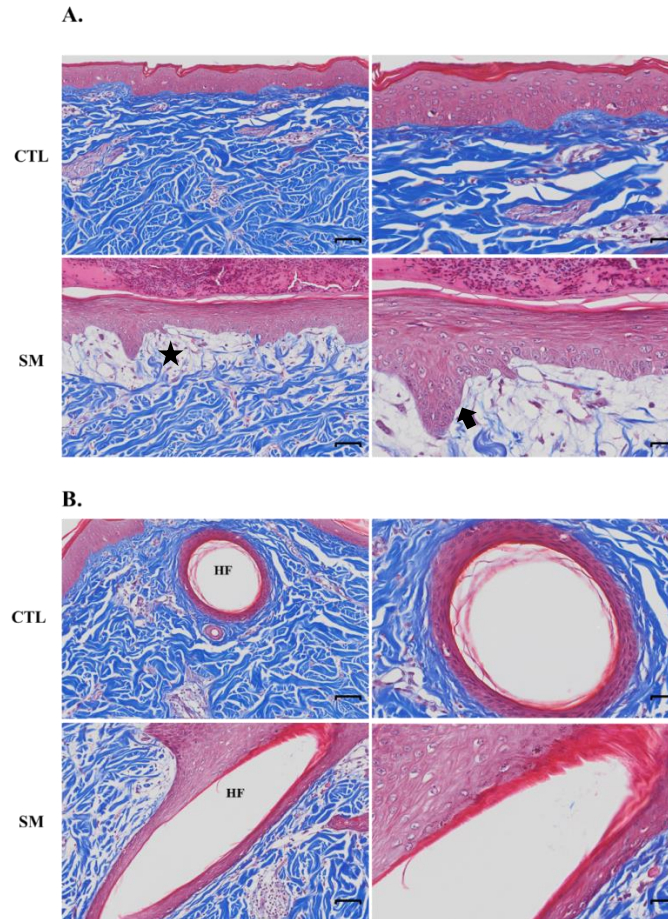
Figure 5.3 Trichrome Staining of Pig Skin Following Exposure to SM.

Histological sections, prepared from control (CTL) pig skin and pig skin 9 days post SM, were stained with Gomori's trichrome containing hematoxylin which stains nuclei dark blue/black, eosin which stains keratin and cytoplasm red, and aniline blue which stains collagen I/III royal blue (original magnification, ×400). **A.** Panels show trichrome staining in the epidermal layers of CTL (*upper panels*) and SM (*lower panels*) exposed skin at low (*left panels*) and high (*right panels*) magnification. **B.** Panels show trichrome staining in the hair follicles of CTL (*upper panels*) and SM (*lower panels*) exposed skin at low (*left panels*) and high (*right panels*) magnification. Left scale bars = 100 μm; right scale bars = 20 μm. **HF**, hair follicle; **Black star**, disorganized reticular dermis; **black arrow**, elongated rete ridges.

Figure 5.4 Effects of SM on PCNA Expression in Pig Skin.

Histological sections, prepared from control (CTL) pig skin and pig skin 9 days post SM, were stained with an antibody to proliferating cell nuclear antigen (PCNA) (original magnification, ×400). Panels show PCNA staining in the epidermal layers of CTL (*upper panels*) and SM (*lower panels*) exposed skin at low (*left panels*) and high (*right panels*) magnification. Left scale bars = 100 µm; right scale bars = 20 µm. **HF**, hair follicle; **Black arrows**, increased expression of PCNA expressing cells at the basal layer.

Figure 5.5 Effects of SM on Cytokeratin-10 Expression in Pig Skin.

Histological sections, prepared from control (CTL) pig skin and pig skin 9 days post SM, were stained with an antibody to cytokeratin-10 (original magnification, ×400). **A.** Panels show cytokeratin-10 staining in the epidermal layers of CTL (*upper panels*) and SM (*lower panels*) exposed skin at low (*left panels*) and high (*right panels*) magnification. **B.** Panels show cytokeratin-10 staining in the hair follicles of CTL (*upper panels*) and SM (*lower panels*) exposed skin at low (*left panels*) and high (*right panels*) magnification. Left scale bars = 100 μm; right scale bars = 20 μm. **HF**, hair follicle; **Black star**, suprabasal keratinocytes expressing cytokeratin-10.
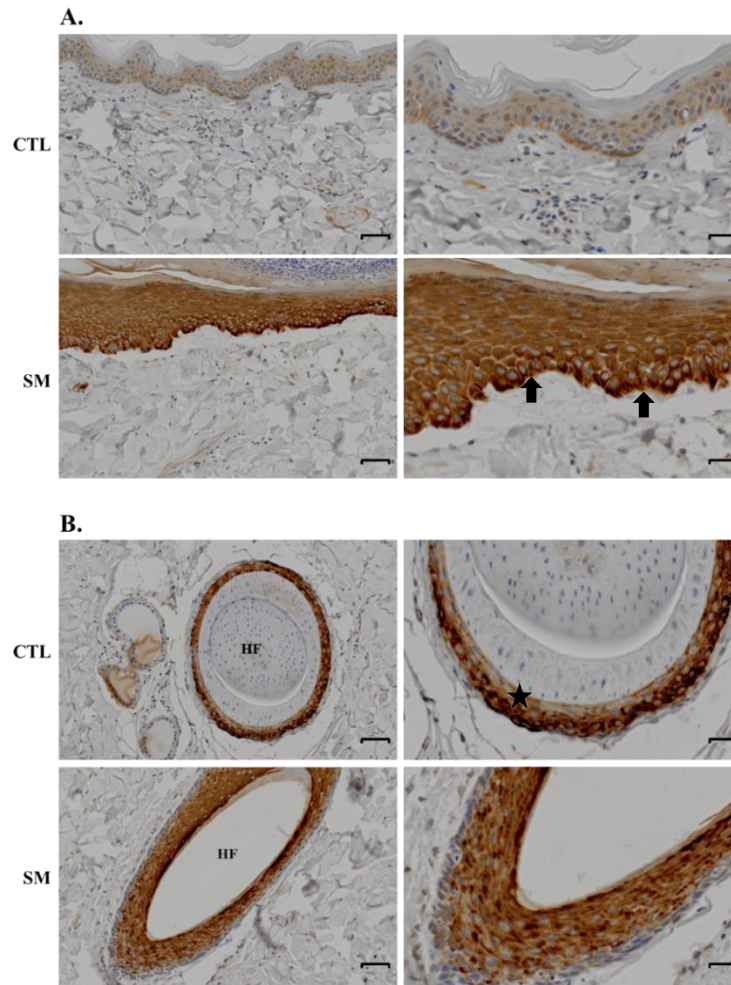
Figure 5.6 Effects of SM on Cytokeratin-17 Expression in Pig Skin.

Histological sections, prepared from control (CTL) pig skin and pig skin 9 days post SM, were stained with an antibody to cytokeratin-17 (original magnification, ×400). **A.** Panels show cytokeratin-17 staining in the epidermal layers of CTL (*upper panels*) and SM (*lower panels*) exposed skin at low (*left panels*) and high (*right panels*) magnification. **B.** Panels show cytokeratin-17 staining in the hair follicles of CTL (*upper panels*) and SM (*lower panels*) exposed skin at low (*left panels*) and high (*right panels*) magnification. Left scale bars = 100 μm; right scale bars = 20 μm. **HF**, hair follicle; **Black arrows**, cytokeratin-17 staining in the basal layer; **Black star**, cytokeratin-17 expression in hair follicle outer root sheath.
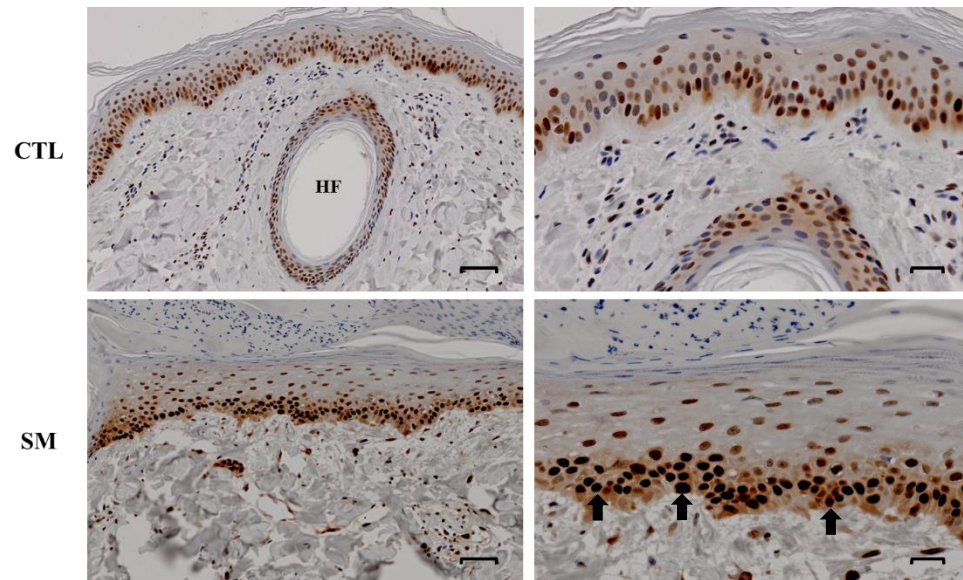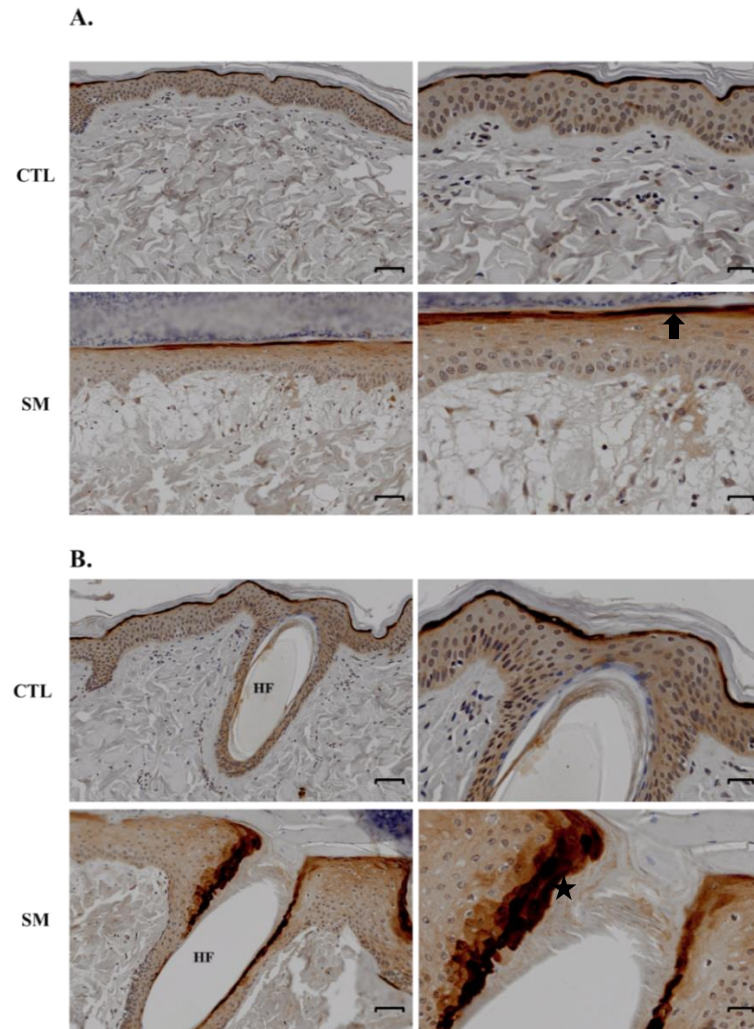
Figure 5.7 Effects of SM on Loricrin Expression in Pig Skin.

Histological sections, prepared from control (CTL) pig skin and pig skin 9 days post SM, were stained with an antibody to loricrin (original magnification, ×400). **A.** Panels show loricrin staining in the epidermal layers of CTL (*upper panels*) and SM (*lower panels*) exposed skin at low (*left panels*) and high (*right panels*) magnification. **B.** Panels show loricrin staining in the hair follicles of CTL (*upper panels*) and SM (*lower panels*) exposed skin at low (*left panels*) and high (*right panels*) magnification. Left scale bars = 100 µm; right scale bars = 20 µm. **HF**, hair follicle; **Black arrow**, loricrin expression in the stratum corneum; **Black star**, loricrin expression in hair follicles.
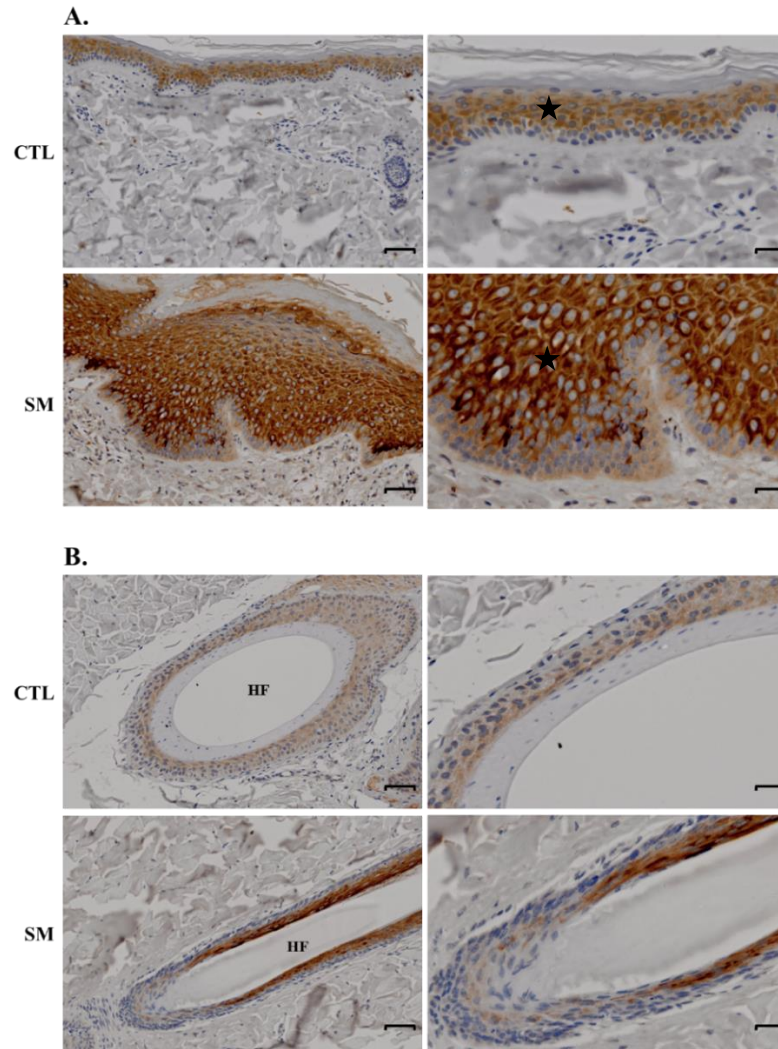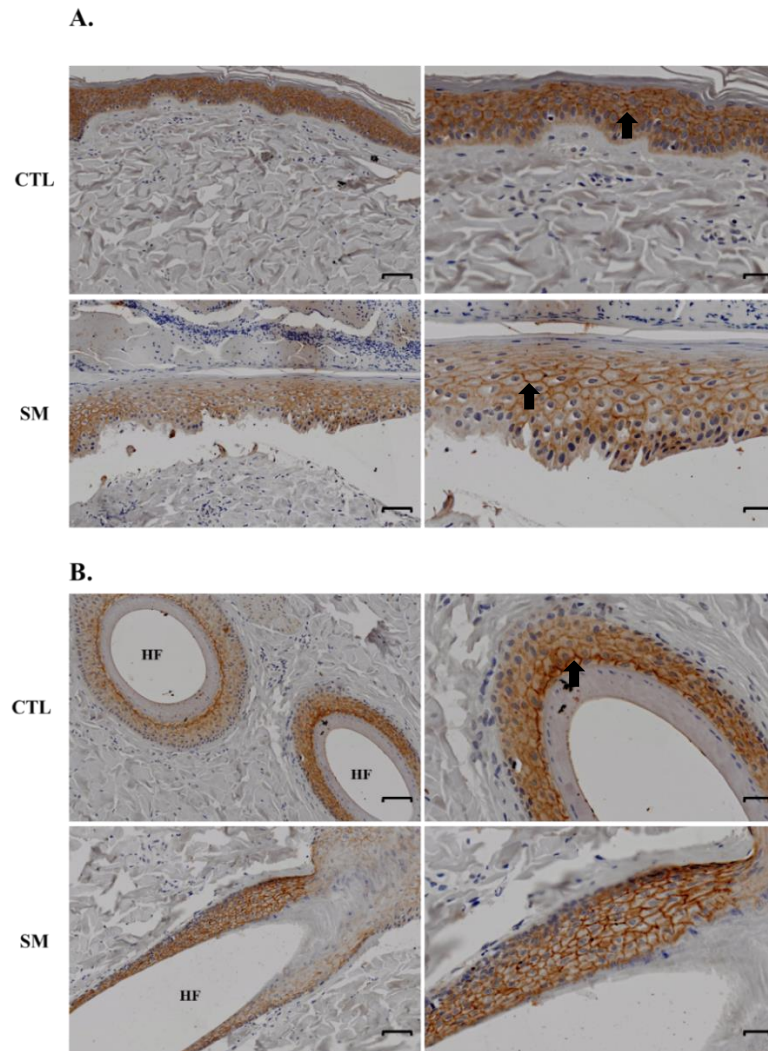
Figure 5.8 Effects of SM on E-Cadherin Expression in Pig Skin.

Histological sections, prepared from control (CTL) pig skin and pig skin 9 days post SM, were stained with an antibody to E-cadherin (original magnification, ×400). **A.** Panels show E-cadherin staining in the epidermal layers of CTL (*upper panels*) and SM (*lower panels*) exposed skin at low (*left panels*) and high (*right panels*) magnification. **B.** Panels show E-cadherin staining in the hair follicles of CTL (*upper panels*) and SM (*lower panels*) exposed skin at low (left panels) and high (right panels) magnification. Left scale bars = 100 μm; right scale bars = 20 μm. **HF**, hair follicle; **black arrows**, adheren junctions.

CHAPTER 6: OVERALL DISCUSSION

Summary

Exposure to mustard gas is a current issue. With the recent mustard gas attacks that have occurred in the Middle East leaving individuals with respiratory problems, irritation to the eyes and damage to the skin, characterization of these mustard agents is crucial to protect individuals from future attacks. An increased cause for concern is the lack of appropriate treatment for mustard induced injuries. The stratum corneum is the skins first line of defense against such agents, and if damaged the body's defense against environmental toxins and bacterial infection is impaired. Disruptions in the skin barrier results in delayed wound healing and chronic wounds, both of which are associated with mustard exposures (Kondo*, et al.*, 2010; Sandoval*, et al.*, 2007; Shakarjian*, et al.*, 2010). Both SM and NM are bifunctional alkylating agents known to induce oxidative stress, DNA damage and inflammation resulting in extensive skin damage (Arck*, et al.*, 2006; Ghabili*, et al.*, 2010; Shakarjian*, et al.*, 2010; Vogt*, et al.*, 1984). SM exposure can be localized using vapor cup models due to its lipophilic properties and countless *in-vivo* and *in-vitro* studies have been performed to better understand its mechanisms of action for the development of therapeutics. NM however, is hydrophobic and application in solvents results in spreading over large areas of skin. To better understand the mechanism of action of NM and for testing potential countermeasures the ability to generate injury in localized areas of the skin is needed. The use of the modified semi-occlusive patch test model resulted in localized and controlled NM exposures and development of wounds that were easily characterized. This allowed for a better understanding of the events immediately following NM exposure, allowing for the development and testing of potential therapeutics as countermeasures.

Vesicating Agents

Chemical agents such as mustard gas have been used in warfare since their development in the 1940s by Germany and the United States. Although NM has never been used in warfare it was stockpiled during WWII and may still be in use (Inturi*, et al.,* 2014). The ability of vesicating agents such as, SM and NM to undergo nucleophilic substitution forming a cyclic aziridinium ion is what allows them to react with nearby nucleophilic sites resulting in adduct formation and crosslinking of DNA and proteins.

Multi-Functional Anti-Inflammatory Combination Drugs

Use of a cutaneous *in-vivo* model in these studies allowed for the testing of a potential prodrug (AIDNX) as treatment against vesicant-induced skin damage. The advantage of AIDNX is that it provides a simple dosage form for two drug targets. AIDNX also has a facilitated mechanism for onsite controlled release of its individual therapeutic components. Additional prodrugs have been tested in this system and have proved to be beneficial in reducing edema resulting from NM exposures.

Conclusion

Chemical warfare is a current issue and there are currently no treatments. Because of the lack of treatment, individuals who have become exposed to mustard agents, either in warfare or in random chemical attacks can only hope they heal in time before chronic wounds and infections develop. The lack of treatment relies heavily on the fact that dermal exposures to mustard agents are hard to study and understand. NM is a commonly studied mustard agent because of its structural similarity to SM, however its hydrophobic nature makes it difficult to study in *in-vivo* models. Use of our patch test model allows for dermal toxicity studies following exposure to NM leading to wounds that are reproducible and easily studied. With this model the responses in the skin can be

observed early following exposure and potential therapeutics can be tested to determine their ability in speeding up the wound healing process, ultimately decreasing wound damage and increasing an individual's quality of life **(Fig. 6.1)**.

The prevalence of chemical warfare and the lack of countermeasures make the risk of exposure a significant concern. This work aims to shed light on skin injury following mustard exposure to understand its mode of action. My thesis research fills knowledge gaps in the fields of skin biology, dermal toxicology, environmental exposure science and chemical warfare. These studies enlist complementary methods to assess the toxic response of mustard agents on the skin and the development of countermeasures to target pathways affected. This work is aimed at identifying the mechanisms underlying the function of mustard agents, toxins used in chemical warfare, through the development of suitable *in-vivo* and *in-vitro* models to ameliorate skin injury following exposure.
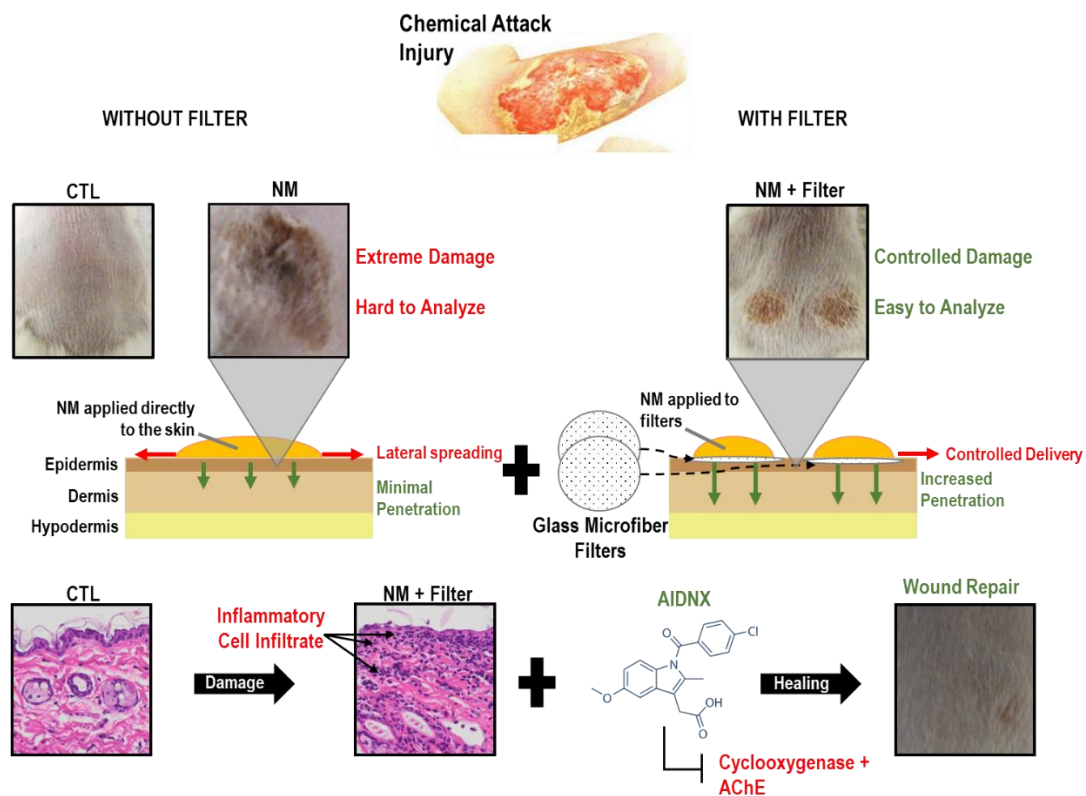
108

Figure 6.1 Graphical summary of overall project.

BIBLIOGRAPHY

Akasaka, E., Takekoshi, S., Horikoshi, Y., Toriumi, K., Ikoma, N., Mabuchi, T., Tamiya, S., Matsuyama, T., and Ozawa, A. (2010). Protein oxidative damage and heme oxygenase in sunlight-exposed human skin: roles of MAPK responses to oxidative stress. *Tokai J Exp Clin Med* **35**(4), 152-64.

Alagpulinsa, D. A., Ayyadevara, S., and Shmookler Reis, R. J. (2014). A Small-Molecule Inhibitor of RAD51 Reduces Homologous Recombination and Sensitizes Multiple Myeloma Cells to Doxorubicin. *Front Oncol* **4**, 289.

Alestas, T., Ganceviciene, R., Fimmel, S., Muller-Decker, K., and Zouboulis, C. C. (2006). Enzymes involved in the biosynthesis of leukotriene B4 and prostaglandin E2 are active in sebaceous glands. *J. Mol. Med. (Berl.)* **84**(1), 75-87.

Alrobaiea, S. M., Ding, J., Ma, Z., and Tredget, E. E. (2016). A Novel Nude Mouse Model of Hypertrophic Scarring Using Scratched Full Thickness Human Skin Grafts. *Adv Wound Care* **5**(7), 299-313.

Anderson, D. R., Mitcheltree, L. W., Brobst, D. E., Byers, S. L., Merz, D. F., and Gold, M. B. (2002). A vapor exposure model for neonatal mice. *Toxicol Mech Methods* **12**(1), 59-70.

Anishkin, A., Loukin, S. H., Teng, J., and Kung, C. (2014). Feeling the hidden mechanical forces in lipid bilayer is an original sense. *Proc Natl Acad Sci U S A* **111**(22), 7898-905.

Arck, P., and Paus, R. (2006). From the brain-skin connection: the neuroendocrine-immune misalliance of stress and itch. *Neuroimmunomodulation* **13**(5-6), 347-56.

Aredia, F., and Scovassi, A. I. (2014). Poly(ADP-ribose): a signaling molecule in different paradigms of cell death. *Biochem Pharmacol* **92**(1), 157-63.

Au, L., Meisch, J. P., Das, L. M., Binko, A. M., Boxer, R. S., Wen, A. M., Steinmetz, N. F., and Lu, K. Q. (2015). Suppression of Hyperactive Immune Responses Protects against Nitrogen Mustard Injury. *J Invest Dermatol* **135**(12), 2971-2981.

Avci, P., Sadasivam, M., Gupta, A., De Melo, W. C., Huang, Y. Y., Yin, R., Chandran, R., Kumar, R., Otufowora, A., Nyame, T., and Hamblin, M. R. (2013). Animal models of skin disease for drug discovery. *Expert Opin Drug Discov* **8**(3), 331-55.

Barnard, A., and Gordon, M. R. (2017). Worst Chemical Attack in Years in Syria; U.S. Blames Assad. In *NY Times* (

Barnes, L., Dumas, M., Juan, M., Noblesse, E., Tesniere, A., Schnebert, S., Guillot, B., and Moles, J. P. (2010). GammaH2AX, an accurate marker that analyzes UV genotoxic effects on human keratinocytes and on human skin. *Photochem. Photobiol.* **86**(4), 933-41.

Barnum, K. J., and O'Connell, M. J. (2014). Cell cycle regulation by checkpoints. *Methods Mol Biol* **1170**, 29-40.

Barrett, C. W., Hadgraft, J. W., and Sarkany, I. (1964). The Influence of Vehicles on Skin Penetration. *J Pharm Pharmacol* **16**, SUPPL:104-7T.

Batal, M., Boudry, I., Mouret, S., Clery-Barraud, C., Wartelle, J., Berard, I., and Douki, T. (2014). DNA damage in internal organs after cutaneous exposure to sulphur mustard. *Toxicol Appl Pharmacol* **278**(1), 39-44.

Black, A. T., Hayden, P. J., Casillas, R. P., Heck, D. E., Gerecke, D. R., Sinko, P. J., Laskin, D. L., and Laskin, J. D. (2010). Expression of proliferative and inflammatory markers in a full-thickness human skin equivalent following exposure to the model sulfur mustard vesicant, 2-chloroethyl ethyl sulfide. *Toxicol. Appl. Pharmacol.* **249**(2), 178-87.

Blattner, C. M., Coman, G., Blickenstaff, N. R., and Maibach, H. I. (2014). Percutaneous absorption of water in skin: a review. *Rev Environ Health* **29**(3), 175-80.

Bragulla, H. H., and Homberger, D. G. (2009). Structure and functions of keratin proteins in simple, stratified, keratinized and cornified epithelia. *J Anat* **214**(4), 516-59.

Brown, R. F., and Rice, P. (1997). Histopathological changes in Yucatan minipig skin following challenge with sulphur mustard. A sequential study of the first 24 hours following challenge. *Int J Exp Pathol* **78**(1), 9-20.

Bruser, L., and Bogdan, S. (2017). Adherens Junctions on the Move-Membrane Trafficking of E-Cadherin. *Cold Spring Harb Perspect Biol* **9**(3).

Buehler, E. V. (1994). Occlusive patch method for skin sensitization in guinea pigs: the Buehler method. *Food Chem Toxicol* **32**(2), 97-101.

Cals-Grierson, M. M., and Ormerod, A. D. (2004). Nitric oxide function in the skin. *Nitric Oxide* **10**(4), 179-93.

Candi, E., Schmidt, R., and Melino, G. (2005). The cornified envelope: a model of cell death in the skin. *Nat Rev Mol Cell Biol* **6**(4), 328-40.

Casillas, R. P., Kiser, R. C., Truxall, J. A., Singer, A. W., Shumaker, S. M., Niemuth, N. A., Ricketts, K. M., Mitcheltree, L. W., Castrejon, L. R., and Blank, J. A. (2000). Therapeutic approaches to dermatotoxicity by sulfur mustard. I. Modulaton of sulfur mustard-induced cutaneous injury in the mouse ear vesicant model. *J Appl Toxicol* **20 Suppl 1**, S145-51.

Chang, Y. C., Sabourin, C. L., Lu, S. E., Sasaki, T., Svoboda, K. K., Gordon, M. K., Riley, D. J., Casillas, R. P., and Gerecke, D. R. (2009). Upregulation of gamma-2 laminin-332 in the mouse ear vesicant wound model. *J Biochem Mol Toxicol* **23**(3), 172-84.

Chang, Y. C., Wang, J. D., Hahn, R. A., Gordon, M. K., Joseph, L. B., Heck, D. E., Heindel, N. D., Young, S. C., Sinko, P. J., Casillas, R. P., Laskin, J. D., Laskin, D. L., and Gerecke, D. R. (2014). Therapeutic potential of a non-steroidal bifunctional anti-inflammatory and anti-cholinergic agent against skin injury induced by sulfur mustard. *Toxicol. Appl. Pharmacol.* **280**(2), 236-44.

Chang, Y. C., Wang, J. D., Svoboda, K. K., Casillas, R. P., Laskin, J. D., Gordon, M. K., and Gerecke, D. R. (2013). Sulfur mustard induces an endoplasmic reticulum stress response in the mouse ear vesicant model. *Toxicol Appl Pharmacol* **268**(2), 178-87.

Chantasart, D., and Li, S. K. (2012). Structure Enhancement Relationship of Chemical Penetration Enhancers in Drug Transport across the Stratum Corneum. *Pharmaceutics* **4**(1), 71-92.

Chaquour, B., Seite, S., Coutant, K., Fourtanier, A., Borel, J. P., and Bellon, G. (1995). Chronic UVB- and all-trans retinoic-acid-induced qualitative and quantitative changes in hairless mouse skin. *J Photochem Photobiol B* **28**(2), 125-35.

Chew, A. L., and Maibach, H. I. (2003). Occupational issues of irritant contact dermatitis. *Int Arch Occup Environ Health* **76**(5), 339-46.

Chilcott, R. P., Dalton, C. H., Ashley, Z., Allen, C. E., Bradley, S. T., Maidment, M. P., Jenner, J., Brown, R. F., Gwyther, R. J., and Rice, P. (2007). Evaluation of barrier creams against sulphur mustard: (II) In vivo and in vitro studies using the domestic white pig. *Cutan Ocul Toxicol* **26**(3), 235-47.

Chilcott, R. P., Jenner, J., Hotchkiss, S. A., and Rice, P. (2002). Evaluation of barrier creams against sulphur mustard. I. In vitro studies using human skin. *Skin Pharmacol Appl Skin Physiol* **15**(4), 225-35.

Clingen, P. H., Wu, J. Y., Miller, J., Mistry, N., Chin, F., Wynne, P., Prise, K. M., and Hartley, J. A. (2008). Histone H2AX phosphorylation as a molecular pharmacological marker for DNA interstrand crosslink cancer chemotherapy. *Biochem Pharmacol* **76**(1), 19-27.

Composto, G. M., Laskin, J. D., Laskin, D. L., Gerecke, D. R., Casillas, R. P., Heindel, N. D., Joseph, L. B., and Heck, D. E. (2016). Mitigation of nitrogen mustard mediated skin injury by a novel indomethacin bifunctional prodrug. *Exp Mol Pathol* **100**(3), 522-31.

Debiak, M., Lex, K., Ponath, V., Burckhardt-Boer, W., Thiermann, H., Steinritz, D., Schmidt, A., Mangerich, A., and Burkle, A. (2016). Immunochemical analysis of poly(ADP-ribosyl)ation in HaCaT keratinocytes induced by the mono-alkylating agent 2-chloroethyl ethyl sulfide (CEES): Impact of experimental conditions. *Toxicol Lett* **244**, 72-80.

Dutagaci, B., Becker-Baldus, J., Faraldo-Gomez, J. D., and Glaubitz, C. (2014). Ceramide-lipid interactions studied by MD simulations and solid-state NMR. *Biochim Biophys Acta* **1838**(10), 2511-9.

El Maghraby, G. M., Ahmed, A. A., and Osman, M. A. (2015). Penetration enhancers in proniosomes as a new strategy for enhanced transdermal drug delivery. *Saudi Pharm J* **23**(1), 67-74.

Elias, P. M. (2008). Skin barrier function. *Curr Allergy Asthma Rep* **8**(4), 299-305.

Elias, P. M. (2014). Lipid abnormalities and lipid-based repair strategies in atopic dermatitis. *Biochim Biophys Acta* **1841**(3), 323-30.

Elkholi, R., and Chipuk, J. E. (2014). How do I kill thee? Let me count the ways: p53 regulates PARP-1 dependent necrosis. *Bioessays* **36**(1), 46-51.

Emanuele, E., Spencer, J. M., and Braun, M. (2014). An experimental double-blind irradiation study of a novel topical product (TPF 50) compared to other topical products with DNA repair enzymes, antioxidants, and growth factors with sunscreens: implications for preventing skin aging and cancer. *J Drugs Dermatol* **13**(3), 309-14.

Farage, M. A., Maibach, H. I., Andersen, K. E., Lachapelle, J. M., Kern, P., Ryan, C., Ely, J., and Kanti, A. (2011). Historical perspective on the use of visual grading scales in evaluating skin irritation and sensitization. *Contact Dermatitis* **65**(2), 65-75.

Fischer, T., and Kihlman, I. (1989). Patch testing technique. *J Am Acad Dermatol* **21**(4 Pt 2), 830-2.

Frank, S., Kampfer, H., Wetzler, C., and Pfeilschifter, J. (2002). Nitric oxide drives skin repair: novel functions of an established mediator. *Kidney Int.* **61**(3), 882-8.

Ghabili, K., Agutter, P. S., Ghanei, M., Ansarin, K., and Shoja, M. M. (2010). Mustard gas toxicity: the acute and chronic pathological effects. *J Appl Toxicol* **30**(7), 627-43.

Gopee, N. V., Cui, Y., Olson, G., Warbritton, A. R., Miller, B. J., Couch, L. H., Wamer, W. G., and Howard, P. C. (2005). Response of mouse skin to tattooing: use of SKH-1 mice as a surrogate model for human tattooing. *Toxicol Appl Pharmacol* **209**(2), 145-58.

Goswami, D. G., Kumar, D., Tewari-Singh, N., Orlicky, D. J., Jain, A. K., Kant, R., Rancourt, R. C., Dhar, D., Inturi, S., Agarwal, C., White, C. W., and Agarwal, R. (2015). Topical nitrogen mustard exposure causes systemic toxic effects in mice. *Exp Toxicol Pathol* **67**(2), 161-70.

Gozzelino, R., Jeney, V., and Soares, M. P. (2010). Mechanisms of cell protection by heme oxygenase-1. *Annu Rev Pharmacol Toxicol* **50**, 323-54.

Graham, J. S., Chilcott, R. P., Rice, P., Milner, S. M., Hurst, C. G., and Maliner, B. I. (2005). Wound healing of cutaneous sulfur mustard injuries: strategies for the development of improved therapies. *J Burns Wounds* **4**, e1.

Graham, J. S., Reid, F. M., Smith, J. R., Stotts, R. R., Tucker, E. S., Shumaker, S. M., Niemuth, N. A., and Janny, S. J. (2000). A cutaneous full-thickness liquid sulfur mustard burn model in weanling swine: clinical pathology and urinary excretion of thiodiglycol. *J Appl Toxicol* **20 Suppl 1**, S161-72.

Graham, J. S., Schomacker, K. T., Glatter, R. D., Briscoe, C. M., Braue, E. H., Jr., and Squibb, K. S. (2002). Efficacy of laser debridement with autologous split-thickness skin grafting in promoting improved healing of deep cutaneous sulfur mustard burns. *Burns* **28**(8), 719-30.

Graham, J. S., and Schoneboom, B. A. (2013). Historical perspective on effects and treatment of sulfur mustard injuries. *Chem Biol Interact* **206**(3), 512-22.

Grando, S. A., Kist, D. A., Qi, M., and Dahl, M. V. (1993). Human keratinocytes synthesize, secrete, and degrade acetylcholine. *J. Invest. Dermatol.* **101**(1), 32-6.

Gutteridge, J. M. (1995). Lipid peroxidation and antioxidants as biomarkers of tissue damage. *Clin Chem* **41**(12 Pt 2), 1819-28.

Hadebe, S. I., Ngubane, P. S., Serumula, M. R., and Musabayane, C. T. (2014). Transdermal delivery of insulin by amidated pectin hydrogel matrix patch in streptozotocin-induced diabetic rats: effects on some selected metabolic parameters. *PLoS One* **9**(7), e101461.

Heck, D. E., Laskin, D. L., Gardner, C. R., and Laskin, J. D. (1992). Epidermal growth factor suppresses nitric oxide and hydrogen peroxide production by keratinocytes. Potential role for nitric oxide in the regulation of wound healing. *J Biol Chem* **267**(30), 21277-80.

Hogan, M. B., Peele, K., and Wilson, N. W. (2012). Skin barrier function and its importance at the start of the atopic march. *J Allergy* **2012**, 901940.

Hojer, J., Personne, M., Hulten, P., and Ludwigs, U. (2002). Topical treatments for hydrofluoric acid burns: a blind controlled experimental study. *J Toxicol Clin Toxicol* **40**(7), 861-6.

Hosnuter, M., Melikoglu, C., Aslan, C., Saglam, G., and Sutcu, R. (2015). The Protective Effects of Epigallocatechin Gallate Against Distant Organ Damage After Severe Skin Burns--Experimental Study Using a Rat Model of Thermal Trauma. *Adv Clin Exp Med* **24**(3), 409-17.

Huang, Y., and Li, L. (2013). DNA crosslinking damage and cancer - a tale of friend and foe. *Transl Cancer Res* **2**(3), 144-154.

Huang, Y., Li, W., and Kong, A. N. (2012). Anti-oxidative stress regulator NF-E2-related factor 2 mediates the adaptive induction of antioxidant and detoxifying enzymes by lipid peroxidation metabolite 4-hydroxynonenal. *Cell Biosci* **2**(1), 40.

Hulten, P., Hojer, J., Ludwigs, U., and Janson, A. (2004). Hexafluorine vs. standard decontamination to reduce systemic toxicity after dermal exposure to hydrofluoric acid. *J Toxicol Clin Toxicol* **42**(4), 355-61.

Ibrahim, S. A., and Li, S. K. (2010). Chemical enhancer solubility in human stratum corneum lipids and enhancer mechanism of action on stratum corneum lipid domain. *Int J Pharm* **383**(1-2), 89-98.

Inturi, S., Tewari-Singh, N., Agarwal, C., White, C. W., and Agarwal, R. (2014). Activation of DNA damage repair pathways in response to nitrogen mustard-induced DNA damage and toxicity in skin keratinocytes. *Mutat. Res.* **763-764**, 53-63.

Inturi, S., Tewari-Singh, N., Jain, A. K., Roy, S., White, C. W., and Agarwal, R. (2013). Absence of a p53 allele delays nitrogen mustard-induced early apoptosis and inflammation of murine skin. *Toxicology* **311**(3), 184-90.

Jafari, M. (2007). Dose- and time-dependent effects of sulfur mustard on antioxidant system in liver and brain of rat. *Toxicology* **231**(1), 30-9.

Jain, A. K., Tewari-Singh, N., Gu, M., Inturi, S., White, C. W., and Agarwal, R. (2011). Sulfur mustard analog, 2-chloroethyl ethyl sulfide-induced skin injury involves DNA damage and induction of inflammatory mediators, in part via oxidative stress, in SKH-1 hairless mouse skin. *Toxicol. Lett.* **205**(3), 293-301.

Jain, A. K., Tewari-Singh, N., Inturi, S., Orlicky, D. J., White, C. W., and Agarwal, R. (2014). Histopathological and immunohistochemical evaluation of nitrogen mustard-induced cutaneous effects in SKH-1 hairless and C57BL/6 mice. *Exp Toxicol Pathol* **66**(2-3), 129-38.

Jan, Y. H., Heck, D. E., Gray, J. P., Zheng, H., Casillas, R. P., Laskin, D. L., and Laskin, J. D. (2010). Selective targeting of selenocysteine in thioredoxin reductase by the half mustard 2-chloroethyl ethyl sulfide in lung epithelial cells. *Chem Res Toxicol* **23**(6), 1045-53.

Jan, Y. H., Heck, D. E., Malaviya, R., Casillas, R. P., Laskin, D. L., and Laskin, J. D. (2014). Cross-linking of thioredoxin reductase by the sulfur mustard analogue mechlorethamine (methylbis(2-chloroethyl)amine) in human lung epithelial cells and rat lung: selective inhibition of disulfide reduction but not redox cycling. *Chem Res Toxicol* **27**(1), 61-75.

Jasin, M., and Rothstein, R. (2013). Repair of strand breaks by homologous recombination. *Cold Spring Harb Perspect Biol* **5**(11), a012740.

Jiang, A., and Maibach, H. (2018). Dermatotoxicology of sulfur mustard: Historical perspectives from World War I. *J Appl Toxicol* **38**(1), 108-112.

Joseph, L. B., Composto, G. M., Perez, R. M., Kim, H. D., Casillas, R. P., Heindel, N. D., Young, S. C., Lacey, C. J., Saxena, J., Guillon, C. D., Croutch, C. R., Laskin, J. D., and Heck, D. E. (2018). Sulfur mustard induced mast cell degranulation in mouse skin is inhibited by a novel anti-inflammatory and anticholinergic bifunctional prodrug. *Toxicol Lett* **293**, 77-81.

Joseph, L. B., Gerecke, D. R., Heck, D. E., Black, A. T., Sinko, P. J., Cervelli, J. A., Casillas, R. P., Babin, M. C., Laskin, D. L., and Laskin, J. D. (2011). Structural changes in the skin of hairless mice following exposure to sulfur mustard correlate with inflammation and DNA damage. *Exp Mol Pathol* **91**(2), 515-27.

Joseph, L. B., Heck, D. E., Cervelli, J. A., Composto, G. M., Babin, M. C., Casillas, R. P., Sinko, P. J., Gerecke, D. R., Laskin, D. L., and Laskin, J. D. (2014). Structural changes in hair follicles and sebaceous glands of hairless mice following exposure to sulfur mustard. *Exp. Mol. Pathol.* **96**(3), 316-27.

Jowsey, P. A., and Blain, P. G. (2015). Checkpoint kinase 1 is activated and promotes cell survival after exposure to sulphur mustard. *Toxicol Lett* **232**(2), 413-21.

Jowsey, P. A., Williams, F. M., and Blain, P. G. (2009). DNA damage, signalling and repair after exposure of cells to the sulphur mustard analogue 2-chloroethyl ethyl sulphide. *Toxicology* **257**(3), 105-12.

Jung, E. C., and Maibach, H. I. (2015). Animal models for percutaneous absorption. *J Appl Toxicol* **35**(1), 1-10.

Kapoor, M., Kojima, F., Yang, L., and Crofford, L. J. (2007). Sequential induction of pro- and anti-inflammatory prostaglandins and peroxisome proliferators-activated receptor-gamma during normal wound healing: a time course study. *Prostaglandins Leukot. Essent. Fat. Acids* **76**(2), 103-12.

Kehe, K., Balszuweit, F., Steinritz, D., and Thiermann, H. (2009). Molecular toxicology of sulfur mustard-induced cutaneous inflammation and blistering. *Toxicology* **263**(1), 12-9.

Kehe, K., Raithel, K., Kreppel, H., Jochum, M., Worek, F., and Thiermann, H. (2008). Inhibition of poly(ADP-ribose) polymerase (PARP) influences the mode of sulfur mustard (SM)-induced cell death in HaCaT cells. *Arch Toxicol* **82**(7), 461-70.

Kehe, K., and Szinicz, L. (2005). Medical aspects of sulphur mustard poisoning. *Toxicology* **214**(3), 198-209.

Kim, B. E., Leung, D. Y., Boguniewicz, M., and Howell, M. D. (2008). Loricrin and involucrin expression is down-regulated by Th2 cytokines through STAT-6. *Clin Immunol* **126**(3), 332-7.

King, A., and Bowe, J. (2015). Animal models for diabetes: Understanding the pathogenesis and finding new treatments. *Biochem Pharmacol* doi: 10.1016/j.bcp.2015.08.108.

Kligman, L. H. (1996). The hairless mouse model for photoaging. *Clin Dermatol* **14**(2), 183-95.

Kondo, T., and Ishida, Y. (2010). Molecular pathology of wound healing. *Forensic Sci Int* **203**(1-3), 93-8.

Kumar, D., Tewari-Singh, N., Agarwal, C., Jain, A. K., Inturi, S., Kant, R., White, C. W., and Agarwal, R. (2015). Nitrogen mustard exposure of murine skin induces DNA damage, oxidative stress and activation of MAPK/Akt-AP1 pathway leading to induction of inflammatory and proteolytic mediators. *Toxicol Lett* **235**(3), 161-71.

Kurzen, H., Wessler, I., Kirkpatrick, C. J., Kawashima, K., and Grando, S. A. (2007). The non-neuronal cholinergic system of human skin. *Horm Metab Res* **39**(2), 125-35.

Langerak, P., and Russell, P. (2011). Regulatory networks integrating cell cycle control with DNA damage checkpoints and double-strand break repair. *Philos Trans R Soc Lond B Biol Sci* **366**(1584), 3562-71.

Laplante, A. F., Germain, L., Auger, F. A., and Moulin, V. (2001). Mechanisms of wound reepithelialization: hints from a tissue-engineered reconstructed skin to long-standing questions. *FASEB J.* **15**(13), 2377-89.

Laskin, J. D., Black, A. T., Jan, Y. H., Sinko, P. J., Heindel, N. D., Sunil, V., Heck, D. E., and Laskin, D. L. (2010). Oxidants and antioxidants in sulfur mustard-induced injury. *Ann N Y Acad Sci* **1203**, 92-100.

Lee, J. L., Mukhtar, H., Bickers, D. R., Kopelovich, L., and Athar, M. (2003). Cyclooxygenases in the skin: pharmacological and toxicological implications. *Toxicol Appl Pharmacol* **192**(3), 294-306.

Lee, Y., Je, Y. J., Lee, S. S., Li, Z. J., Choi, D. K., Kwon, Y. B., Sohn, K. C., Im, M., Seo, Y. J., and Lee, J. H. (2012). Changes in transepidermal water loss and skin hydration according to expression of aquaporin-3 in psoriasis. *Ann Dermatol* **24**(2), 168-74.

Lefkowitz, L. J., and Smith, W. J. (2002). Sulfur mustard-induced arachidonic acid release is mediated by phospholipase D in human keratinocytes. *Biochem. Biophys. Res. Commun.* **295**(5), 1062-7.

Lieber, M. R. (2010). The mechanism of double-strand DNA break repair by the nonhomologous DNA end-joining pathway. *Annu Rev Biochem* **79**, 181-211.

Liu, F., Jiang, N., Xiao, Z. Y., Cheng, J. P., Mei, Y. Z., Zheng, P., Wang, L., Zhang, X. R., Zhou, X. B., Zhou, W. X., and Zhang, Y. X. (2016). Effects of poly (ADP-ribose) polymerase-1 (PARP-1) inhibition on sulfur mustard-induced cutaneous injuries in vitro and in vivo. *PeerJ* **4**, e1890.

Mah, L. J., El-Osta, A., and Karagiannis, T. C. (2010). gammaH2AX: a sensitive molecular marker of DNA damage and repair. *Leukemia* **24**(4), 679-86.

Mahajan, K., and Mahajan, N. P. (2015). Cross talk of tyrosine kinases with the DNA damage signaling pathways. *Nucleic Acids Res* **43**(22), 10588-601.

Mann, D. J. (2010). Aziridinium ion ring formation from nitrogen mustards: mechanistic insights from ab initio dynamics. *J Phys Chem A* **114**(13), 4486-93.

Mao, Z., Bozzella, M., Seluanov, A., and Gorbunova, V. (2008). DNA repair by nonhomologous end joining and homologous recombination during cell cycle in human cells. *Cell Cycle* **7**(18), 2902-6.

Margulis, A., Chaouat, M., Ben-Bassat, H., Eldad, A., Ickson, M., Breiterman, S., and Neuman, R. (2007). Comparison of topical iodine and silver sulfadiazine as therapies against sulfur mustard burns in a pig model. *Wound Repair Regen* **15**(6), 916-21.

Mazzalupo, S., Wong, P., Martin, P., and Coulombe, P. A. (2003). Role for keratins 6 and 17 during wound closure in embryonic mouse skin. *Dev Dyn* **226**(2), 356-65.

Mejia-Ramirez, E., Limbo, O., Langerak, P., and Russell, P. (2015). Critical Function of gammaH2A in S-Phase. *PLoS Genet.* **11**(9), e1005517.

Mendonsa, A. M., Na, T. Y., and Gumbiner, B. M. (2018). E-cadherin in contact inhibition and cancer. *Oncogene* **37**(35), 4769-4780.

Menon, G. K., Cleary, G. W., and Lane, M. E. (2012). The structure and function of the stratum corneum. *Int J Pharm* **435**(1), 3-9.

Mershon, M. M., Mitcheltree, L. W., Petrali, J. P., Braue, E. H., and Wade, J. V. (1990). Hairless guinea pig bioassay model for vesicant vapor exposures. *Fundam Appl Toxicol* **15**(3), 622-30.

Meyyappan, M., Wong, H., Hull, C., and Riabowol, K. T. (1998). Increased expression of cyclin D2 during multiple states of growth arrest in primary and established cells. *Mol Cell Biol* **18**(6), 3163-72.

Mitchell, J. A., Larkin, S., and Williams, T. J. (1995). Cyclooxygenase-2: regulation and relevance in inflammation. *Biochem. Pharmacol.* **50**(10), 1535-42.

Moldovan, G. L., Pfander, B., and Jentsch, S. (2007). PCNA, the maestro of the replication fork. *Cell* **129**(4), 665-79.

Moll, R., Divo, M., and Langbein, L. (2008). The human keratins: biology and pathology. *Histochem Cell Biol* **129**(6), 705-33.

Moncada, S. (1999). Nitric oxide: discovery and impact on clinical medicine. *J. R. Soc. Med.* **92**(4), 164-9.

Monteiro-Riviere, N. A., Inman, A. O., Babin, M. C., and Casillas, R. P. (1999). Immunohistochemical characterization of the basement membrane epitopes in bis(2-chloroethyl) sulfide-induced toxicity in mouse ear skin. *J Appl Toxicol* **19**(5), 313-28.

Murdock, H. (2017). Suspected Mosul Mustard Gas Victims Recovering; Foul Smells Remain. In (Murdock, Ed.), Vol. 2017.

Murphrey, M. B., and Zito, P. M. (2019). Histology, Stratum Corneum. In *StatPearls*, Treasure Island (FL).

Ng, M. F. (2010). The role of mast cells in wound healing. *Int. Wound J.* **7**(1), 55-61.

Nicholson, M., and Willis, C. M. (1999). The influence of patch test size and design on the distribution of erythema induced by sodium lauryl sulfate. *Contact Dermatitis* **41**(5), 264-7.

Nithya, S., Radhika, T., and Jeddy, N. (2015). Loricrin - an overview. *J Oral Maxillofac Pathol* **19**(1), 64-8.

Noli, C., and Miolo, A. (2001). The mast cell in wound healing. *Vet. Dermatol.* **12**(6), 303-13.

Notman, R., Anwar, J., Briels, W. J., Noro, M. G., and den Otter, W. K. (2008). Simulations of skin barrier function: free energies of hydrophobic and hydrophilic transmembrane pores in ceramide bilayers. *Biophys J* **95**(10), 4763-71.

Nyska, A., Lomnitski, L., Maronpot, R., Moomaw, C., Brodsky, B., Sintov, A., and Wormser, U. (2001). Effects of iodine on inducible nitric oxide synthase and

cyclooxygenase-2 expression in sulfur mustard-induced skin. *Arch. Toxicol.* **74**(12), 768-74.

Oehmichen, M., Gronki, T., Meissner, C., Anlauf, M., and Schwark, T. (2009). Mast cell reactivity at the margin of human skin wounds: an early cell marker of wound survival? *Forensic Sci. Int.* **191**(1-3), 1-5.

Ogiso, T., Hata, T., Iwaki, M., and Tanino, T. (2001). Transdermal absorption of bupranolol in rabbit skin in vitro and in vivo. *Biol Pharm Bull* **24**(5), 588-91.

Pan, T. L., Wang, P. W., Aljuffali, I. A., Huang, C. T., Lee, C. W., and Fang, J. Y. (2015). The impact of urban particulate pollution on skin barrier function and the subsequent drug absorption. *J Dermatol Sci* **78**(1), 51-60.

Papirmeister, B., Gross, C. L., Meier, H. L., Petrali, J. P., and Johnson, J. B. (1985). Molecular basis for mustard-induced vesication. *Fundam Appl Toxicol* **5**(6 Pt 2), S134-49.

Park, E. J., Kim, Y. M., and Chang, K. C. (2017). Hemin Reduces HMGB1 Release by UVB in an AMPK/HO-1-dependent Pathway in Human Keratinocytes HaCaT Cells. *Arch Med Res* **48**(5), 423-431.

Park, S. Y., Jeong, M. S., Han, C. W., Yu, H. S., and Jang, S. B. (2015). Structural and functional insight into proliferating cell nuclear antigen. *J. Microbiol. Biotechnol.* **26**, 637-642.

Paromov, V., Suntres, Z., Smith, M., and Stone, W. L. (2007). Sulfur mustard toxicity following dermal exposure: role of oxidative stress, and antioxidant therapy. *J Burns Wounds* **7**, e7.

Patel, G. K., Wilson, C. H., Harding, K. G., Finlay, A. Y., and Bowden, P. E. (2006). Numerous keratinocyte subtypes involved in wound re-epithelialization. *J. Invest. Dermatol.* **126**(2), 497-502.

Pentland, A. P., and Needleman, P. (1986). Modulation of keratinocyte proliferation in vitro by endogenous prostaglandin synthesis. *J. Clin. Invest.* **77**(1), 246-51.

Povirk, L. F., and Shuker, D. E. (1994). DNA damage and mutagenesis induced by nitrogen mustards. *Mutat Res* **318**(3), 205-26.

Rao, K. N., and Brown, M. A. (2008). Mast cells: multifaceted immune cells with diverse roles in health and disease. *Ann. N. Y. Acad. Sci.* **1143**, 83-104.

Raymond, A. A., Gonzalez de Peredo, A., Stella, A., Ishida-Yamamoto, A., Bouyssie, D., Serre, G., Monsarrat, B., and Simon, M. (2008). Lamellar bodies of human epidermis: proteomics characterization by high throughput mass spectrometry and possible involvement of CLIP-170 in their trafficking/secretion. *Mol Cell Proteomics* **7**(11), 2151-75.

Rice, P. (2003). Sulphur mustard injuries of the skin. Pathophysiology and management. *Toxicol Rev* **22**(2), 111-8.

Richardson, M. (2003). Understanding the structure and function of the skin. *Nurs Times* **99**(31), 46-8.

Ricketts, K. M., Santai, C. T., France, J. A., Graziosi, A. M., Doyel, T. D., Gazaway, M. Y., and Casillas, R. P. (2000). Inflammatory cytokine response in sulfur mustard-exposed mouse skin. *J Appl Toxicol* **20 Suppl 1**, S73-6.

Rietschel, R. L. (1989). Contact dermatitis and diagnostic techniques. *Allergy Proc* **10**(6), 403-11.

Rissmann, R., Oudshoorn, M. H., Hennink, W. E., Ponec, M., and Bouwstra, J. A. (2009). Skin barrier disruption by acetone: observations in a hairless mouse skin model. *Arch Dermatol Res* **301**(8), 609-13.

Rogakou, E. P., Nieves-Neira, W., Boon, C., Pommier, Y., and Bonner, W. M. (2000). Initiation of DNA fragmentation during apoptosis induces phosphorylation of H2AX histone at serine 139. *J. Biol. Chem.* **275**(13), 9390-5.

Rosso, J. D., Zeichner, J., Alexis, A., Cohen, D., and Berson, D. (2016). Understanding the Epidermal Barrier in Healthy and Compromised Skin: Clinically Relevant Information for the Dermatology Practitioner: Proceedings of an Expert Panel Roundtable Meeting. *J Clin Aesthet Dermatol* **9**(4 Suppl 1), S2-S8.

Sandby-Moller, J., Poulsen, T., and Wulf, H. C. (2003). Epidermal thickness at different body sites: relationship to age, gender, pigmentation, blood content, skin type and smoking habits. *Acta Derm Venereol* **83**(6), 410-3.

Sandoval, M., Morales, M., Tapia, R., del Carmen Alarcon, L., Sordo, M., Ostrosky-Wegman, P., Ortega, A., and Lopez-Bayghen, E. (2007). p53 response to arsenic exposure in epithelial cells: protein kinase B/Akt involvement. *Toxicol Sci* **99**(1), 126-40.

Saunders, J., Davis, H., Coetzee, L., Botha, S., Kruger, A., and Grobler, A. (1999). A novel skin penetration enhancer: evaluation by membrane diffusion and confocal microscopy. *J Pharm Pharm Sci* **2**(3), 99-107.

Schlereth, T., Birklein, F., an Haack, K., Schiffmann, S., Kilbinger, H., Kirkpatrick, C. J., and Wessler, I. (2006). In vivo release of non-neuronal acetylcholine from the human skin as measured by dermal microdialysis: effect of botulinum toxin. *Br. J. Pharmacol.* **147**(2), 183-7.

Scully, R., and Xie, A. (2013). Double strand break repair functions of histone H2AX. *Mutat. Res.* **750**(1-2), 5-14.

Senturk, E., and Manfredi, J. J. (2013). p53 and cell cycle effects after DNA damage. *Methods Mol Biol* **962**, 49-61.

Shahin, S., Cullinane, C., and Gray, P. J. (2001). Mitochondrial and nuclear DNA damage induced by sulphur mustard in keratinocytes. *Chem. Biol. Interact.* **138**(3), 231-45.

Shakarjian, M. P., Heck, D. E., Gray, J. P., Sinko, P. J., Gordon, M. K., Casillas, R. P., Heindel, N. D., Gerecke, D. R., Laskin, D. L., and Laskin, J. D. (2010). Mechanisms mediating the vesicant actions of sulfur mustard after cutaneous exposure. *Toxicol Sci* **114**(1), 5-19.

Sharma, A., Singh, K., and Almasan, A. (2012). Histone H2AX phosphorylation: a marker for DNA damage. *Methods Mol. Biol.* **920**, 613-26.

Shiota, N., Nishikori, Y., Kakizoe, E., Shimoura, K., Niibayashi, T., Shimbori, C., Tanaka, T., and Okunishi, H. (2010). Pathophysiological role of skin mast cells in wound healing after scald injury: study with mast cell-deficient W/W(V) mice. *Int. Arch. Allergy Immunol.* **151**(1), 80-8.

Shoumali, K., and Yeginsu, C. (2015). New Report of ISIS using Poison Gas in Syria. In *NY Times* (

Simon, G. A., and Maibach, H. I. (1998). Relevance of hairless mouse as an experimental model of percutaneous penetration in man. *Skin Pharmacol Appl Skin Physiol* **11**(2), 80-6.

Singer, A. J., Hirth, D., McClain, S. A., Crawford, L., Lin, F., and Clark, R. A. (2011). Validation of a vertical progression porcine burn model. *J Burn Care Res* **32**(6), 638-46.

Singer, A. J., Toussaint, J., Chung, W. T., Thode, H. C., McClain, S., and Raut, V. (2015). Effects of burn location and investigator on burn depth in a porcine model. *Burns* doi: 10.1016/j.burns.2015.09.016.

Singh, N. P. (2016). The comet assay: Reflections on its development, evolution and applications. *Mutat Res Rev Mutat Res* **767**, 23-30.

Smith, K. J., Skelton, H. G., Martin, J. L., Hurst, C. G., and Hackley, B. E., Jr. (1997). CO2 laser debridement of sulphur mustard (bis-2-chloroethyl sulphide) induced cutaneous lesions accelerates production of a normal epidermis with elimination of cytological atypia. *Br J Dermatol* **137**(4), 590-4.

Snider, T. H., Perry, M. R., Richter, W. R., Plahovinsak, J. L., Rogers, J., Reid, F. M., and Graham, J. S. (2014). A dynamic system for delivering controlled bromine and chlorine vapor exposures to weanling swine skin. *Cutan Ocul Toxicol* **33**(2), 161-7.

Stenn, K. S., and Karnik, P. (2010). Lipids to the top of hair biology. *J Invest Dermatol* **130**(5), 1205-7.

Sternberg, T. P. S. (1999). Studies of Aging, 17-18 (Book).

Strozyk, E., and Kulms, D. (2013). The role of AKT/mTOR pathway in stress response to UV-irradiation: implication in skin carcinogenesis by regulation of apoptosis, autophagy and senescence. *Int J Mol Sci* **14**(8), 15260-85.

Surh, I., Behl, M., Elmore, S. A., and Chhabra, R. S. (2012). Comparative dermal toxicity of dicyclohexylcarbodiimide and diisopropylcarbodiimide in rodents. *Cutan Ocul Toxicol* **31**(3), 177-87.

Talreja, P., Kleene, N. K., Pickens, W. L., Wang, T. F., and Kasting, G. B. (2001). Visualization of the lipid barrier and measurement of lipid pathlength in human stratum corneum. *AAPS PharmSci* **3**(2), E13.

Tewari-Singh, N., and Agarwal, R. (2016). Mustard vesicating agent-induced toxicity in the skin tissue and silibinin as a potential countermeasure. *Ann N Y Acad Sci* **1374**(1), 184-92.

Tewari-Singh, N., Jain, A. K., Inturi, S., White, C. W., and Agarwal, R. (2013). Clinically-relevant cutaneous lesions by nitrogen mustard: useful biomarkers of vesicants skin injury in SKH-1 hairless and C57BL/6 mice. *PLoS One* **8**(6), e67557.

Tewari-Singh, N., Jain, A. K., Orlicky, D. J., White, C. W., and Agarwal, R. (2014). Cutaneous injury-related structural changes and their progression following topical nitrogen mustard exposure in hairless and haired mice. *PLoS One* **9**(1), e85402.

Tewari-Singh, N., Rana, S., Gu, M., Pal, A., Orlicky, D. J., White, C. W., and Agarwal, R. (2009). Inflammatory biomarkers of sulfur mustard analog 2-chloroethyl ethyl sulfide-induced skin injury in SKH-1 hairless mice. *Toxicol Sci* **108**(1), 194-206.

Valerie, K., Yacoub, A., Hagan, M. P., Curiel, D. T., Fisher, P. B., Grant, S., and Dent, P. (2007). Radiation-induced cell signaling: inside-out and outside-in. *Mol Cancer Ther* **6**(3), 789-801.

Vane, J. R., Mitchell, J. A., Appleton, I., Tomlinson, A., Bishop-Bailey, D., Croxtall, J., and Willoughby, D. A. (1994). Inducible isoforms of cyclooxygenase and nitric-oxide synthase in inflammation. *Proc. Natl. Acad. Sci. U. S. A.* **91**(6), 2046-50.

Veuger, S. J., Curtin, N. J., Richardson, C. J., Smith, G. C., and Durkacz, B. W. (2003). Radiosensitization and DNA repair inhibition by the combined use of novel inhibitors of DNA-dependent protein kinase and poly(ADP-ribose) polymerase-1. *Cancer Res* **63**(18), 6008-15.

Vieille-Petit, A., Blickenstaff, N., Coman, G., and Maibach, H. (2015). Metrics and clinical relevance of percutaneous penetration and lateral spreading. *Skin Pharmacol Physiol* **28**(2), 57-64.

Vogt, R. F., Jr., Dannenberg, A. M., Jr., Schofield, B. H., Hynes, N. A., and Papirmeister, B. (1984). Pathogenesis of skin lesions caused by sulfur mustard. *Fundam Appl Toxicol* **4**(2 Pt 2), S71-83.

Wang, X., Sistrunk, C., Miliani de Marval, P. L., Kim, Y., and Rodriguez-Puebla, M. L. (2012). Combined effect of cyclin D3 expression and abrogation of cyclin D1 prevent mouse skin tumor development. *Cell Cycle* **11**(2), 335-42.

Weller, K., Foitzik, K., Paus, R., Syska, W., and Maurer, M. (2006). Mast cells are required for normal healing of skin wounds in mice. *FASEB J.* **20**(13), 2366-8.

Wessler, I., Michel-Schmidt, R., and Kirkpatrick, C. J. (2015). pH-dependent hydrolysis of acetylcholine: Consequences for non-neuronal acetylcholine. *Int. Immunopharmacol.* **29**, 27-30.

Wickett, R. R., and Visscher, M. O. (2006). Structure and function of the epidermal barrier. *American Journal of Infection Control* **34**(10).

Williams, C. S., Mann, M., and DuBois, R. N. (1999). The role of cyclooxygenases in inflammation, cancer, and development. *Oncogene* **18**(55), 7908-16.

Williams, J. S., Williams, R. S., Dovey, C. L., Guenther, G., Tainer, J. A., and Russell, P. (2010). gammaH2A binds Brc1 to maintain genome integrity during S-phase. *EMBO J.* **29**(6), 1136-48.

Wormser, U., Brodsky, B., and Sintov, A. (2002). Skin toxicokinetics of mustard gas in the guinea pig: effect of hypochlorite and safety aspects. *Arch Toxicol* **76**(9), 517-22.

Wormser, U., Langenbach, R., Peddada, S., Sintov, A., Brodsky, B., and Nyska, A. (2004). Reduced sulfur mustard-induced skin toxicity in cyclooxygenase-2 knockout and celecoxib-treated mice. *Toxicol. Appl. Pharmacol.* **200**(1), 40-7.

Wu, C. L., Su, S. B., Lien, H. Y., and Guo, H. R. (2012). The role of the chemical burns caused by hydroxide ion in the toxicity of dermal exposure to tetramethylammonium ion in a rat model. *Burns* **38**(7), 1051-7.

Yamaguchi, Y., Madhyastha, H., Madhyastha, R., Choijookhuu, N., Hishikawa, Y., Pengjam, Y., Nakajima, Y., and Maruyama, M. (2016). Arsenic acid inhibits proliferation of skin fibroblasts, and increases cellular senescence through ROS mediated MST1-FOXO signaling pathway. *J Toxicol Sci* **41**(1), 105-13.

Yang, L., Zhang, S., and Wang, G. (2019). Keratin 17 in disease pathogenesis: from cancer to dermatoses. *J Pathol* **247**(2), 158-165.

Ye, L., Wang, Z., Li, Z., Lv, C., and Man, M. Q. (2019). Validation of GPSkin Barrier((R)) for assessing epidermal permeability barrier function and stratum corneum hydration in humans. *Skin Res Technol* **25**(1), 25-29.

Young, S., Fabio, K., Guillon, C., Mohanta, P., Halton, T. A., Heck, D. E., Flowers, R. A., 2nd, Laskin, J. D., and Heindel, N. D. (2010). Peripheral site acetylcholinesterase inhibitors targeting both inflammation and cholinergic dysfunction. *Bioorg Med Chem Lett* **20**(9), 2987-90.

Young, S. C., Fabio, K. M., Huang, M. T., Saxena, J., Harman, M. P., Guillon, C. D., Vetrano, A. M., Heck, D. E., Flowers, R. A., 2nd, Heindel, N. D., and Laskin, J. D. (2012). Investigation of anticholinergic and non-steroidal anti-inflammatory prodrugs which reduce chemically induced skin inflammation. *J. Appl. Toxicol.* **32**(2), 135-41.

Yousef, H., and Sharma, S. (2019). Anatomy, Skin (Integument), Epidermis. In *StatPearls*, Treasure Island (FL).

Zhang, X., Mei, Y., Wang, T., Liu, F., Jiang, N., Zhou, W., and Zhang, Y. (2017). Early oxidative stress, DNA damage and inflammation resulting from subcutaneous injection of sulfur mustard into mice. *Environ Toxicol Pharmacol* **55**, 68-73.

Zhaorigetu, S., Yanaka, N., Sasaki, M., Watanabe, H., and Kato, N. (2003). Inhibitory effects of silk protein, sericin on UVB-induced acute damage and tumor promotion by reducing oxidative stress in the skin of hairless mouse. *J Photochem Photobiol B* **71**(1-3), 11-7.

Zheng, R., Heck, D. E., Mishin, V., Black, A. T., Shakarjian, M. P., Kong, A. N., Laskin, D. L., and Laskin, J. D. (2014). Modulation of keratinocyte expression of antioxidants by 4-hydroxynonenal, a lipid peroxidation end product. *Toxicol Appl Pharmacol* **275**(2), 113-21.

Zheng, R., Po, I., Mishin, V., Black, A. T., Heck, D. E., Laskin, D. L., Sinko, P. J., Gerecke, D. R., Gordon, M. K., and Laskin, J. D. (2013). The generation of 4-hydroxynonenal, an electrophilic lipid peroxidation end product, in rabbit cornea organ cultures treated with UVB light and nitrogen mustard. *Toxicol Appl Pharmacol* **272**(2), 345-55.

Zhu, H., Jung, E. C., Hui, X., and Maibach, H. (2015). Proposed human stratum corneum water domain in chemical absorption. *J Appl Toxicol* doi: 10.1002/jat.3208.